International Atomic Energy Agency

INDC(BLR)-010
Distr. G

INDC INTERNATIONAL NUCLEAR DATA COMMITTEE

EVALUATION OF NEUTRON DATA FOR PLUTONIUM-242

V.M. Maslov, Yu.V. Porodzinskij, E.Sh. Sukhovitskij, G.B. Morogovskij

Radiation Physics & Chemistry Problems Institute
220109, Minsk-Sosny, Belarus

November 1997

IAEA NUCLEAR DATA SECTION, WAGRAMERSTRASSE 5, A-1400 VIENNA

Reproduced by the IAEA in Austria
November 1997

INDC(BLR)-010
Distr. G

EVALUATION OF NEUTRON DATA FOR PLUTONIUM-242

V.M. Maslov, Yu.V. Porodzinskij, E.Sh. Sukhovitskij,
G.B. Morogovskij

Radiation Physics & Chemistry Problems Institute
220109, Minsk-Sosny, Belarus

Abstract

The evaluation of neutron data for ^{242}Pu is made in the energy region from 10^{-5} eV up to 20 MeV. The results of the evaluation are compiled in the ENDF/B-VI format.

This work is performed under the Project Agreement CIS-03-95 with the International Science and Technology Center (Moscow). The Financing Party for the Project is Japan. The evaluation was requested by Japan Nuclear Data Center (JAERI).

Date of Manuscript: October 9, 1997

Contents

1. **Introduction** 7

2. **Resolved resonance region** 7
   - 2.1 Previous evaluations of resolved resonance parameters 7
   - 2.2 Measured data fitting 8
     - 2.2.1 Status of measured data 8
     - 2.2.2 Energy region below 200 eV 9
     - 2.2.3 Energy region 200 - 1300 eV 10
     - 2.2.4 Resonance parameter analysis 11

3. **Unresolved resonance region** 13
   - 3.1 Review 13
   - 3.2 The s-wave average resonance parameter evaluation 14
     - 3.2.1 Estimate of resonance level missing influence on $<D_{obs}>$ and S_0 14
     - 3.2.2 Evaluation of $<D_{obs}>$, S_0, $<\Gamma_\gamma>$ and $<\Gamma_f>$ based on the resolved resonance parameters 14
   - 3.3 The s-, p- and d-wave average resonance parameter evaluation 15
     - 3.3.1 Neutron width 15
     - 3.3.2 Neutron resonance spacing 16
     - 3.3.3 Fission width 16
     - 3.3.4 Radiative capture width 16
   - 3.4 Cross section evaluation in the region 1.3-44.7256 keV 16
     - 3.4.1 Total section energy dependence 16
     - 3.4.2 Fitting of fission cross section structure 16
     - 3.4.3 Capture cross section energy dependence 17
     - 3.4.4 Comparison of current and JENDL-3 and ENDF-B-VI evaluated data 17
     - 3.4.5 Drawbacks of ENDF/B-VI format and associated inconsistencies in evaluated neutron cross sections 18

4. **Fast neutron cross sections** 19
   - 4.1 Optical potential 19
   - 4.2 Fission cross section 20
     - 4.2.1 Status of the experimental data 20
     - 4.2.2 Statistical model calculation of fission cross section 22
     - 4.2.3 Fission transmission coefficient, level density and transitition state spectrum 22
     - 4.2.4 Fission cross section above emissive fission threshold 25
   - 4.3 Inelastic scattering cross section 26
     - 4.3.1 Levels of ^{242}Pu 26
     - 4.3.2 ^{242}Pu level density 26
     - 4.3.3 ^{243}Pu level density 26
     - 4.3.4 Compound inelastic scattering 27
     - 4.3.5 Direct inelastic scattering 27
   - 4.4 Radiative capture cross section 27
   - 4.5 Cross sections of (n,2n) and (n,3n) reactions 28

5. **Energy distributions of secondary neutrons** 29
5.1 Model calculations of (n,nx) reaction spectra 29
5.2 Prompt fission neutron spectra 30
5.2.1 Prompt fission neutron spectra evaluation 30

6. **Number of neutrons per fission** 32

7. **Angular distributions of secondary neutrons** 33

8. **Conclusions** 33

9. **Figure captions** 39

1 Introduction

The advanced nuclear fuel cycle studies request the nuclear data of minor actinides [1]. The buildup of higher actinides in fast breeder reactors is strongly affected by the neutron capture cross section of ^{242}Pu. In this work the evaluation of ^{242}Pu neutron data is performed. The quantities evaluated are resolved and unresolved resonance parameters, total, elastic and inelastic scattering, fission, capture, (n,2n) and (n,3n) reaction cross sections, angular and energy distributions of secondary neutrons, including partial (n,xn) and (n,xnf) reaction spectra, fission spectra and number of neutrons per fission. The incident neutron energy range covered is from 10^{-5} eV up to 20 MeV. The evaluated quantities are compared with JENDL-3.2 [2], ENDF/B-VI [3] and JEF-2 [4] evaluations.

2 Resolved resonance region

2.1 Previous evaluations of resolved resonance parameters

In ENDF/B-VI evaluation Breit-Wigner single-level parameters recommended in BNL-325 [5] up to 986 eV are adopted. Negative and first 2.68-eV resonance parameters are fitted to thermal total cross section values by Young and Reeder [6] and by Young and Simpson [7].

In JEF-2 evaluation resonance parameters of JENDL -2 are adopted, i.e. neutron and capture width values up to 1290 eV calculated by Poortmans et al.[8] and Auchampaugh and Bowman [9]. Fission resonance area values, obtained by Auchampaugh and Bowman [9] and Bergen et al.[10] are employed. Negative resonance is introduced instead of smooth background cross section, as it was done in JENDL-2. Scattering radius value is used to fit total cross section data in resonance valleys.

In JENDL-3 evaluation basically resonance parameters by Poortmans et al. [8] and Auchampaugh and Bowman [9] up to 1115 eV are adopted, fission widths are obtained by fitting fission resonance areas measured by Weigmann et al. [11]. Thermal cross section values estimated by Mughabghab [12] were fitted with two negative resonance parameters.

The purpose of current resonance parameter evaluation is to extract the resolved resonance parameters up to 1300 eV by consistent analysis of measured total and fission data base. As a first order approximation resonance parameters by Poortmans et al. [8] were adopted.

2.2 Measured data fitting

2.2.1 Status of measured data

2.2.1.1 Total cross section data A number of total cross section measurements are available. Auchampaugh et al.[13] have measured total cross section in the energy range of 0.02-389 eV with time-of-flight method. The oxide samples were used. Resonance shape and area analysis provides reduced neutron width Γ_n^o values. Total cross section was measured by Young et al.[6] from 0.0015 up to 150 eV for high purity oxide sample. They provide resonance parameters Γ_n^o and Γ_γ below 150 eV. Total cross section data by Young et al.[6, 7], as well as that by Auchampaugh et al.[13] exhibit strong sensitivity to the sample, specifically the total cross section value, obtained for oxide target [6, 7] is much higher than for metallic target [7]. However when the influence of powder scattering and water impurity is taken into account [7], the total and capture data [14, 15, 16, 17, 18] seem to be compatible with the estimates of potential and elastic scattering [19].

Cote et al. [20] have measured the transmission and obtained the 2.65-eV and 53.6-eV resonance parameters. The measurements were performed for two sample thicknesses, so capture width Γ_γ of 2.65-eV resonance was obtained.

Pattenden et al. [21] have measured transmission with time-of-flight method below 850 eV. Resonance areas were obtained below 320 eV, a number of resonances have been detected, not seen by Auchampaugh et al.[13] and Young and Reeder [6].

James al.[22] have measured total cross section in the energy range from 16 eV up to 35 keV with time-of-flight method. Fission areas for 767-eV and 799-eV resonances are estimated.

Auchampaugh and Bowman [9] have measured total cross section in the energy range of 600 eV - 81 keV. Resonance parameters of strong fission resonances up to 4 keV are estimated. The values of Γ_n and Γ_f are extracted by combined analysis of transmission and fission data [23].

Simpson et al. [24] have measured transmission for metallic samples from 15 eV up to 30 keV, resolved resonance parameters are provided from 20 eV up to 500 eV.

Hockenbury et al.[28] have investigated energy region of 205-383 eV using metallic sample.

2.2.1.2 Fission data Bergen et al. [10] have measured fission cross section relative to that of ^{235}U with the bomb-shot from 51 up to 5000 eV and from 0.1 to 3 MeV. Fission resonance areas are provided up to 790 eV. Bomb-shot measurement was made by Auchampaugh et al.[23] from 20 eV up to 10 MeV. Fission resonance areas are provided for energy range of 370

eV - 4 keV. Fission resonance areas are reported for 49 resonances below 500 eV. Intermediate structure is observed with average spacing $\langle D_{II} \rangle = 600^{+189}_{-116}$ eV.

Fission cross section was measured by Weigmann et al.[11] from 2 eV up to 10 MeV. Neutrons were produced with 150-MeV electron linac of CBNM. ^{235}U sample was used as neutron flux monitor, to normalize fission data below 25 keV fission integral of ^{235}U, measured by Wagemans et al.[29] was used. The fission width values were obtained based on measured fission resonance areas. Lower limits for the neutron width values of 468.4-eV and 762.4-eV strong fission resonances are given. Resonances of 2.68 eV and 53.5 eV are assumed to be of class I type. The other resonances are supposed to belong to class II clusters of resonances. The approximate energies of class II states are provided, but only in case of 468.4-eV and 762.4-eV resonances the major strength is concentrated on these resonances, otherwise the average energy of fission resonance area is assumed to be class II state energy. The resonances at still higher energies up to 70 keV are just individual class II clusters, so only total class II fission areas are provided. Much less resonances were observed by Weigmann et al.[11] below 10 keV than in the measurement by Auchampaugh et al.[23], while more pronounced structure have been revealed above 10 keV.

The characteristic features of the whole measured fission data base may be summarized as follows. The bomb-shot measurement [10, 23] are inherently very sensitive, while the energy resolution is poorer than that attainable with linacs [11]. Below a few keV incident neutron energy the sensitivity factor turns out to be more important than resolution. Weak resonances observed in bomb-shot measurements remain undetected in measurements with linac. However above ~10 keV incident neutron energy the opposite is true. Fission areas as obtained in linac' measurements tend to be somewhat higher than those of bomb-shot measurement [23]. Unfortunately it is difficult to find a way to renormalize lower energy data of ref. [10, 23] to more accurate data by Weigmann et al. [11].

2.2.1.3 Capture cross section data Capture cross section was measured with activation method by Studier et al. [14] , Butler et al.[15], Durham et al. [16], Halperin et al.[17] and Folger et al. [18]. The evaluated data are based on capture and total data and coherent scattering length obtained by Lander et al. [19].

2.2.2 Energy region below 200 eV

The first resonance occurs at 2.66 eV. To fit the data at lower energies the first resonance parameters, available thermal total and capture cross sections as well as coherent scattering length [19] were used. The total data by

Young et al. [6, 7] at higher energies were also of relevance. First resonance parameters fit the total data base, however only increasing reduced neutron width value we can get a better fit of thermal cross section values (see Fig. 2.1). To avoid this increase we introduced single negative resonance at E_r= - 70 eV. First resonance parameters influence only weakly on thermal cross section values, hence measured total data by Young and Reeder [7] and Auchampaugh et al.[13] discrepancy around 2.66-eV resonance peak is of no consequences for the thermal total cross section value (see Fig. 2.2).

Total cross section measurements listed above provide basically only neutron width values. Most comprehensive measurements by Poortmans et al.[8] of total, capture and elastic scattering cross sections up to 1300 eV for oxide sample provide Γ_n^o values for 71 resonances and Γ_γ values for 25 resonances.

Radiative capture width Γ_γ values obtained by Poortmans et al.[8] for 25 resonances in the energy range 50 -950 eV were adopted. For the other resonances the average value of Γ_γ =22.72 meV was assumed. Fission width values were obtained by fission data fitting. Reference fission data were that by Bergen et al.[10] and Auchampaugh et al.[23]. Fission widths of negative, 14.6-eV, 22.56-eV and 40.93-eV resonances were assumed to be equal to 0.002 meV. Resonance energies as deduced from capture measurements by Poortmans et al. [8] were adopted.

Fission data by Bergen et al.[10] were used up to 200.13 eV, except low energy resonances measured by Weigmann et al.[11]. Fission area of 53.5-eV resonance obtained by Weigmann et al.[11] is ~20 lower than that obtained by Bergen et al.[10]. Resonance fission areas measured by Weigmann et al.[11] were used to extract fission width values of 2.66-eV and 53.5-eV resonances for adopted Γ_n^o and Γ_γ values. Parameters of higher resonances (up to 163.3 eV) were obtained by shape analysis of data by Bergen et al.[10].

2.2.3 Energy region 200 ÷ 1300 eV

Above 200 eV fission width values were extracted by shape analysis of data by Auchampaugh et al.[23]. Values of reduced neutron width Γ_n^o and radiative width Γ_γ were fixed in the same manner as at lower energies. Figures 2.3, 2.4 show the comparison of fission cross section, calculated with present resonance parameters with measured data. Table 2.1 shows the comparison of fission areas as obtained by Bergen et al.[10], Auchampaugh et al.[23] and Weigmann et al.[11]. In some cases (see for instance 788.5-eV resonance on Fig. 2.4), the discrepancy of calculated and quoted measured data is due to discrepancies in resonance valleys. There is almost a systematic difference between fission data by Bergen et al.[10] and Auchampaugh et al.[23], the former being essentially higher. In any case it is hardly possible to interpret high level of non-resonance background in measured data..

Above 980 eV neutron width Γ_n^o values obtained by Poortmans et al. [8]

were adopted, while the average value of capture width $\Gamma_\gamma = 22.72$ meV was assumed. Five resonances at 996.9 eV, 1158 eV, 1231.6 eV, 1239.8 eV, 1304 eV are added to improve fit of fission data by Auchampaugh et al.[23].

Table 2.1

E_r, eV	A_f [10]	A_f[23]	A_f[11]	A_f, [3]	A_f, [4]	A_f, [2]	A_f, Present
474.6		0.14±0.03	0.12±0.06		0.032	0.104	0.136
482.3	2.83±0.24	1.29±0.22	1.70±0.20		2.826	1.664	1.069
536.2	1.12±0.09	0.46±0.09	0.27±0.10		1.113	0.271	0.334
548.3	1.08±0.11	0.53±0.08	0.44±0.10		1.079	0.429	0.429
669.2		0.23±0.07	0.12±0.09	0.239	0.197	0.109	0.1221
692.9	2.16±0.22	0.90±0.16	0.85±0.14	1.009	1.502	0.866	0.538
736.6	4.23±0.50	2.70±0.39	2.08±0.21	2.756	3.458	2.023	2.073
754.8		6.96±0.80	7.27±0.43	7.512	12.510	7.284	4.149
761.7		22.97±2.57	28.71±1.39	15.236	19.216	28.179	13.848
788.5	7.34±1.27	4.85±0.58	6.16±0.36	4.644	6.109	6.024	2.942
865.1		0.45±0.10	0.27±0.13	0.485	0.414	0.272	0.269
1304		0.23±0.04	0.32±0.12			0.005	0.165

2.2.4 Resonance parameter analysis

We have got 89 resonance parameters up to 1310 eV. The average resonance parameters, thermal cross sections and resonance integrals are presented in Table 2.2. Thermal cross sections, except fission one, and resonance integrals are fairly consistent with previous evaluations.

Intermediate structure is evident in subthreshold fission cross section data of ^{242}Pu target nuclide. A large number of class II resonances are observed below 70 keV incident neutron energy. It is a common assumption that resonances above 53.5 eV exhibit intermediate structure due to second minimum of double humped fission barrier. Fission width values of the intermediate structure resonances and matrix elements for coupling of class I and class II levels were studied by Weigmann et al. [11] and Auchampaugh and Bowman [9]. Total width of class II resonance $\Gamma_{II} = \Gamma^{\uparrow} + \Gamma^{\cdot}$ is the sum of class II fission width $\Gamma^{\uparrow}$ and spreading width $\Gamma^{\cdot}$. In a weak coupling limit, when Γ_{II} is much less than neutron resonance spacing $\langle D_{II} \rangle$ in second well, class I fission width $\Gamma_{\mu f}$ are defined by equation

$$\Gamma_{\mu f} = \frac{v^2_{II\mu}}{(E_{II} - E\mu)^2}\Gamma^{\uparrow}, \mu = 1, ..., k. \quad (1)$$

The averaged over class II states square of coupling matrix element $\overline{v^2_{II\mu}}$

between class I state μ in primary well and class II state E_{II} in the second well is given as

$$\overline{v^2_{II\mu}} = \langle \Gamma_{\mu f}(E_{II} - E\mu)^2 \rangle / \Gamma^{\uparrow}. \tag{2}$$

This matrix element could be computed also using the penetrability of inner (A) hump of fission barrier. Specifically,

$$\overline{v^2_{II\mu}} = \frac{\langle D_I \rangle \langle D_{II} \rangle}{4\pi^2} \left[1 + \exp\left(\frac{2\pi\,(E_A - B_n - E_n)}{\hbar\omega_A} \right) \right]^{-1}. \tag{3}$$

When inner fission barrier parameters are fixed by description of fission cross section data above ~100 keV up to emissive fission threshold (E_A= 6.05 MeV, $\hbar\omega_A$ = 0.725 MeV, E_B= 5.45 MeV, $\hbar\omega_B$ = 0.52 MeV), using Eq.(3) we get $\overline{v^2_{II\mu}}$ = 0.049 (eV)^2, assuming that $\langle D_{II} \rangle$ = 1000 eV, D_I = 12.903 eV. Estimate of class II resonance spacing $\langle D_{II} \rangle$ = 1000 eV was obtained by Weigmann et al.[11]. Class II fission width $\Gamma^{\uparrow}$ is just the sum of fission widths of fine structure resonances of a given cluster E_{II} :

$$\Gamma^{\uparrow} = \sum_{\mu=0}^{n} \Gamma_{\mu f}. \tag{4}$$

An upper limit of class II fission width might be obtained as

$$\Gamma^{\uparrow} < \left[\sum_{\mu \neq II} \sqrt{\Gamma_{\mu f} \Gamma^{o}_{\mu n} / \Gamma_{IIn}}. \right]^2 \tag{5}$$

Average class II fission width $\langle \Gamma^{\uparrow} \rangle$ could be related to the outer fission barrier penetrability as

$$\langle \Gamma^{\uparrow} \rangle = \frac{\langle D_{II} \rangle}{2\pi} \left[1 + \exp\left(\frac{2\pi\,(E_B - B_n - E_n)}{\hbar\omega_B} \right) \right]^{-1}. \tag{6}$$

We obtain $\Gamma^{\uparrow}$= 1.04 eV for E_B= 5.45 MeV, while $\Gamma^{\uparrow}$= 0.118 eV for E_B= 5.63 MeV. Inner barrier height E_B= 5.63 MeV allows to describe fission cross section data by Auchampaugh et al. [23] below 100 keV. Below we will comment that fission data above 100 keV and below 100 keV can not be described without changing fission barrier parameters.

Established class II resonances are at 468.4 eV and 761.7 eV. 468.4-eV resonance remained unobserved in total cross section measurements, it's neutron width Γ_n = 0.03 meV, an order of magnitude lower than that of 474.6-eV neighbor resonance, isolated by Poortmans et al.[8]. Using value of $\overline{v^2_{II\mu}}\Gamma^{\uparrow}$ = 0.13 (eV)^3 for cluster around 468.4-eV resonance, obtained with Eq.(2), estimate of $\Gamma^{\uparrow}$= 0.21 eV was obtained by Weigmann et al. [11]. Present estimate of $\overline{v^2_{II\mu}}$ = 0.049 (eV)^2 is rather sensitive to the inner barrier

parameters, it yields $\Gamma^{\uparrow}$= 2.65 eV. In other words estimates of $\Gamma^{\uparrow}$ based on Eqs.(2-3) might produce inconsistent results. For 761.7-eV resonance present neutron width value Γ_n = 5.96 meV is compatible with estimate of Γ_n = 5.1 meV by Weigmann et al. [11], being higher than estimate of 3.3±1.5 meV by Poortmans et al.[8]. $\overline{v^2_{I\mu}}\Gamma^{\uparrow}$ = 0.76 (eV)^3 for cluster around 761.7-eV resonance, relevant estimate of $\Gamma^{\uparrow}$ < 0.56 eV was obtained by Weigmann et al. [11] using Eq.(5). Estimate of $\langle\Gamma^{\uparrow}\rangle \approx$ 0.5 MeV was obtained taking into account Porter-Thomas fluctuations, which is roughly compatible with our estimate of $\langle\Gamma^{\uparrow}\rangle$ as given by outer fission barrier estimate E_B= 5.45÷5.63 MeV. Summarizing, it might be concluded, that fission widths are roughly compatible with fission barrier parameters estimated by statistical model fit.

Table 2.2

	ENDF/B-VI	JENDL-3	JEF-2	Present
$\langle\Gamma_n^o\rangle$, meV	1.5983	1.4200	1.3749	1.6316
$\langle\Gamma_f\rangle$, meV	1.2680	5.4920	2.9812	0.4947
$\langle\Gamma_\gamma\rangle$, meV	23.278	24.124	24.191	22.720
$\langle D\rangle$, eV	15.640	17.2593	20.0729	15.6136
S_o	1.03714×10^{-4}	8.32315×10^{-5}	6.92174×10^{-4}	1.05687×10^{-4}
σ_t , barn	26.888	27.111	26.819	26.900
σ_γ , barn	19.158	18.789	18.504	19.034
σ_f , barn	1.0423×10^{-3}	2.5567×10^{-3}	1.4483×10^{-2}	1.9657×10^{-3}
σ_n , barn	7.7290	8.3198	8.3005	7.8636
g_γ	1.01323	1.01322	1.01399	1.01370
g_f	1.00388	1.00920	1.01247	1.01271
I_γ , barn	1273.62	1131.23	1117.05	1123.70
I_f , barn	5.5686	5.5768	6.3010	5.5270

The thermal total σ_t, fission σ_f, capture σ_γ and scattering σ_n cross sections, $g_\gamma-$, and g_f-factors, as well as resonance integrals $I\gamma$ and I_f values are calculated with a code INTER[25]. In case of JENDL-3 and present evaluations the multi-level Breit-Wigner formalism was used, while for ENDF/B-IV evaluation single-level formula was employed.

3 Unresolved resonance region

3.1 Review

Unresolved resonance region of ^{242}Pu is supposed to be from 1.3 keV up to 44.7256 keV. The lower energy is the end-point of resolved resonance

region, the upper energy is the threshold energy of the first excited level. We suppose $s-$, $p-$ and $d-$wave neutron-nucleus interactions to be effective.

3.2 The s-wave average resonance parameter evaluation

3.2.1 Estimate of resonance level missing influence on $\langle D_{obs} \rangle$ and S_o.

Preliminary estimates of average partial widths were obtained by averaging evaluated resolved resonance parameters. Figure 3.1 demonstrates the cumulative sum of resolved resonance levels. Missing of levels above ~600 eV might be noticed. The average resolved resonance parameters are as follows:

$$\langle \Gamma_n^0 \rangle = 1.407 \times 10^{-4} \text{ (eV)}^{1/2}$$
$$\langle \Gamma_f \rangle = 0.4947 \text{ meV}$$
$$\langle D_{obs} \rangle = 14.96 \text{ eV}$$
$$\langle \Gamma_\gamma \rangle = 22.72 \text{ meV}$$

Fission width value $\langle \Gamma_f \rangle = 0.4947$ meV was averaged over energy range of 1 keV, which is compatible with estimate of spacing of class II resonances $\langle D_{II} \rangle$ ~1 keV in second well, estimated by Weigmann et al.[11]. This value of $\langle \Gamma_f \rangle$ strongly depends on fission width of 761.7-eV resonance, strongest in cluster centered on it. On the other hand fission width Γ_f of this 761.7-eV resonance depends on estimate of it's neutron width Γ_n. Adopting estimate of Γ_n= 3.3 meV by Poortmans et al.[8], as compared with our estimate of Γ_n= 5.96 meV might yield three times higher estimate of $\langle \Gamma_f \rangle$. Due to missing of weak resonances values of $\langle \Gamma_n^0 \rangle$ and $\langle D_{obs} \rangle$ may overestimate neutron resonance spacing and average reduced neutron width. To get a physically justified values of $\langle D_{obs} \rangle$ and $\langle \Gamma_n^0 \rangle$ we employ a method, which is described elsewhere [26]. Both reduced neutron width and neutron resonance spacing distributions with account of missing are obtained in a unified approach. We take into account the correlation of weak resonance missing and resonance missing due to poor experimental resolution. The resolution function as well as $\langle D_{obs} \rangle$ and $\langle \Gamma_n^0 \rangle$ values are obtained by maximum likelihood method when comparing experimental distributions of reduced neutron width and neutron resonance spacing with Porter-Thomas and Wigner distributions, modified for resonance missing.

3.2.2 Evaluation of $\langle D_{obs} \rangle$, S_o, $\langle \Gamma_\gamma \rangle$ and $\langle \Gamma_f \rangle$ based on the resolved resonance parameters.

We applied our method [26] to the resolved resonance data base. The evaluated values are:

$$S_o = (0.931 \pm 0.150) \times 10^{-4}\ (\mathrm{eV})^{1/2}$$
$$\langle D_{obs} \rangle = (12.903 \pm 0.72)\ \mathrm{eV}$$

Figure 3.2 shows the cumulative sum of reduced neutron widths. Figure 3.3 shows the comparison of expected and experimental reduced neutron width distributions. Figure 3.4 shows the comparison of distributions for neutron resonance spacing. The expected distributions shown on the figures 3.3 and 3.4 demonstrate the influence of resonance missing. Figures 3.5 and 3.6 present the ratios of the theoretical and experimental distribution quantiles. Figure 3.5 shows that there is surplus of small neutron widths ($\sim$ 4% of total resonance number). Probability for the resolved resonance to be p-wave resonance, estimated based on Porter-Thomas distribution of reduced p-wave neutron width Γ_n^1 with S_1 =2.59$\times 10^{-4}$ (eV)$^{1/2}$, $\langle D_{1/2-} \rangle$ =12.9 eV, $\langle D_{3/2-} \rangle$ = 6.7 eV, yields that three resonances at most could be assigned as p-wave. Fitting of experimental reduced neutron widths distribution with Porter-Thomas distribution (see Fig.3.7) gives the same result. Surplus of small neutron widths lies within statistics $\Delta N = 2\sqrt{N} \simeq 20$, so there is no need to assign any resonances below 1300 eV as $p-$wave. It might be concluded that expected distributions are consistent with experimental data within statistical errors. That is the reason to consider the estimates of $\langle D_{obs} \rangle$ and S_o reliable.

3.3 The s-, p- and d-wave average resonance parameter evaluation

3.3.1 Neutron width

Average neutron width is calculated as follows

$$\langle \Gamma_n^{lJ} \rangle = S_l \langle D_J \rangle E_n^{1/2} P_l,$$

where P_l is the transmission factor for the lth partial wave, which was calculated within black nucleus model. The p-wave neutron strength function S_1 = 2.59$\times 10^{-4}$ (eV)$^{-1/2}$ was calculated with the optical model using the deformed optical potential described below. According to the results of optical model calculations S_o was assumed to decrease linearly from S_o=0.931$\times 10^{-4}$ (eV)$^{-1/2}$ to the value of S_o=0.883$\times 10^{-4}$(eV)$^{-1/2}$ for neutron energy of 44.7256 keV. The d-wave neutron strength function was taken from optical model calculations: S_2 = 1.17$\times 10^{-4}$ (eV)$^{-1/2}$. Since d-wave contribution is rather small, the impact of any reasonable approximation on calculated values is negligible.

3.3.2 Neutron resonance spacing

Neutron resonance spacing $\langle D_J \rangle$ was calculated with the phenomenological model [27], which takes into account the shell, pairing and collective effects. The main parameter of the model $\tilde{a}$ was normalized to the observed neutron resonance spacing of ^{242}Pu $\langle D_{obs} \rangle$ = 12.903 eV.

3.3.3 Fission width

Fission widths are calculated within a double-humped fission barrier model. We constructed transition spectra by supposing the triaxiality of inner saddle and mass asymmetry at outer saddle. Energy and angular momentum dependence of fission width is defined by the transition state spectra at inner and outer barrier humps. They will be described below. One must realize that due to the second well impact on fission width distribution, which can not be taken into account within ENDF/B format, fission widths values fitting measured fission data might be lower than actual fission width values.

3.3.4 Radiative capture width

Energy and angular momentum dependences of radiative capture width are calculated within a two-cascade $\gamma-$emission model with allowance for the (n,γf) and (n,γn') reaction competition to the (n,$\gamma\gamma$) reaction. In this energy region (n,$\gamma\gamma$) reaction appears to be a radiative capture reaction. The radiative capture width was normalized to the value of $\langle \Gamma_\gamma \rangle$ = 22.72 meV determined for ^{242}Pu in resolved resonance region. (For details see Chapter IV).

3.4 Cross section evaluation in the region 1.3-44.7256 keV

3.4.1 Total section energy dependence

Total cross section data by Young and Reeder[6] below 7 keV can be used only for checking present S_o and S_1 strength function values (see Fig. 3.8), as the latter and potential radii, which was adopted from optical calculations define total cross section in a few keV energy region.

3.4.2 Fitting of fission cross section structure

Fission cross section of ^{242}Pu in unresolved energy region is measured in bomb-short experiment by Auchampaugh et al.[23] and Bergen et al.[10]. Data by Bergen et al.[10] are almost order of magnitude higher than data by Auchampaugh et al.[23] in the energy range 0.2- 6 keV, while they are compatible around 0.5 keV and above 100 keV (see Fig. 3.9).

Fission cross section calculations with the adopted fission barrier parameters, giving $\langle \Gamma_f^{1/2+} \rangle$ = 0.36 meV at incident neutron energy of 1.3 keV,

reproduce data by Bergen et al.[10] below ~6 keV and fit measured data above 100 keV. Nevertheless we decided to reproduce data by Auchampaugh et al.[23], specifically intermediate structure, supported by data by Weigmann et al.[11]. However, it is hardly possible to fit that low fission cross section data below ~100 keV and measured data base at higher energies simultaneously, without changing fission barrier parameters (see Chapter IV for details). To reproduce suthreshold data by Auchampaugh et al.[23] we increased outer fission barrier height by ~ 0.2 MeV and excluded $K^{\pi} = 1/2^{-}$ transition state from adopted scheme (see Table 4.1), to suppress fission channel for $p-$ neutrons. Energy dependence of fission width with such barrier parameters ($\langle\Gamma_f^{1/2+}\rangle$=0.15 meV, $\langle\Gamma_f^{1/2-}\rangle$=0.12 meV, $\langle\Gamma_f^{3/2+}\rangle$= 0.12 meV for incident neutron energy 1.3 keV) allows to describe data by Auchampaugh et al.[23]. Intermediate structure in fission cross section was fitted with $s-$neutron fission width $\langle\Gamma_f^{1/2+}\rangle$ value, which fluctuates rather strongly.

3.4.3 Capture cross section energy dependence

Capture cross section of ^{242}Pu was measured by Hockenbery et al. [28] and Wisshak et al.[30, 31] at incident neutron energy range of 6 - 250 keV. These data are consistent within errors (see Fig. 3.10). Calculated capture cross section exhibits low if any sensitivity to subthreshold fission cross section in the unresolved energy region, instead it is determined by neutron strength functions S_o and S_1. Absolute values of average capture width $\langle\Gamma_\gamma\rangle$ and neutron resonance spacing $\langle D_J\rangle$ were fixed by resolved resonance parameter analysis. Description of measured capture cross section data is shown on Fig.3.10, adopted values of $S_o, S_1, \langle\Gamma_\gamma\rangle$ and $\langle D_J\rangle$ maintain acceptable data fit.

3.4.4 Comparison of current and JENDL-3 and ENDF/B-VI evaluated data

Present evaluated fission cross sections is close to those of ENDF/B-VI, JENDL-3 and JEF-2, figure 3.9 gives the comparison of evaluated fission cross sections. Below 2 keV present estimate is rather low as compared with previous evaluations of JENDL-3 and JEF-2. That trend is supported by data by Weigmann et al.[11], which demonstrate a valley between two strong clusters of fission resonances centered at 761.7 eV and 1.837 keV. It is consistent also with average data by Auchampaugh et al.[23], while cluster isolated at 1.378 keV is too weak to maintain fission cross section rise. Next two clusters present in JENDL-3 and JEF-2 evaluation are at 3.5 keV and 4.7 keV. Weigmann et al.[11] had revealed three closely spaced clusters in this energy region at 3.54 keV, 3.68 keV and 4.9 keV. There is some inconsistency of relevant fission resonance area values defined by

Weigmann et al.[11] and Auchampaugh et al.[23]. We represent fission cross section here with one broad cluster. We also added two rather deep valleys around 19.75 keV and 37.5 keV, as they were observed by Auchampaugh et al.[23]. They are consistent with fission areas, measured by Weigmann et al.[11].

Present evaluated capture cross section σ_γ is compatible with that of JENDL-3 at lower energy edge and is ~10% lower at higher boundary of unresolved resonance region. Evaluated capture cross section σ_γ of ENDF/B-VI is consistent with present evaluation above 10 keV and is ~15% lower below 10 keV. Comparison of the evaluated ^{242}Pu capture cross sections is given on Fig 3.10. Evaluated fission and capture cross sections are compared also in Table 3.1.

Table 3.1 Evaluated fission and capture cross sections

Energy, keV	σ_f, b				σ_γ, b			
	present	J-3	JEF-2	B-VI	present	J-3	JEF-2	B-VI
1.3	0.0094	0.027	0.028	0.011	2.86	2.90	3.66	2.30
1.5	0.0072	0.022	0.023	0.011	2.61	2.44	3.29	2.12
1.9	0.0366	0.023	0.029	0.012	2.25	2.25	2.77	1.88
2.25	0.0063	0.010	0.011	0.012	2.04	2.23	2.46	1.73
2.75	0.0051	0.009	0.009	0.013	1.83	1.84	2.14	1.58
3.25	0.0117	0.015	0.016	0.014	1.68	1.81	1.92	1.50
3.75	0.0157	0.015	0.016	0.015	1.57	1.93	1.76	1.44
4.5	0.0141	0.011	0.010	0.017	1.45	1.75	1.58	1.40
5.5	0.0045	0.007	0.007	0.018	1.34	1.48	1.43	1.33
7.5	0.0045	0.004	0.005	0.019	1.18	1.27	1.24	1.22
9.5	0.0057	0.006	0.007	0.020	1.08	1.17	1.14	1.15
13.0	0.0085	0.009	0.009	0.011	0.96	1.05	1.01	0.93
15.0	0.0070	0.010	0.010	0.011	0.91	1.00	0.95	0.88
20.0	0.0055	0.011	0.011	0.011	0.81	0.88	0.84	0.77
27.5	0.0118	0.011	0.012	0.012	0.70	0.76	0.71	0.67
32.5	0.0098	0.012	0.012	0.012	0.65	0.70	0.66	0.62
37.5	0.0082	0.013	0.013	0.012	0.60	0.65	0.62	0.58
40.0	0.0076	0.013	0.013	0.012	0.59	0.62	0.60	0.56
44.7256	0.0132	0.013	0.013	0.012	0.56	0.56	0.56	0.52

3.4.5 Drawbacks of ENDF/B-VI format and associated inconsistencies in evaluated neutron cross sections

Within ENDF/B-VI format number of the degrees of freedom for fission widths distributions must not exceed 4, while structure of transition states

at fission barriers may lead to a greater number for some spin and parity compound states. Intermediate structure of fission resonance widths due to second well cannot be described within the format. This justifies using lower fission width values.

4 Fast neutron cross sections

The measured neutron data in fast energy region, i.e. above ~44 keV are available only for fission and capture cross sections. The detailed fission cross section data are available up to 20 MeV, while capture data only up to 200 keV. The available fission data fit would be used as constraint for (n, n') and (n, γ) reaction cross sections calculation. We reproduce also the average resonance fission width within double-humped fission barrier model. To fix fission channel parameters the systematic trends are used.

4.1 Optical potential

The deformed optical potential for n+^{242}Pu was employed. The starting values for the potential parameters were those for n+^{238}U interaction[32]. The isotopic dependences of real V_R and imaginary W_D parts of the potential were calculated using the optical potential parameter systematics [33]. We modified the original potential geometry parameters[32] to fit total cross section and differential scattering data for N-odd and -even targets above 10 MeV. This procedure of parameter fitting is well tested in case of ^{233}U, ^{239}Pu, ^{235}U, ^{232}Th and ^{238}U targets. Three levels of the ground state rotational band (0^+,2^+,4^+) are coupled. Energy dependence coefficients of real V_R and imaginary W_D well parameters of the potential were slightly changed to fit measured total data by Moore et al.[34]. Deformation parameters of the potential β_2, β_4 were adjusted to predict evaluated S_o value The potential parameters are as follows:

$$V_R = 46.23 - 0.24E, MeV, r_R = 1.26\ fm, a_R = 0.615\ fm$$
$$W_D = \begin{cases} 3.61 + 0.406E, MeV, & E \leq 10 MeV, r_D = 1.24\ fm, a_D = 0.5\ fm \\ 7.63\ MeV, & E > 10\ MeV \end{cases}$$
$$V_{SO} = 6.2\ MeV, r_{SO} = 1.12\ fm, a_{SO} = 0.47\ fm, \beta_2 = 0.194, \beta_4 = 0.071$$

The s-, p-, and d-wave strength functions and potential scattering cross section, calculated with this potential parameters in a coupled channel approach at incident neutron energy of 1.3 keV are:

$$S_o = 0.932 \times 10^{-4} (\mathrm{eV})^{-1/2} \quad , \quad R' = 9.104\ \mathrm{fm}$$

and at 44.7256 keV are:

$S_o = 0.883 \times 10^{-4}(\mathrm{eV})^{-1/2}$ $S_1 = 2.59 \times 10^{-4}(\mathrm{eV})^{-1/2}$ $S_2 = 1.17 \times 10^{-4}(\mathrm{eV})^{-1/2}$

The ^{242}Pu reaction cross sections, calculated with present deformed optical potential, spherical optical potential, which is used above 3 MeV and deformed optical potential by Lagrange [35] which is used below 3 MeV in JENDL-3 evaluation, are compared on Fig. 4.1. Difference above ~12 MeV would be manifested in inelastic scattering cross section and $(n,3n)$ cross section. Evaluated total cross sections appear to be rather similar up to 10 MeV (see Fig.4.2). At higher incident neutron energies evaluated curve of ENDF/B-VI fits measured data by Moore et al.[34] basically due to adding imaginary volume absorption term to coupled channel potential.We can not fit this data with only imaginary surface absorption, while elastic scattering cross sections are compared on Fig. 4.3.

4.2 Fission cross section

4.2.1 Status of the experimental data

Specifically there is only one fission cross section measurement by Behrens et al.[36] covering almost whole energy region of interest. Behrens et al.[36] have measured fission cross section ratio of ^{242}Pu and ^{235}U from 0.1 to 30 MeV. Neutrons were produced with linac, time-of-flight technique (TOF) was employed. Absolute values of fission cross section ratio of ^{242}Pu and ^{235}U were derived using measured with threshold method values of fission cross section ratio of ^{242}Pu and ^{239}Pu and fission cross section ratio of ^{239}Pu and ^{235}U by Carlson and Behrens [37].

Fission cross section ratio of ^{242}Pu and ^{235}U was defined by Fomushkin et al.[43] in the range of incident neutron energy from 0.45 MeV to 3.62 MeV. They have used mica detectors, neutron were produced via T(p,n)^{3}He reaction. The sample weight was defined using $T_{\alpha_{1/2}} = 3.76\times10^5$ years, renormalization of their results to new value of $T_{\alpha_{1/2}} = 3.73\times10^5$ years changes original values only slightly. Data appear to be ~15% lower than data by Behrens et al.[36] and Butler [38] up to ~1.5 MeV, which are compatible with the latter data set.

The ratio of fission cross sections of ^{242}Pu and ^{235}U was measured in the energy range from 0.13 to 7.0 MeV by Kupriyanov et al.[39]. The energy dependence of fission ratios was defined using ionization fission chambers, neutrons were produced via ^{7}Li(p,n)^{7}Be, T(p,n)^{3}He and D(d,n)^{3}He. Absolute values of fission cross section ratio of ^{242}Pu and ^{235}U were derived using measured with threshold method values of fission cross section ratio of ^{242}Pu and ^{239}Pu and fission cross section ratio of ^{239}Pu and ^{235}U by Fursov et al.[40]. There is some discrepancy with data by Behrens et al.[36] around 1 MeV.

Fission cross section ratio of ^{242}Pu and ^{235}U nuclides was measured by Meadows [41] above 396 keV up to 9.9 MeV. Neutrons were produced via ^{7}Li(p,n)^{7}Be, T(p,n)^{3}He and D(d,n)^{3}He reactions. ^{242}Pu sample weight was defined by low geometry $\alpha-$counting. The agreement of this measurement with data by Behrens et al.[36] is within errors.

Iwasaki et al.[42] have measured ^{242}Pu and ^{235}U fission cross sections ratio from 600 keV up to 7 MeV with TOF method. The influence of the background due to α-particle pileup and spontaneous fission is reduced using fast timing back-to-back fission chamber. Monoenergetic neutrons were produced via ^{7}Li(p,n) (0.6-1.4 MeV), T(p,n) (0.9-2.7 MeV) and D(d,n) (3.6-6.9 MeV) reactions. Total ratio errors are from 1.8 to 2.7%. There is a pronounced discrepancy with data by Behrens et al. [36] above 6 MeV, which might be due to energy scale calibration procedures in either experiment with the mono-energetic or white source. Around 1 MeV there is a discrepancy ~4% with data by Behrens et al. [36], while the data by Iwasaki et al.[42] are compatible with data by Kupriyanov et al.[39].

Fission cross section ratio of ^{242}Pu and ^{235}U was measured by Weigmann et al.[11] from 2 eV up to 10 MeV. Neutrons were produced with 150-MeV electron linac. Correction due to spontaneous fission of ^{242}Pu nuclides was determined. Cross section values for ^{242}Pu given for rather broad energy intervals seem to be systematically higher than other data in the first plateau region.

Fission cross section was measured at 14.5 MeV by Fomushkin et al.[43]. When renormalized to recent values of ^{238}U fission cross section, the resulting value appears to be too low as compared with other data.

Meadows [44] measured fission cross section ratio of ^{242}Pu and ^{235}U at an average neutron energy 14.74 MeV. Neutrons were produced via T(d,n)^{4}He reaction. Sample weight was defined by low geometry $\alpha-$counting. The ratio value is well compatible with data by Behrens et al. [36].

Fission cross section around 14.7 MeV was measured by Kovalenko et al. [46], Arlt et al. [47] with time correlated associated particle method (TCAMP). The highest value is predicted by Arlt et al. [47], however covariation analysis of TCAMP data [46] for to ^{235}U, ^{233}U, ^{238}U, ^{237}Np, ^{239}Pu ^{242}Pu target nuclides yields lower value of absolute fission cross section.

In summary, some discrepancy exists between TCAMP and TOF measurements by Kovalenko et al. [46] and Behrens et al. [36], respectively, at 14.7 MeV. Below emissive fission threshold data by Kuprijanov et al.[?] and Meadows [41] are quite compatible. The data by Iwasaki et al. [42] are also compatible with them, while the data by Behrens et al. [36] are somewhat lower than previous data sets.

4.2.2 Statistical model calculation of fission cross section

The most peculiar feature of data base is the irregularity around 1 MeV, i.e. above fission threshold, evident as a step-like structure in data by Kuprijanov et al.[39] and Meadows [41] and resonance-like shape in data by Behrens et al. [36]. We choose to fit data by Kuprijanov et al.[39] above 100 keV. Another feature is a decreasing trend of data above ~2 MeV incident neutron energies. Step-like structure of the same kind is evident in ^{238}Pu and ^{240}Pu neutron-induced fission cross section [48, 49]. Both features could be reproduced within the statistical model calculations. To describe the step-like structure above 1 MeV, we assume it to be due to interplay of level densities of even-odd ^{243}Pu fissioning nuclide and even-even ^{242}Pu residual nuclide. Below 100 keV there is a systematic discrepancy of bomb-shot experiment data by Auchampaugh et al.[23] and Bergen et al.[10]. Calculated curve is compatible with the latter data below 6 keV, if calculated with fission barrier parameters fitted to the cross section shape above 100 keV and up to emissive fission threshold. Data by Auchampaugh et al.[23], which seem to be rather low could be described by increase of inner barrier height $\Delta E_A \sim$ 0.2 MeV. Comparison of calculated fission cross section with measured data is shown in figs. 4.4, 4.5 and 4.6. The statistical theory calculation of fission cross section was accomplished within the double-humped fission barrier model. The approach employed in code STAT is described in more details elsewhere [50, 51]. The procedure of calculating fission transmission coefficients is briefly described below.

4.2.3 Fission transmission coefficient, level density and transition state spectrum

Different behavior of level densities of even-even and even-odd nuclei at low excitation energies should be taken into account. The one-quasiparticle neutron states of even-odd ^{243}Pu fissioning nuclide, lying below the three-quasiparticle states excitation threshold define the shape of ^{242}Pu(n,f) fission cross section below incident neutron energy of ~1.7 MeV. At higher excitation energies three-quasiparticle states are excited. Each one-quasiparticle state is assumed to have a rotational band built on it with a rotational constant, dependent upon the respective saddle deformation. These levels comprise the discrete transition spectra at both saddles. We construct the discrete transition spectra up to 100 keV, using basically one-quasiparticle states of Bolsterli et al. [52] (see Table 4.1). However to describe very low subthreshold fission cross section we assumed lowest barrier with $K^\pi = 3/2^-$ and abandoned rotational band $K^\pi = 1/2^+$, to suppress fission channel of $s-$wave neutrons. At higher excitation energies the continuous level densities are used.

The discrete transition spectra, as well as continuous level contribution to the fission transmission coefficient are dependent upon the order of symmetry for ^{243}Pu fissioning nucleus at inner and outer saddles. Due to the axial asymmetry at the inner saddle [53] we additionally assume $(2J+1)$ rotational levels for each J value. The negative parity bands $K^{\pi} = 1/2^-, 3/2^-, 5/2^-$ ... at outer saddle are assumed to be degenerate with positive parity bands due to mass asymmetry [53]. With transition state spectra thus defined (see Table 4.1) the fission barrier parameters are obtained (see table 4.2). The fission width $\Gamma_f^{1/2+} = 0.359$ meV calculated at incident neutron energy of 1.3 keV is lower than average fission width obtained in unresolved resonance region.

The generalized pairing model provides the means of taking into account the discrete character of few-quasiparticle excitations. It was shown to be important in case of even-even fissioning nucleus ^{236}U in the ^{235}U(n,f) reaction [50]. However that is a general effect, which is evident in neutron-induced fission cross sections of even-even, Z-even, N-odd and odd-odd target nuclei [48, 49]. We will model the discrete few-quasiparticle excitation effects in level density in the following approximate way. The level density of axially symmetric fissioning nucleus is calculated in constant temperature approximation, i.e. $\rho(U) = T_f^{-1}\exp((U - U_o)/T_f)$. The respective parameters, nuclear temperature T_f and excitation energy shift U_o are defined at the matching energy U_c =2.4 MeV. At excitation energies above U_c the continuum part of the transition state spectrum is represented with the phenomenological model [27], which takes into account pairing, shell and collective effects at saddle deformations. The asymptotic value of the main parameter of the level density for fissioning nucleus ^{243}Pu is assumed to be the same, as that of ^{243}Pu compound nuclide at stable deformations. After that the effects of non-axiality and mass asymmetry are included. The detailed procedure of calculating fission transmission coefficient is described elsewhere [50, 51]. The respective parameters: shell correction at saddles δW, pairing correlation function Δ, quadrupole deformation ε,and momentum of inertia at zero temperature $F_0/\hbar^2$ are given in Table 4.3.

The threshold energies for the excitations of few-quasiparticle states are calculated within generalized pairing model [27] using closed-form equations derived by Fu [54]. The procedure is described in more detail elsewhere [55]. In case of even-odd nuclei the nuclear level density $\rho(U)$ up to the three-quasiparticle excitation threshold depends on the excitation energy only weakly, since the intrinsic state density is constant. In this excitation energy region we will model the level density as $\rho(U) \simeq T_f^{-1}(1 + 1.5(U - 0.5U_3))\exp((\Delta_f - U_o)/T_f)$. The one- and three-quasiparticle states level density of even-odd fissioning nucleus ^{243}Pu defines the fission cross section shape at incident neutron energies below ~2.5 MeV (see Fig. 4.5). Above

~2.5 MeV incident neutron energy fission cross section data were fitted (see Fig. 4.5) by slight increase of pairing correlation function Δ. The parameters used for calculation of residual nuclide ^{242}Pu level density for neutron emission competition are described below.

Table 4.1

Transition spectra band-heads of ^{243}Pu

inner saddle		outer saddle	
K^π	E_{K^π}, MeV	K^π	E_{K^π}, MeV
$3/2^+$	0.0	$1/2^+$	0.0
$5/2^+$	0.08	$1/2^-$	0.0
$1/2^-$	0.05	$3/2^+$	0.08
$3/2^-$	0.0	$3/2^-$	0.08
		$5/2^+$	0.0
		$5/2^-$	0.0

Table 4.2

Fission barrier parameters

Nucleus	Barrier	Barrier height, MeV	Curvature, MeV
^{243}Pu	inner	6.05	0.725
^{243}Pu	outer	5.45	0.52
^{242}Pu	inner	5.85	0.9
^{242}Pu	outer	5.05	0.6
^{241}Pu	inner	6.15	0.7
^{241}Pu	outer	5.50	0.5
^{240}Pu	inner	6.05	1.0
^{240}Pu	outer	5.05	0.6

Table 4.3

Level density parameters of ^{243}Pu fissioning nucleus and residual nucleus ^{242}Pu

Parameter	inner saddle	outer saddle	neutron channel
δW, MeV	2.5	0.6	-1.917
Δ, MeV	Δ_0 +0.13	Δ_0 +0.13	Δ_0
ε	0.6	0.8	0.24
$F_0/\hbar^2$, MeV^{-1}	100	200	73

Below incident neutron energy of 1.14 MeV the neutron cross sections are calculated within Hauser-Feshbach approach with a width fluctuation correction taken into account. For width fluctuation correction calculation only Porter-Thomas fluctuations are taken into account. Effective number of degrees of freedom for fission channel is defined at the higher (inner) saddle as $\nu_f^{J\pi} = T_f^{J\pi}/T_{f\,\mathrm{max}}^{J\pi}$, where $T_{f\,\mathrm{max}}^{J\pi}$ is the maximum value of the fission transmission coefficient $T_f^{J\pi}$. Above incident neutron energy of 1.14 MeV the Tepel et al. [56] approach is employed.

4.2.4 Fission cross section above emissive fission threshold

The first chance fission cross section of ^{242}Pu(n,f) reaction above the emissive fission threshold is fixed with the level density and fission barrier parameters systematics [57] (see Tables 4.2, 4.3) and secondary neutron spectra parameterization (see Fig. 4.7). A consistent description of a complete set of measured data on (n,f), (n,2n) and (n,3n) for ^{238}U and ^{235}U targets was accomplished with the secondary neutron spectra parameterization [57], which is used here.

Fission barrier parameters of ^{242}Pu are fixed by ^{241}Pu(n,f) neutron-induced fission data description. Figure 4.8 shows ^{241}Pu(n,f) reaction measured data description. We modelled the fissioning even-even nuclide ^{242}Pu nuclear level density $\rho(U)$ above the pairing gap up to the four-quasiparticle excitation threshold as $\rho(U) = \rho(\hat{U})/(1 + \exp(U_2 - U + \delta_1)/\delta_2)$. The two-quasiparticle states level density of even-even fissioning nucleus ^{242}Pu defines the fission cross section shape at incident neutron energies $\sim 0.5 \div 2$MeV (see Fig. 4.8), the parameters $\hat{U} = 1.7$ MeV, $\delta_1 = \delta_2 = 0.2$ MeV are fixed U and Pu fission data analysis.

Fission barrier parameters of ^{241}Pu are fixed by ^{240}Pu(n,f) neutron-induced fission data description. Figure 4.9 shows the ^{240}Pu(n,f) reaction measured data description [49]. Step-like irregularity evident above $\sim$1 MeV incident neutron energy is of the same nature as that in ^{238}Pu(n,f) [48] and ^{242}Pu(n,f) reactions data.

Calculated fission cross section is rather different from previous evaluated curves from 8 MeV up to 13 MeV (see Fig. 4.10). Calculated fission cross section at $\sim$15 MeV neutron energy appears to be consistent with absolute fission cross section data by Kovalenko et al.[46], which are higher than those by Behrens et al.[36] and Meadows [44]. Some discrepancy of the calculated cross section with data by Behrens et al. [36] from 10 MeV up to 12 MeV could be avoided, however it seems unjustified viewing discrepancy of measured data at higher energies.

4.3 Inelastic scattering cross section

The inelastic scattering cross section is calculated with the statistical codes STAT and STAPRE [58]. The discrete level excitation (compound and direct), continuum excitation and pre-equilibrium emission contribute to the inelastic scattering cross section.

4.3.1 Levels of ^{242}Pu

The low-lying levels of scheme of Nuclear Data Sheets [59] appears incomplete at excitation energy above 1.14 MeV (see Fig. 4.11). In JENDL-3 evaluation there are 29 discrete excited levels up to 1.636 MeV, i.e. the missing of levels above ~1.14 MeV is ignored.

4.3.2 ^{242}Pu level density

The continuum level density below excitation energy U_c = 3.6 MeV is calculated with the constant temperature model

$$\rho(U) = T^{-1}\exp((U - U_o)/T),$$

here, energy shift U_0 = -0.01557 MeV, nuclear temperature T = 0.37201 MeV are the constant temperature model parameters. The cumulative number of observed levels is compared with constant temperature approximation on Fig.4.11. At higher excitation energies the phenomenological model [27] is used. The main model parameter a for ^{242}Pu residual nucleus is obtained by fitting neutron resonance spacing of ^{241}Pu nuclide [60].

The generalized pairing model provides the means of taking into account the discrete character of few-quasiparticle excitations just above the pairing gap. It was shown to be important in case of even-even residual nucleus ^{238}Pu in the ^{239}Pu(n,2n) reaction [55]. We modelled the nuclear level density $\rho(U)$ above the pairing gap U_2 up to the four-quasiparticle excitation threshold U_4 as $\rho(U) = \rho(U_4 - 0.3)/(1+\exp(U_2 - U + \delta_1)/\delta_2)$. The two-quasiparticle states level density of even-even residual nuclide ^{242}Pu influences the fission cross section shape at incident neutron energies above ~1.6 MeV, the parameters, $\delta_1 = \delta_2 = 0.4$ MeV values were extracted. Below pairing gap the collective levels of Nuclear Data Sheets [59] were employed.

4.3.3 ^{243}Pu level density

The level density of even-odd compound nuclide ^{243}Pu one needs to calculate radiative capture width and (n,γn') reaction contribution to the compound inelastic scattering cross section. The continuum level density below excitation energy U_c = 2.4 MeV is calculated with the constant temperature

model, the constant temperature model parameters are: energy shift U_0 = -0.60585 MeV, nuclear temperature T = 0.35146 MeV. The cumulative number of observed levels is compared with constant temperature approximation on Fig. 4.12. At higher excitation energies the phenomenological model [27] is used. The main model parameter $\tilde{a}$ for ^{243}Pu residual nucleus is obtained by fitting the evaluated neutron resonance spacing of ^{242}Pu target nuclide $\langle D_{obs} \rangle$ = 12.903 eV.

4.3.4 Compound inelastic scattering

The residual nucleus ^{242}Pu level density modelling, adopted in present work changes the inelastic scattering cross section below 5 MeV as compared with ENDF/B-VI, JEF-2 and JENDL-3.2 evaluations. The most close to our estimate is that of JEF-2 evaluation (see figs. 4.13 - 4.27). However the discrepacies still remain in the range below 1 MeV and above 10 MeV. Above ~10 MeV incident neutron energy the discrepancy is due to different estimates of direct excitation of the ground state band levels. Above 1 MeV incident neutron energy inelastic scattering to the continuum gives a major contribution to the total inelastic scattering cross section (see Fig. 4.14). Above 5 MeV incident neutron energy pre-equilibrium emission and direct inelastic scattering are the two reaction mechanisms which define inelastic scattering cross section (see Fig. 4.13). The pre-equilibrium model parameters were tested by the statistical model description of ^{238}U+n interaction secondary neutron spectra and consistent description of fission and (n,xn) reaction data for major actinides [57].

4.3.5 Direct inelastic scattering

The direct inelastic scattering changes the shape of ground state band levels excitation cross sections above 1 MeV incident neutron energy (see figs. 4.15 - 4.16). This mechanism defines partly the hard-energy tail in total inelastic scattering cross section (see Fig. 4.13).

4.4 Radiative capture cross section

The radiative capture cross section is calculated within a statistical approach up to 5 MeV. Radiative capture strength function equals $S_{\gamma 0}$ = 17.608. At higher incident neutron energies we assume radiative capture cross section to be 1 mbarn. The radiative capture width was calculated with (n,γf) and (n,γn$'$) reactions competition against "true" capture reaction (n,$\gamma\gamma$). Due to high fission threshold for ^{243}Pu compound nuclide the competition of (n,γn$'$) reaction is stronger than that of (n,γf) reaction. The influence of (n,γn$'$) and (n,γf) reaction competition on radiative capture cross section is illustrated on Fig.4.18 by sharp decrease of capture cross section above 1 MeV incident

neutron energy, as compared with (n,γx) reaction cross section. Present capture cross section shape and that of JENDL-3.2 are rather similar.

Table 4.4

Level scheme of ^{242}Pu

$E^J_{K^\pi}$, MeV	J	π	K	band
0.0	0	+	0	A
0.04454	2	+	0	A
0.1473	4	+	0	A
0.3064	6	+	0	A
0.5181	8	+	0	A
0.7787	10	+	0	A
0.78046	1	-	0	B
0.8323	3	-	0	B
0.9270	5	-	0	B
0.956	0	+	0	C
0.9925	2	+	0	C
1.0194	3	-	3	D
1.0392	1	+	1	
1.064	4	-	3	D
1.084	12	+	0	A
1.0921	6	+	1	
1.102	2	+	2	E
1.122	5	-	0	D
1.1501	2	-		
1.1546	3	-		
1.1816	2	+	2	

4.5 Cross sections of (n,2n) and (n,3n) reactions

The current and JENDL-3 evaluated (n,2n) and (n,3n) cross sections are drastically different. The magnitude of (n,2n) cross section below the (n,2nf) reaction threshold is defined by (n,nf), (n,nγ) and (n,2n) reaction competition. The present and JENDL-3 evaluated fission cross sections are rather different, as well as reaction cross sections above 10 MeV incident neutron energy (see Fig. 4.1). To calculate the (n,2n) reaction cross section we use an approach, developed for description of the ^{238}U(n,2n) reaction cross section [57]. The present and previous evaluations are compared in Fig. 4.19. There is no hard-energy tail in (n,2n) reaction cross sections of previous

evaluations. In case of (n,3n) reaction the difference in reaction cross section above 11 MeV (see Fig. 4.1) contributes essentially to the discrepancy, shown on Fig. 4.20.

5 Energy distributions of secondary neutrons

There is no measured data on secondary neutron spectra. To calculate neutron energy distributions of (n,xnγ) and (n,xnf), x=1, 2, 3 reactions we use a simple Weisscopf-Ewing evaporation model [61] taking into account fission and gamma emission competition to neutron emission. The pre-equilibrium emission of first neutron is included.

5.1 Model calculations of (n,nx) reaction spectra

The first neutron spectra for the (n,nx) reaction is the sum of evaporated and pre-equilibrium emitted neutron contributions. The pre-equilibrium emission contribution is calculated with a parameter systematics tested in case of n+^{238}U and n+^{235}U interactions [57]. We have calculated the 1st, 2nd and 3d neutron spectra for the (n,nγ), (n,2n) and (n,3n), where applicable. According to the ENDF/B-VI format we included the secondary neutron spectra in the following way. The calculated spectra were summed up and tabular spectra for the (n,nγ), (n,2n) and (n,3n) reactions were obtained. To clarify the competition of neutron, γ-emission and fission in case of (n,nx) and (n,2nx) reactions we have chosen the following presentation of spectra. Figure 5.1 shows the spectrum of 1st neutron of the reaction (n,nx) and its partial contributions for (n,nγ), (n,2n), (n,nf) (n,2nf) and (n,3n) reactions. Figure 5.2 shows the spectrum of 2nd neutron of the reaction (n,2nx) and its partial contributions for (n,2n), (n,3n) and (n,2nf) reactions. The spectra of 1st and 2nd neutrons are normalized to unity. The partial neutron spectra shown on figs. 5.1, 5.2 are normalized to the contributions of appropriate cross sections to the (n,nx) and (n,2nx) reaction cross sections, respectively.

The inclusion of pre-equilibrium emission changes significantly the average energies of emitted neutron spectra. That is shown in Table 5.1, where the average secondary neutron energies for current, ENDFB-VI and JENDL-3 evaluations are compared. The most significant is the change of neutron spectra of (n,nγ) reaction. Figures 5.3-5.7 demonstrate the discrepancies of secondary neutron spectra in current, ENDF/B and JENDL-3 evaluations. One can see that current and JENDL-3 evaluated spectra are in good agrement as JENDL-3 evaluation of (n,n'), (n,2n) and (n,3n) spectra uses code Pegasus[62], that takes into account pre-equilibrium emission, evaluated spectra of ENDF/B-VI are much softer.

Table 5.1 Average energies of secondary neutron spectra

E_n , MeV	average neutron energy, MeV									
	(n, n')			(n, 2n)			(n, n'f)	(n, 3n)		(n, 2n'f)
	pres.	B-VI	J - 3	pres.	B-VI	J - 3	pres.	pres.	J - 3	pres.
2.0	0.39	0.66	0.33							
8.0	3.22	1.12	2.44	0.54	0.68	0.60	1.04			
14.0	9.53	1.48	9.37	2.20	1.14	1.84	2.75	0.66	0.68	0.64
20.0	15.5	1.76	15.3	5.35	1.50	5.59	4.53	1.69	1.13	1.97

First neutron spectra of (n, n'f) reaction also becomes harder, that influences prompt fission neutron spectra. On the other hand, the spectra of 2nd and 3d neutrons become softer.

5.2 Prompt fission neutron spectra

Prompt fission neutron spectra were calculated with the account of pre-fission neutron emission above emissive fission threshold.

5.2.1 Prompt fission neutron spectra evaluation

Prompt fission neutron spectra are calculated involving Watt formula with the parameters given in Table 5.2. Approach employed by Watt assumes neutron evaporation from fully accelerated fission fragments.

Above emissive fission threshold the fission neutron spectra $N(E, E_n)$ is the superposition of emissive fission spectra, i.e.

$$N(E,E_n) = \left(\frac{\sigma_{nf}}{\sigma_{nF}}\nu_1(E_n)N_1(E,E_n) + \frac{\sigma_{nn'f}}{\sigma_{nF}}\left[\Phi_{nn'f}(E,E_n) + \nu_2(E_n)N_2(E,E_n)\right]\right.$$
$$\left. + \frac{\sigma_{n2nf}}{\sigma_{nF}}\left[\Phi^1_{n2nf}(E,E_n) + \Phi^2_{n2nf}(E,E_n) + \nu_3(E_n)N_3(E,E_n)\right]\right) /$$
$$\left[\frac{\sigma_{nf}}{\sigma_{nF}}\nu_1(E_n) + \frac{\sigma_{nn'f}}{\sigma_{nF}}(1+\nu_2(E_n)) + \frac{\sigma_{n2nf}}{\sigma_{nF}}(2+\nu_3(E_n))\right],$$

where σ_{nF}, σ_{nf}, $\sigma_{nn'f}$, σ_{n2nf} are the total and i-the chance fission cross sections (i = 1,2,3); $\Phi_{nn'f}$, Φ^1_{n2nf}, and Φ^2_{n2nf} are emitted neutron spectra: for (n,nf) reaction, 1st and 2nd neutrons of (n,2nf) reaction, respectively; ν_i and N_i are multiplicity and prompt neutron spectra for the i-th fissioning nucleus. Prompt neutron multiplicities ν_i are described in Chapter 6. Average neutron energy dependences of prompt neutron spectra for the i-th fissioning nucleus $N_i(E, E_n)$ were calculated using assumption by Terrell [63] $\overline{E_i} = a + b\sqrt{1+\nu_i(E_n)}$(for parameters see Table 5.2). The pre-equilibrium

emission of the first neutron is included, the $\Phi^{i}_{n,xnf}$ spectra for the emissive fission are calculated with Weisscopf-Ewing evaporation model [61].

Table 5.2

Parameters a and b of Terrel systematic and Watt spectrum E_{fi}.

Fissioning nucleus	E_{fi}, MeV	a, MeV	b, MeV
^{243}Pu	0.749	0.75	0.645
^{242}Pu	0.749	0.75	0.645
^{241}Pu	0.749	0.75	0.645

Table 5.3
Comparison of average fission spectra energies for different evaluations.

E_n,	Present	JENDL-3	ENDF/B-VI
MeV	Average fission spectrum energy, MeV		
Thermal	2.014	2.0096	2.0055
2.0	2.059	2.096	2.0565
5.0	2.126	2.0096	2.1300
10.0	2.121	2.0096	2.2440
15.0	2.259	2.0096	2.3490
20.0	2.454	2.0096	2.4495

For ^{242}Pu fissioning nucleus average neutron energy $\overline{E} = 2.017$ calculated with the parameters from Table 5.2 within Terrell approximation [63], could be compared with $\overline{E} = 2.003 \pm 0.051$ measured by Smith [64] (for ν_i^{th} see next Chapter). Figure 5.8 shows the comparison of calculated prompt fission neutron spectra involving maxwellian and Watt spectrum with the same average neutron energies. Maxwellian spectrum overestimates number of emitted neutrons below 1MeV and above 6 MeV energy of emitted neutron. Average energies of fission spectrum for thermal neutron predicted with the adopted parameters are 2.014 MeV for ^{243}Pu, 2.027 MeV for ^{242}Pu and 2.017 MeV for ^{241}Pu fissioning nuclei. It is compatible with evaluated value 2.022 MeV of JENDL-3 for ^{243}Pu, however the spectra shapes are significantly different. Figure 5.9 demonstrates the differences between our spectra taking into account pre-fission neutrons and those calculated using Watt formula with the same average energy of emitted neutron. Large differences can be found above 3 MeV emission energies. Figures 5.10-5.12 show the partial contributions of i-th chance fission to the total fission neutron spectrum at

incident neutron energies of 6, 14 and 20 MeV. Figure 5.13 demonstrates difference of our and ENDF/B and JENDL-3 evaluated spectra. Table 5.3 gives comparison of average neutron energies for our JENDL-3 and ENDFB-VI evaluations.

Our estimate of average fission spectrum energy almost coincides with ENDF/B-VI and is much higher than that of JENDL-3 at high neutron incident energies. Both JENDL-3 and ENDF/B-VI evaluation use simple maxwellian approximation for fission spectra, without taking into account emission of pre-fission neutrons. Differences which may arise because of this simplification are shown on Figs. 5.9 and 5.13.

6 Number of neutrons per fission

There are no experimental data on number of prompt fission neutrons ν_p for ^{242}Pu. Thermal value suggested by Malinovski et al.[65] for ^{242}Pu neutron-induced fission ν_p^{th} =2.87 is higher than ν_p^{th} =2.74, predicted by Howerton [66] systematics. Similar discrepancy occurs for ^{240}Pu target nuclide. Malinovski et al.[65] recommend ν_p^{th} =2.92, while estimate by Howerton systematics [66] is ν_p^{th} =2.72. Estimate obtained by Manero et al.[67] based on experimental data is ν_p^{th} =2.86. We assume that ν_p^{th} for even plutonium targets is overestimated by Malinovski et al.[65] due to linear extrapolation of ν_p from 1-15 MeV energy region down to thermal energy. Energy dependence of ν_p above emissive fission threshold might be essentially non-linear due to decrease of excitation energy by pre-equilibrium emission of pre-fission neutrons. We adopted ν_p^{th} =2.84 for ^{242}Pu, following the tendencies noticed for ^{240}Pu target nuclide. Number of prompt fission neutrons ν_p^{th} =2.92 for ^{241}Pu target nuclide, based on experimental data [65], while ν_p^{th} =2.86 for ^{240}Pu, as evaluated by Manero et al.[67]. The systematics by Howerton[66] used in JENDL-3 and ENDF/B-6 gives too sharp increase of $\nu_p(E)$ with energy. Present evaluation of $\nu_p(E)$ is based on assumption that energy dependence of number of neutrons for first chance fission of ^{243}Pu, ^{242}Pu, ^{241}Pu fissioning nuclides has a linear dependence on excitation energy, with the slopes of $d\nu_p/dE$ =0.142, 0.140, 0.145 MeV^{-1}, respectively. The excitation energies of emerging nuclei took into account binding and average energies of pre-fission neutrons. The comparison of $\nu_p(E)$, calculated with fixed parameters, with JENDL-3 and ENDF/B-VI evaluations is shown in Fig. 6.1. The adopted slope of $d\nu_p/dE$ = 0.142 is considerably lower than that of systematics by Howerton [66], adopted in JENDL-3 and ENDF/B-VI. However, it is consistent with $d\nu_p/dE$ for neighboring nuclei. Our calculations predict non-linear shape of $\nu_p(E)$ above emissive fission threshold. The influence of pre-equilibrium pre-fission neutrons manifests in additional appreciable decrease of $d\nu_p/dE$ above 12 MeV.

The delayed number of neutrons per fission ν_d for ^{242}Pu was measured by Krick et al.[68]: $\nu_d = 0.016 \pm 0.005$ for low neutron incident energies. Within errors it is consistent with systematics by Tuttle et al.[69] predicting $\nu_d = 0.0208$ for incident neutron energies up to 6 MeV and $\nu_d = 0.0142$ for $E_n \geq$ 8MeV. Value of ν_d estimated by Tuttle et al.[69] for $E_n \geq$ 8MeV virtually coincides with measured value $\nu_d = 0.015$ for ^{241}Pu [70] for low energies. In systematics by Tuttle et. al. [69] ν_d for ^{242}Pu for $E_n \geq 8$ MeV, since this nuclide emerges after pre-fission neutron emission in (n,nf) reaction. That explains why values, derived using systematics by Tuttle[69] are adopted in our evaluation. Values of ν_d between 6 and 8 MeV are obtained by linear interpolation. The decay constants for six groups of delayed neutrons are taken from Brady et al.[71]

7 Angular distributions of secondary neutrons

The angular distributions of elastically scattered neutrons and those for neutrons, scattered on four levels of ground state band are calculated with the coupled channel method. The isotropic compound scattering contribution is taken into account by renormalizing l-th Legendre polynomial coefficients A_l^{cc}, calculated with coupled channels:

$$A_l = A_l^{cc}\sigma_{dir}/(\sigma_{dir}+\sigma_{comp}),$$

where σ_{dir} and σ_{comp} are the scattering cross section direct and compound contributions, respectively. For the other contributing reactions angular distributions of secondary neutrons are assumed isotropic.

8 Conclusions

The evaluated neutron data file for ^{242}Pu is compiled in ENDF/B-VI format and sent to the International Science and Technology Center (Moscow), Japan Nuclear Data Center at Japan Atomic Energy Research Institute and Nuclear Data Section of International Atomic Energy Institute.

The scarcity of experimental data coupled with possibility of some new data becoming available may urge some revision of data file. Present version of ^{242}Pu data file may be revised before March of 1998, the expiration date of Project CIS-03-95.

References

[1]Nakagawa T., Kikuchi Y., Proc. of the Int. Conf. on Nuclear Data and Technology, Gatlinburg, Tenn., USA, 9-13 May, 1994, Dickens J.K. (Editor), 709, ANS Inc., 1994.

[2]Japanese Evaluated Data Library, Version 3, JAERI 1319, 1990.

[3]Dunford C.L. Nuclear Data for Science and Technology, Proc. Int. Conf. Julich, 1991,788.Springer-Verlag,1992, Berlin.

[4]Nordborg C., Salvatores M. Nuclear Data for Science and Technology, Proc. of the Int. Conf., Gatlinburg, Tennessee, USA, May 9-13, 1994, v.2, p. 680.

[5]Mughabghab S.F., Garber D.I., BNL-325, 3d edition, vol. 1, 1973.

[6]Young T.E., Reeder S.D. Nucl. Sci. Eng. 40, 389 (1970).

[7]Young T.E., Simpson F.B., Tate R.E. Nucl. Sci. Engng. 43, 341 (1971).

[8]Poortmans F., Vanpraet G.J. Nucl. Phys., A207, 342 (1973).

[9]Auchampaugh G.F., Bowman C.D. Phys. Rev. C47, 2085 (1973).

[10]Bergen D.W., Fullwood R.R. Nucl. Phys., A163, 577 (1971).

[11]Weigmann H., Wartena J.A., Burkholz C. Nucl. Phys. A438, 333 (1985).

[12]Mughabghab S.F. Neutron Cross Sections, vol. 1. Part B. Academic Press, 1984.

[13]Auchampaugh G.F., Bowman C.D., Coops M.S., Fultz S.C. Phys. Rev. 146, 840 (1966).

[14]Studier M.H., Maedler D., Wapstra A.M. Phys. Rev. 93, 1433 (1954).

[15]Butler J.P., Lounsbury M., Merritt J.S. Can. J. Phys. 35, 147 (1957).

[16]Durham R.W., Molson F. Can. J. Phys. 48, 716 (1970).

[17]Halperin J., Oliver J.H. ORNL-3679, 1964, 13.

[18]Folger R.L., Smith J.A., Brown L.C. et al. Proc. Conf. on Neutron Cross Sections and Technology, Washington, vol. 2, 1968, 1279.

[19]Lander G.H., Mudler M.H. Acta Crystallografica 107, 1294 (1957).

[20]Cote R.E., Bollinger L.M., Burnes R.F., Diamond H. Phys. Rev. 114, 505 (1959).

[21]Pattenden N. EANDC-50 S, 1965.

[22]James J.D. Nucl. Phys., A123, 24 (1969).

[23]Auchampaugh G.F., Farrell J.A., Bergen D.W. Nucl. Phys. A171, 31 (1971).

[24]Simpson O.B, Simpson O.D., Miller H.G. et al. USNDC-3, 1972, 2.

[25]Dunford C.L.: "ENDF Utility Codes Release 6.9", IAEA-NDS-29 (1993).

[26]Porodzinskij Yu.V., Sukhovitskij E.Sh., Nuclear Constants, 4, p.27, 1987 (in Russian).

[27]Ignatjuk A.V., Istekov K.K., Smirenkin G.N. Sov. J. Nucl. Phys. 29, 450 (1979).

[28]Hockenbury R.W., Sanislo A.J., Kaushal N.N. Proc. Conf. on Neutron Cross Sections and Technology, Washington, vol. 2, 1972, 584.

[29]Wagemans C. and Deruytter A.J., Ann. Nucl. Energy 3, 437 (1976).

[30]Wisshak K., Kappeler F. Nucl. Sci. Eng. 66, 363 (1978).

[31]Wisshak K., Kappeler F. Nucl. Sci. Eng. 69, 39 (1979).

[32]Haouat, Lachkar J., Lagrange Ch., et al., Nucl.Sci. Engng. 81, 491 (1982).

[33]Klepatskij A.B., Sukhovitskij E.Sh., private communication.

[34]Moore M.S. et al. Proc. Int. Conf. Nuclear Data for Science and Technology, Knoxville, Tennessee, 22-26 October, 1979, USA, p.703, 1980.

[35]Lagrange C.L. and Jary CJ. NEANDC(E) 198 "L" (1978)

[36]Behrens J.W., Newbury R.S., Magana J.W. Nucl. Sci. Eng. 66, 433 (1978).

[37]Carlson G.W., Behrens J.W. Nucl. Sci. Eng. 66, 205 (1978).

[38]Butler D.K. Phys. Rev., 117, 1305 (1960).

[39]Kupriyanov V.M., Fursov B.I., Maslennikov B.K. et al. Sov J. At. Energy, 46, 35 (1979).

[40]Fursov B.I. et al. Sov J. At. Energy, 43, 894 (1977).

[41]Meadows J.W. Nucl. Sci. Eng. 68, 360 (1978).

[42]Iwasaki T., Wanabe F., Baba M. et al. J. Nucl. Sci. Tech. 27, 885 (1990).

[43]Fomushkin E.F., Gutnikova E.K. Sov. J. Nucl. Phys. 10, 529 (1970).

[44]Meadows J.W. Ann. Nucl. Energy, 15, 421 (1988).

[45]Fomushkin E.F., Gutnikova E.K., Zamyatnin Yu.S. et al. Sov. J. Nucl. Phys. 5, 966 (1967).

[46]Kovalenko S.S. et al. Isotopenpraxis 21, 344 (1985).

[47]Arlt R. et al. Sov J. At. Energy, 55, 656 (1984).

[48]Maslov V.M. et al. INDC(BLR)-009, 1997.

[49]Maslov V.M. Int. Conf. Nuclear Data for Science and Technology, Trieste, Italy, May 19-24, 1997, to be published.

[50]Ignatjuk A.V., Maslov V.M., Proc. Int. Symp. Nuclear Data Evaluation Methodology, Brookhaven,USA, October 12-16, 1992, p.440, World Scientific, 1993.

[51]Maslov V.M., Kikuchi Y. JAERI-Research 96-030, June, 1996.

[52]Bolsterli M., Fiset E.O., Nix J.R., Norton J.L. Phys.Rev., C 5, 1050 (1972).

[53]Howard W.M., Moller P. Atomic Data and Nuclear Data Tables,25, 219 (1980).

[54]Fu C. Nucl. Sci. Engng. 86, 344 (1984).

[55]Maslov V.M. Zeit. Phys. A, Hadrons & Nuclei, 347, 211 (1994).

[56]Tepel J.W., Hoffman H.M., Weidenmuller H.A. Phys. Lett. 49, 1 (1974).

[57]Ignatjuk A.V., Maslov V.M., Pashchenko A.B. Sov. J. Nucl. Phys. 47, 224 (1988).

[58]Uhl M. and Strohmaier B., Report IRK - 76/10 (Vienna,1976).

[59]ENSDF, 1995.

[60]Porodzinskij Yu.V., Sukhovitskij E.Sh. and Maslov V.M. Int. Conf. Nuclear Data for Science and Technology, Trieste, Italy, May 19-24, 1997, to be published.

[61]Maslov V.M., Porodzinskij Yu.V.,Sukhovitskij E.Sh., Proc. Int. Conf. on Neutron Physics, 14-18 Sept., Kiev, USSR, V.1, p.413, 1988.

[62]Iijima S., et. al., Report JAERI-M, 87-025, 337 (1987).

[63]Terrell J., Proc. of Symp.on Phys. and Chem. of Fission, Salzburg, vol.2, p.3 (1965)

[64]Smith A.B.,Phys. Rev. 23, 2140 (1961).

[65]Malinovski V.V., Tarasko M.Z., Kuzminov B.D., Sov. Journal of Atomic Energy, 58, 430 (1985).

[66]Howerton R.J., Nucl. Sci. Engng. 62, 438 (1977).

[67]Manero F, Konshin V.A., Atomic Energy Review, 10 (1972).

[68]Krick M.S., Evans A.E., Nucl.Sci.Eng. 47, 311 (1972).

[69]Tuttle R.J. Proc. Consultants Meeting on Delayed Neutron Properties. 1979, Vienna, INDC(NDS)-107/G, p.29

[70]Cox S.A., Dowing Whiting E.E., Report ANL-7610(1970) 45.

[71]Brady M.C., Wright R.Q., England T.R., Report ORNL/CSD/TM-226(1991), IAEA-NDS-102, 1992

9 Figure captions

Fig. 2.1 Total cross section of ^{242}Pu in the energy region below 2 eV.
Fig. 2.2 Total cross section of ^{242}Pu in the energy region 2.5-2.84 eV.
Fig. 2.3 Fission cross section of ^{242}Pu in the energy region 465 - 496 eV.
Fig. 2.4 Fission cross section of ^{242}Pu in the energy region 758- 795 eV.
Fig. 3.1 Cumulative sum of neutron resonance levels of ^{242}Pu
Fig. 3.2 Cumulative sum of reduced neutron widths of ^{242}Pu
Fig. 3.3 Distribution of reduced neutron widths for ^{242}Pu.
Fig. 3.4 Neutron resonance spacing distribution for ^{242}Pu.
Fig. 3.5 Distribution of reduced neutron widths for ^{242}Pu.
Fig. 3.6 Neutron resonance spacing distribution for ^{242}Pu.
Fig. 3.7 Distribution of reduced neutron widths for ^{242}Pu.
Fig. 3.8 Total cross section of ^{242}Pu in unresolved resonance region.
Fig. 3.9 Fission cross section of ^{242}Pu in unresolved resonance region.
Fig. 3.10 Radiative capture cross section of ^{242}Pu in unresolved resonance region.
Fig. 4.1 Compound reaction cross section of ^{242}Pu.
Fig. 4.2 Total cross section of ^{242}Pu.
Fig. 4.3 Elastic scattering cross section of ^{242}Pu.
Fig. 4.4 Fission cross section of ^{242}Pu.
Fig. 4.5 Fission cross section of ^{242}Pu.
Fig. 4.6 Fission cross section of ^{242}Pu.
Fig. 4.7 Fission cross section of ^{242}Pu.
Fig. 4.8 Fission cross section of ^{241}Pu.
Fig. 4.9 Fission cross section of ^{240}Pu.
Fig. 4.10 Fission cross section of ^{242}Pu.
Fig. 4.11 Cumulative number of levels of ^{242}Pu.
Fig. 4.12 Cumulative number of levels of ^{243}Pu.
Fig. 4.13 Inelastic scattering cross section of ^{242}Pu.
Fig. 4.14 Continuum inelastic scattering cross section of ^{242}Pu.
Fig. 4.15 Cross section of ^{242}Pu: 0.04454 MeV, 2^+ level excitation.
Fig. 4.16 Cross section of ^{242}Pu: 0.1473 MeV, 4^+ level excitation.
Fig. 4.17 Cross section of ^{242}Pu: 0.3064 MeV, 6^+ level excitation.
Fig. 4.18 Radiative capture cross section of ^{242}Pu.
Fig. 4.19 ^{242}Pu(n,2n) reaction cross section.
Fig. 4.20 ^{242}Pu(n,3n) reaction cross section.
Fig. 5.1 Components of first neutron spectrum of ^{242}Pu for incident neutron energy 14 MeV.
Fig. 5.2 Components of second neutron spectrum of ^{242}Pu for incident neu-

tron energy 14 MeV.
Fig. 5.3 Comparison of (n,n'γ) reaction neutron spectra of ^{242}Pu for incident neutron energy 8 MeV.
Fig. 5.4 Comparison of (n,2n) reaction neutron spectra of ^{242}Pu for incident neutron energy 8 MeV.
Fig. 5.5 Comparison of (n,n'γ) reaction neutron spectra of ^{242}Pu for incident neutron energy 14 MeV.
Fig. 5.6 Comparison of (n,2n) reaction neutron spectra of ^{242}Pu for incident neutron energy 14 MeV.
Fig. 5.7 Comparison of (n,3n) reaction neutron spectra of ^{242}Pu for incident neutron energy 14 MeV.
Fig. 5.8 Prompt fission neutron spectrum of ^{242}Pu.
Fig. 5.9 Calculated fission neutron spectra of ^{242}Pu ratio to Watt spectrum.
Fig. 5.10 Fission neutron spectra of ^{242}Pu for incident neutron energies 6 MeV.
Fig. 5.11 Fission neutron spectra of ^{242}Pu for incident neutron energy 14 MeV.
Fig. 5.12 Fission neutron spectra of ^{242}Pu for incident neutron energy 20 MeV.
Fig. 5.13 Prompt fission neutron spectra of ^{242}Pu for incident neutron energy 15 MeV.
Fig. 6.1 Prompt fission neutron multiplicity for ^{242}Pu..

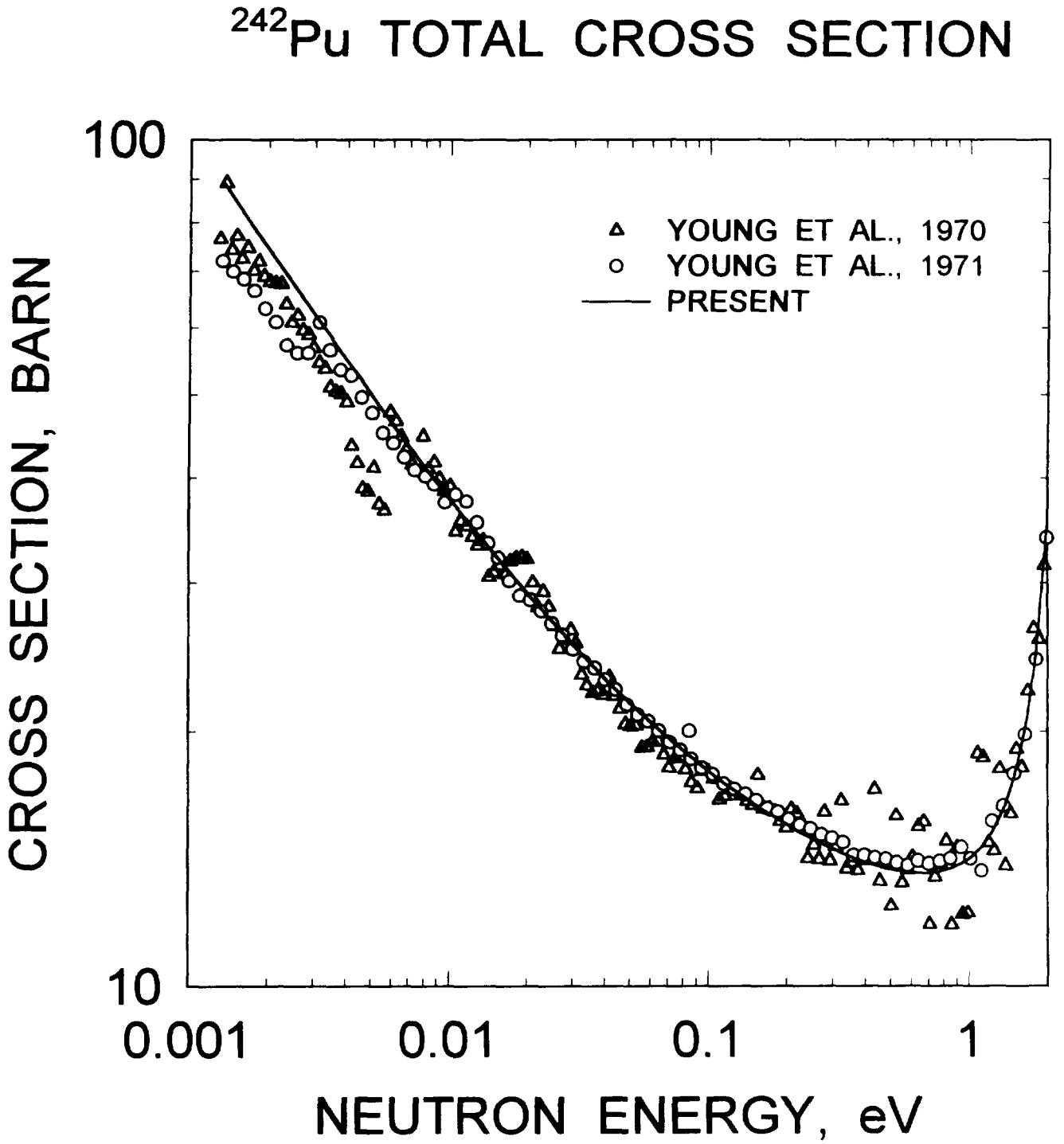
^{242}Pu TOTAL CROSS SECTION
100
10
CROSS SECTION, BARN
0.001
0.01
0.1
1
NEUTRON ENERGY, eV
YOUNG ET AL., 1970
YOUNG ET AL., 1971
PRESENT

FIG. 2.1

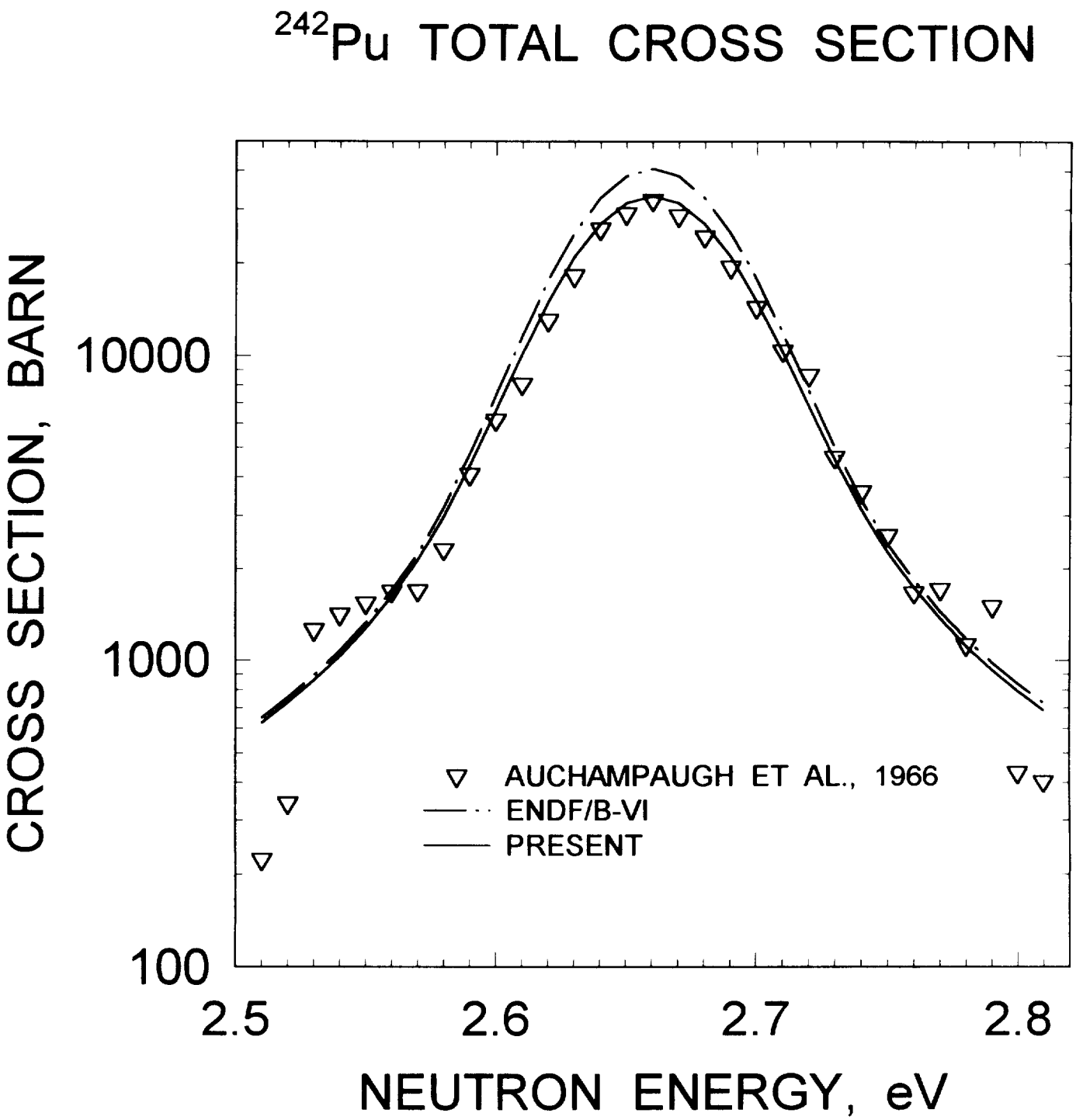
^{242}Pu TOTAL CROSS SECTION
CROSS SECTION, BARN
10000
1000
100
2.5
2.6
2.7
2.8
NEUTRON ENERGY, eV
AUCHAMPAUGH ET AL., 1966
ENDF/B-VI
PRESENT

FIG. 2.2

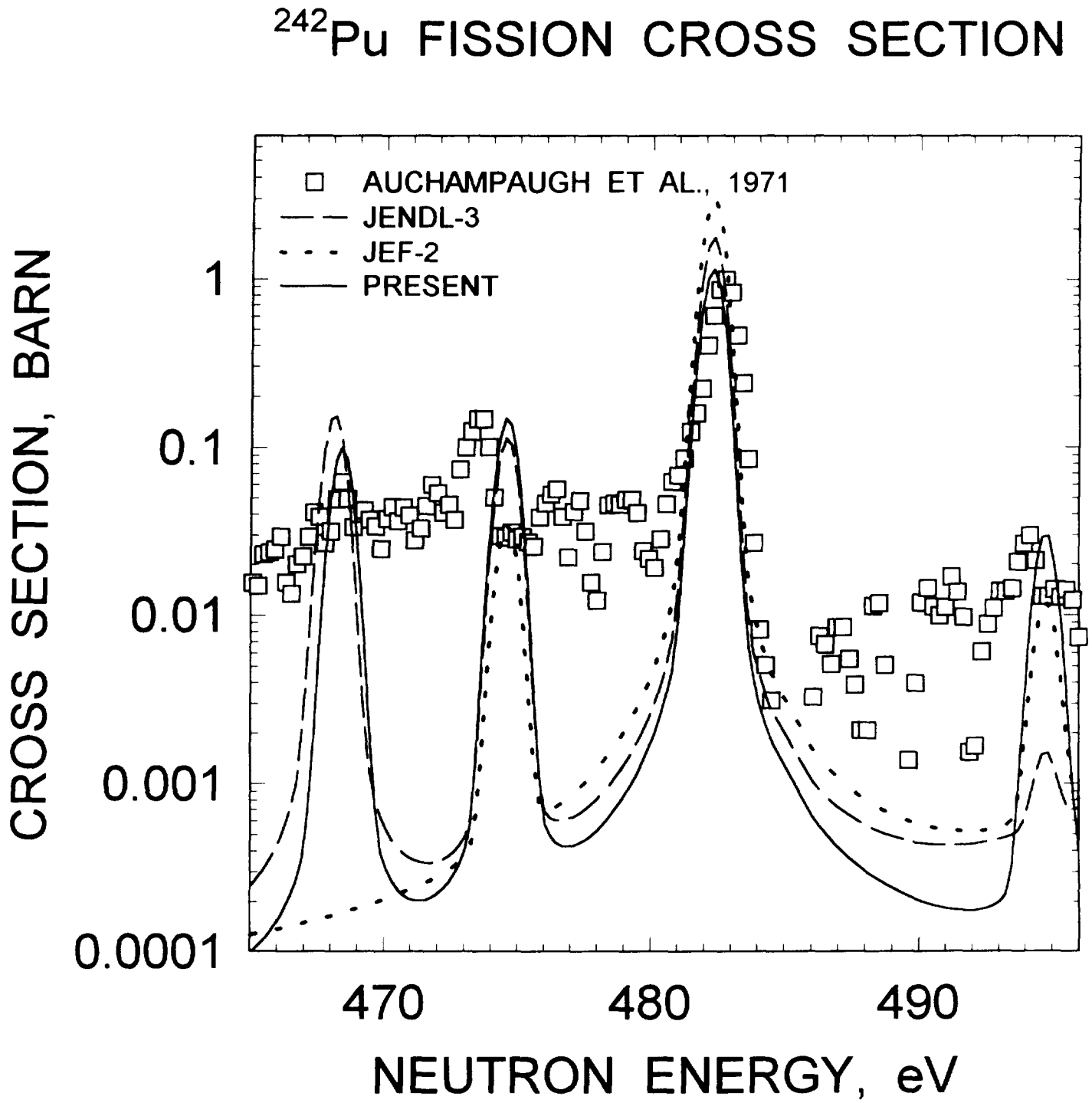
^{242}Pu FISSION CROSS SECTION
AUCHAMPAUGH ET AL., 1971
JENDL-3
JEF-2
PRESENT
CROSS SECTION, BARN
1
0.1
0.01
0.001
0.0001
470
480
490
NEUTRON ENERGY, eV

FIG. 2.3

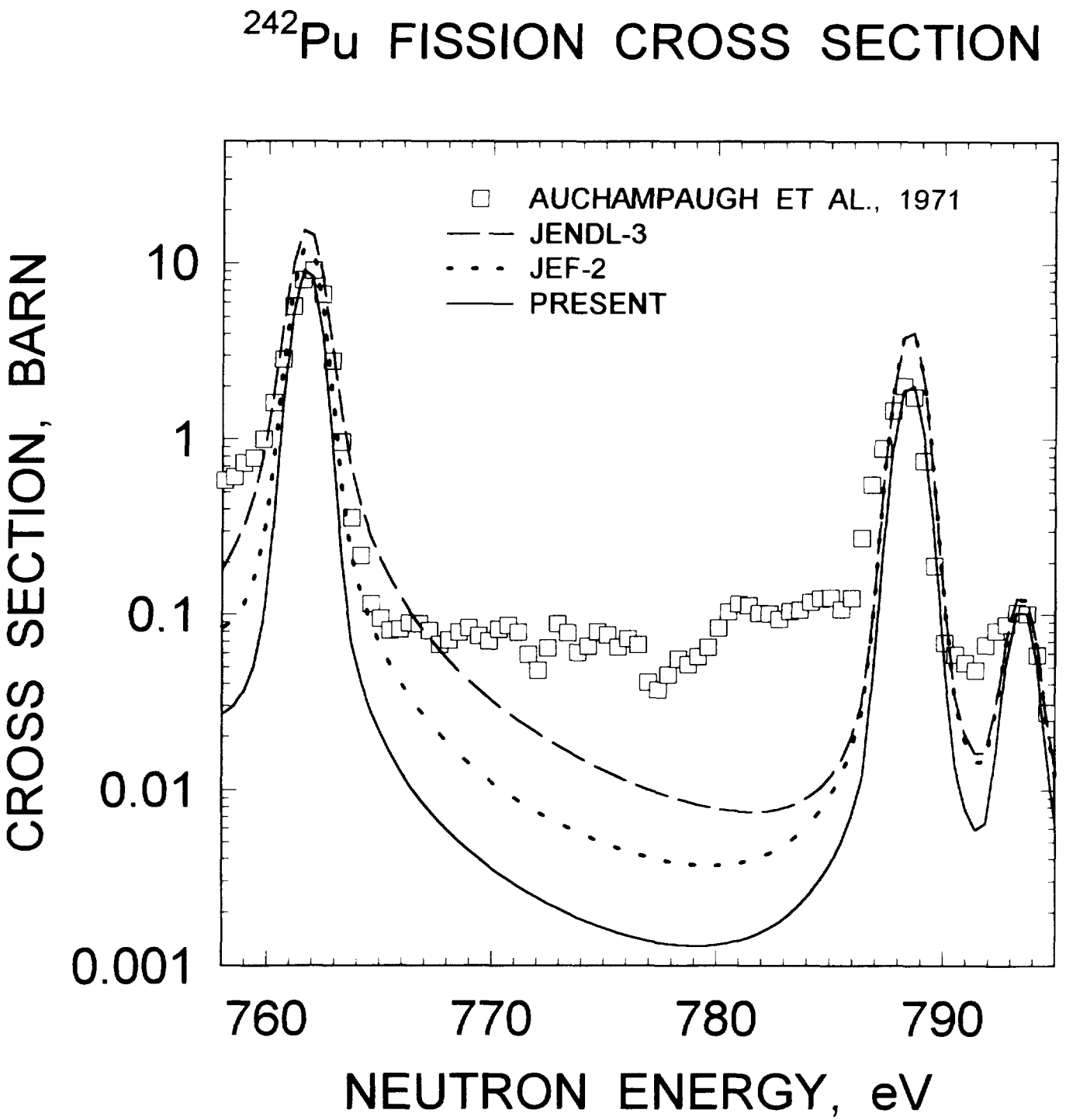
^{242}Pu FISSION CROSS SECTION
AUCHAMPAUGH ET AL., 1971
JENDL-3
JEF-2
PRESENT
CROSS SECTION, BARN
10
1
0.1
0.01
0.001
760
770
780
790
NEUTRON ENERGY, eV

FIG. 2.4

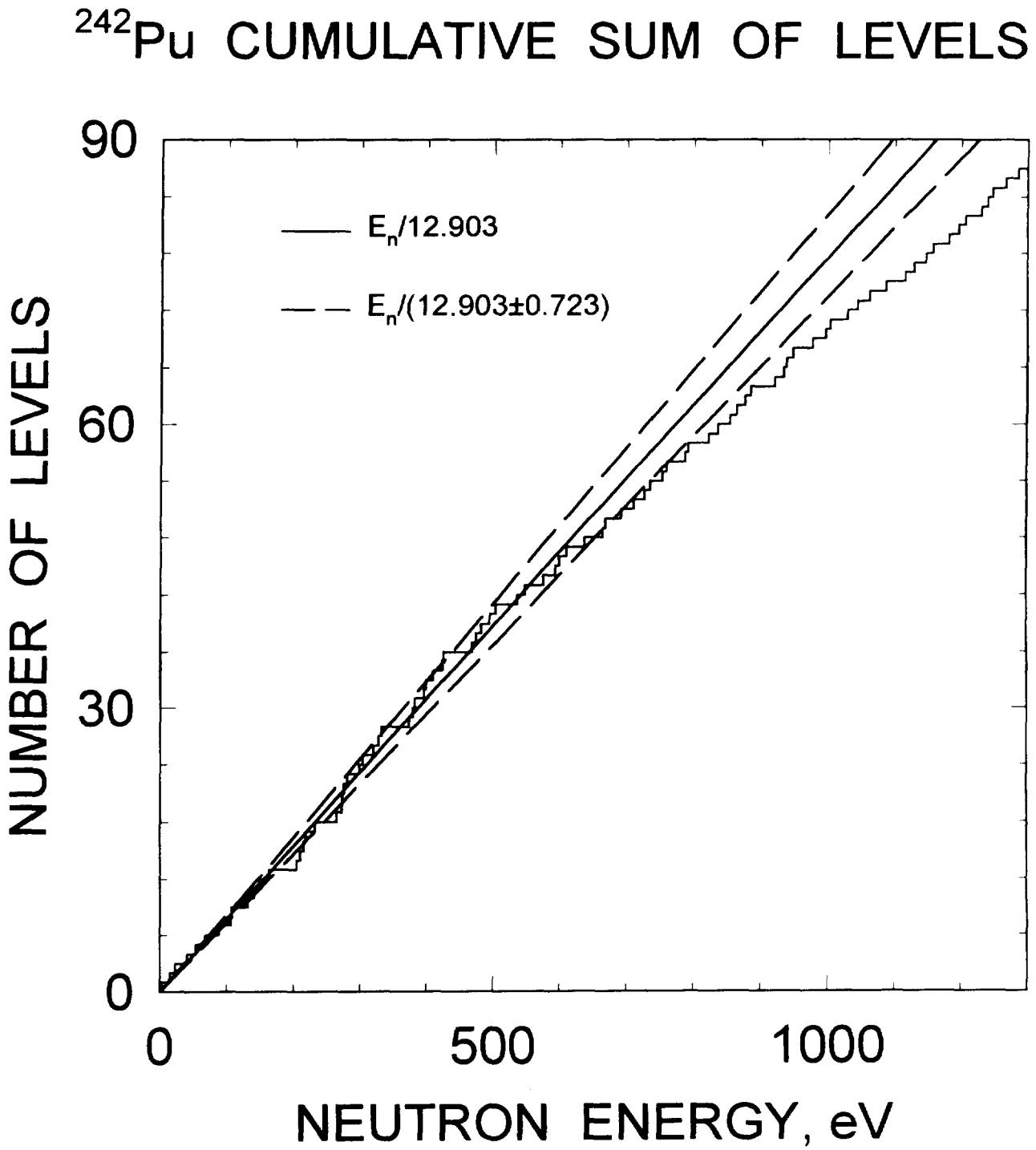
^{242}Pu CUMULATIVE SUM OF LEVELS
90
60
30
0
NUMBER OF LEVELS
E_n/12.903
E_n/(12.903±0.723)
0
500
1000
NEUTRON ENERGY, eV

FIG. 3.1

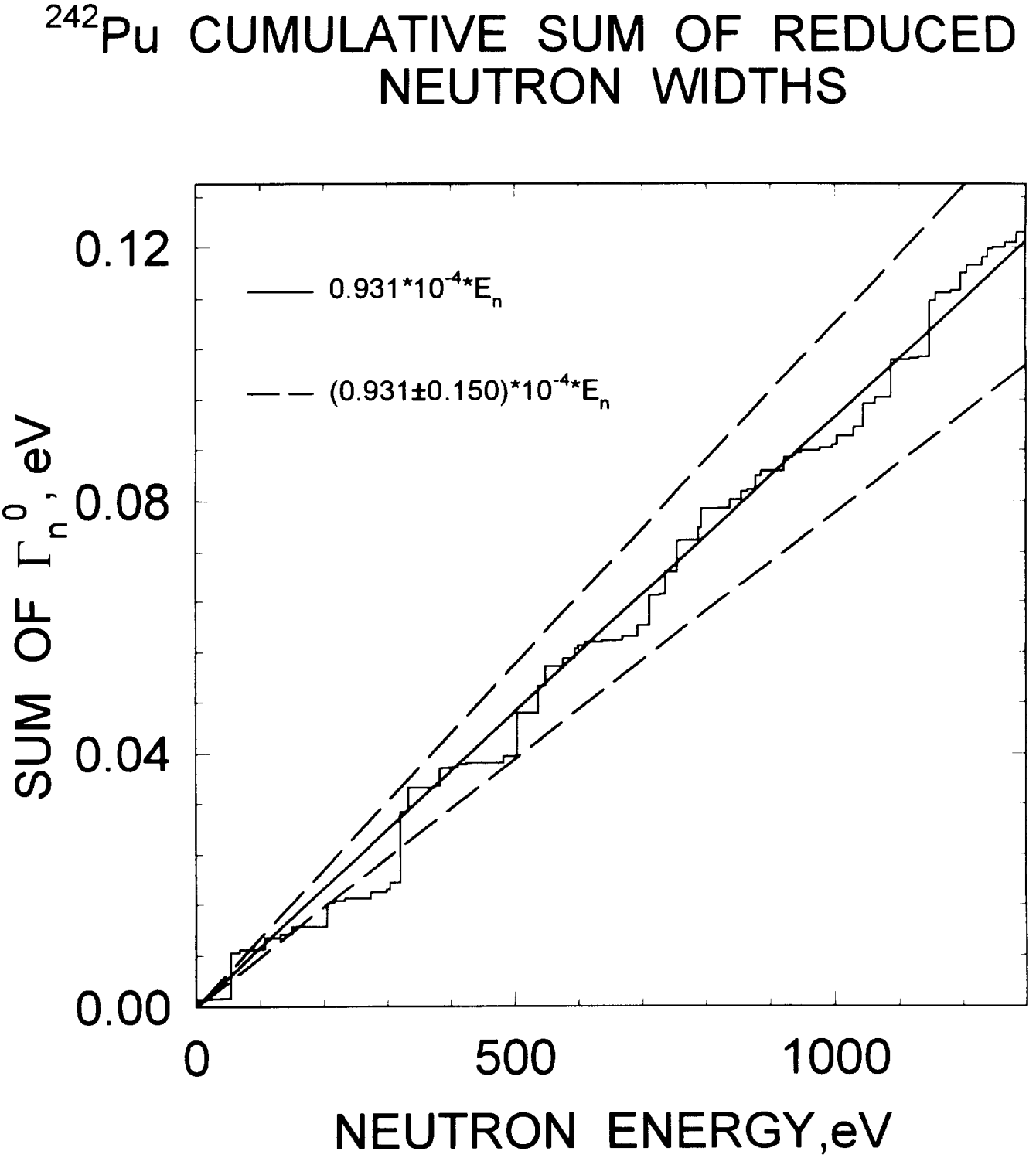
^{242}Pu CUMULATIVE SUM OF REDUCED NEUTRON WIDTHS
0.931*10^{-4}*E$_n$
(0.931±0.150)*10^{-4}*E$_n$
SUM OF Γ_n^0, eV
0.12
0.08
0.04
0.00
0
500
1000
NEUTRON ENERGY,eV

FIG. 3.2

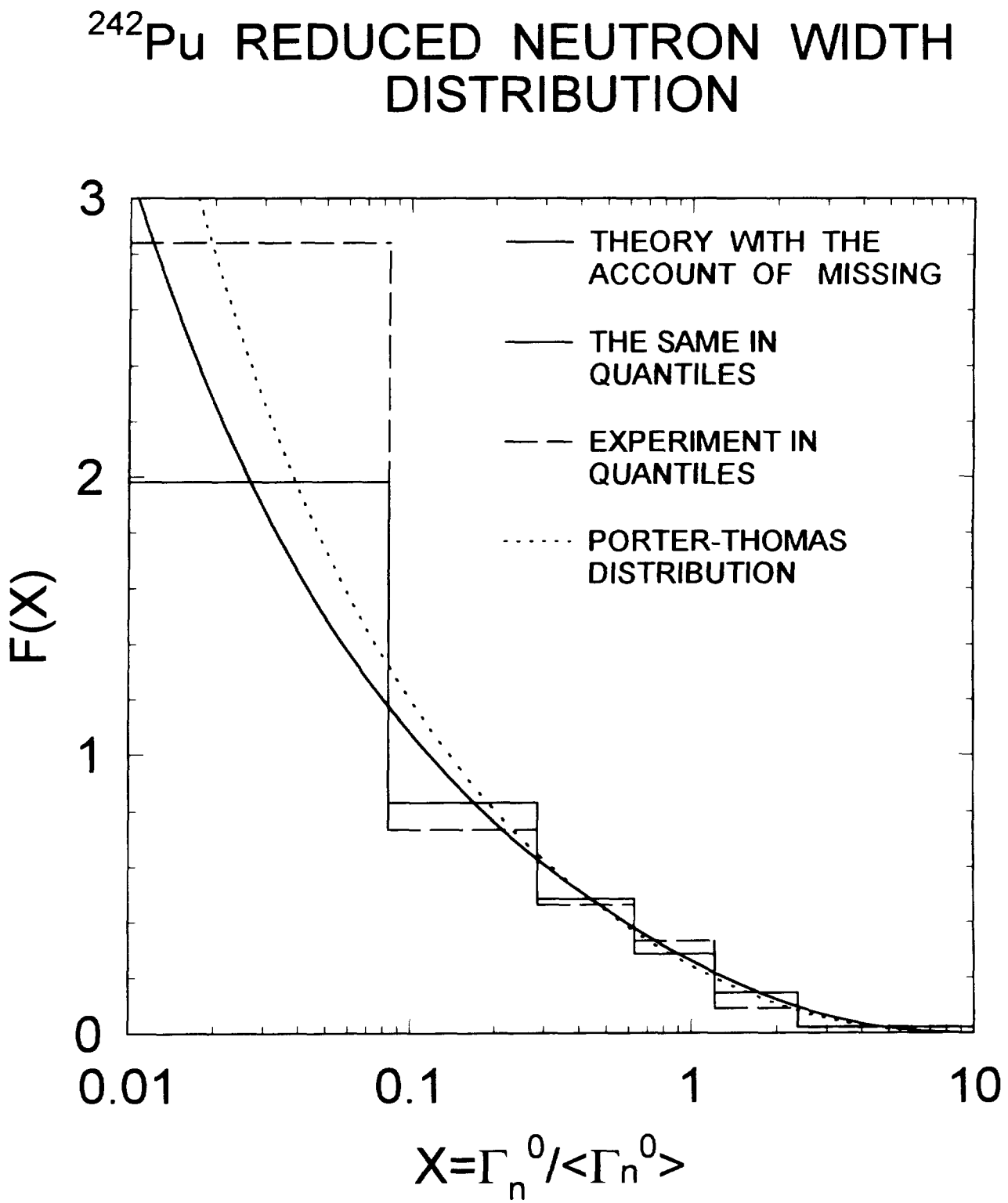
^{242}Pu REDUCED NEUTRON WIDTH DISTRIBUTION
THEORY WITH THE ACCOUNT OF MISSING
THE SAME IN QUANTILES
EXPERIMENT IN QUANTILES
PORTER-THOMAS DISTRIBUTION
F(X)
3
2
1
0
0.01
0.1
1
10
$X=\Gamma_n^0/\langle\Gamma_n^0\rangle$

FIG. 3.3

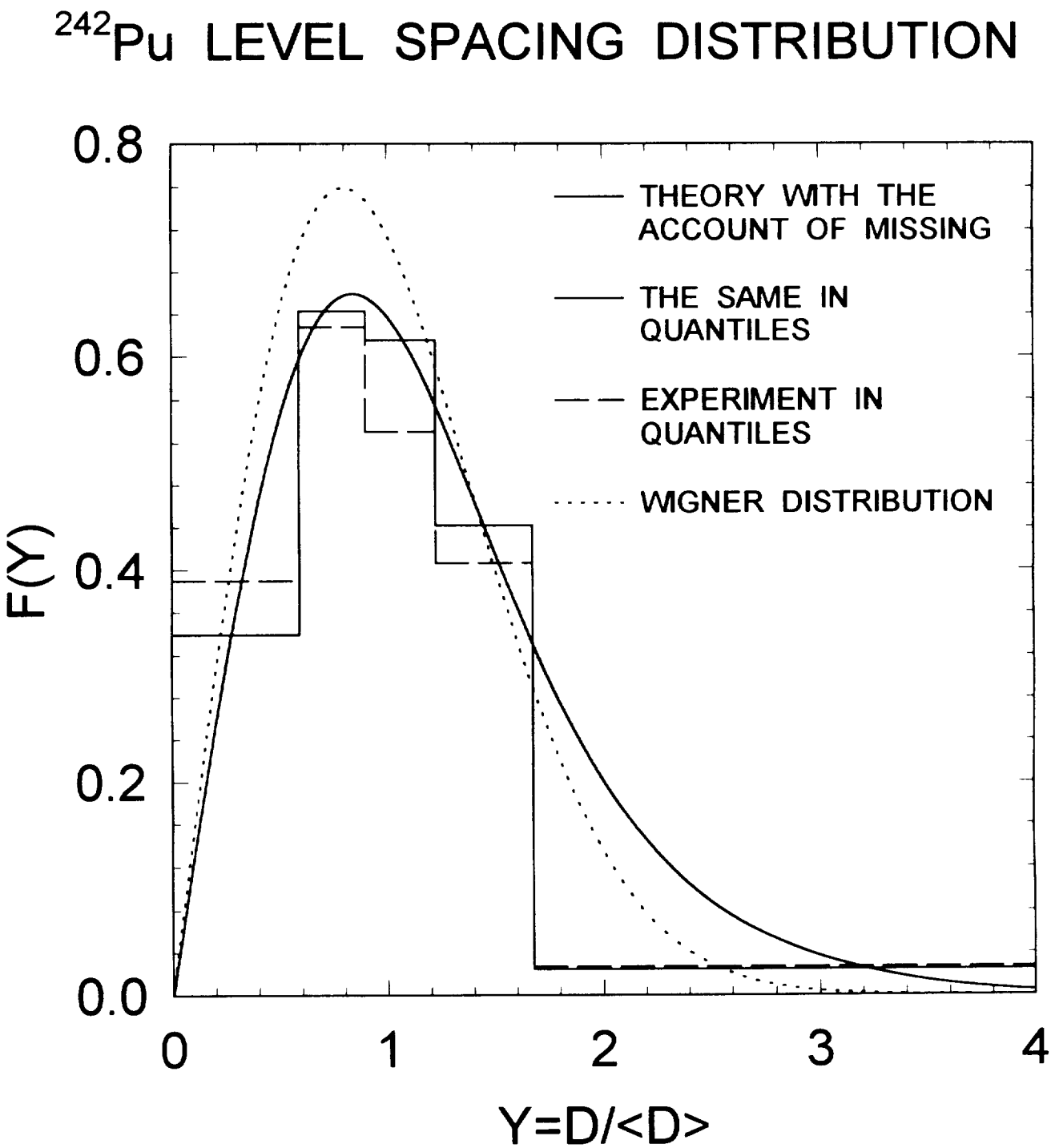
^{242}Pu LEVEL SPACING DISTRIBUTION
0.8
0.6
0.4
0.2
0.0
F(Y)
0
1
2
3
4
Y=D/<D>
THEORY WITH THE ACCOUNT OF MISSING
THE SAME IN QUANTILES
EXPERIMENT IN QUANTILES
WIGNER DISTRIBUTION

FIG. 3.4

^{242}Pu COMPARISON OF REDUCED NEUTRON WIDTH DISTRIBUTIONS PRESENTED IN QUANTILE FORM

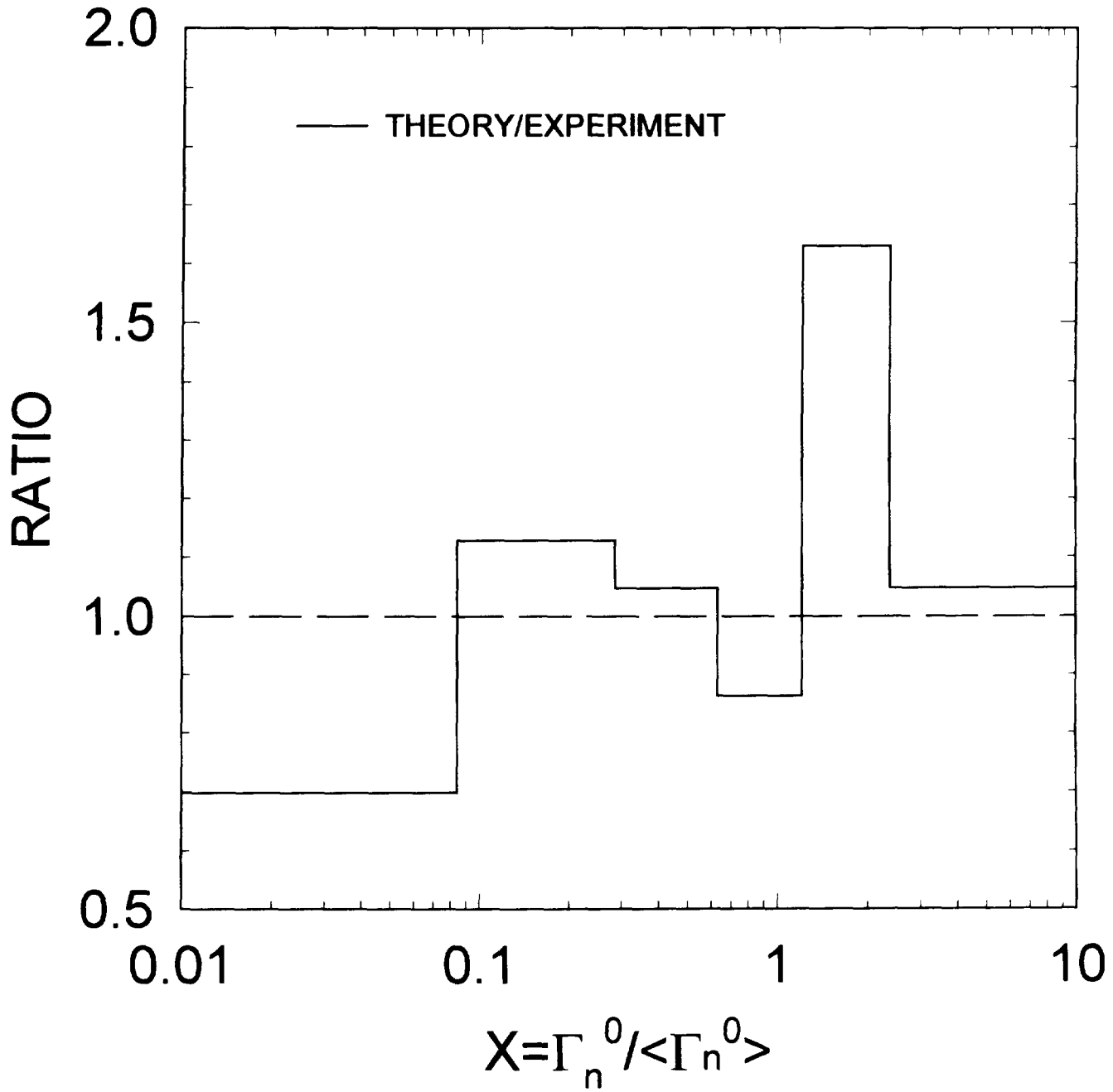

FIG. 3.5

^{242}Pu COMPARISON OF LEVEL SPACING DISTRIBUTIONS PRESENTED IN QUANTILE FORM

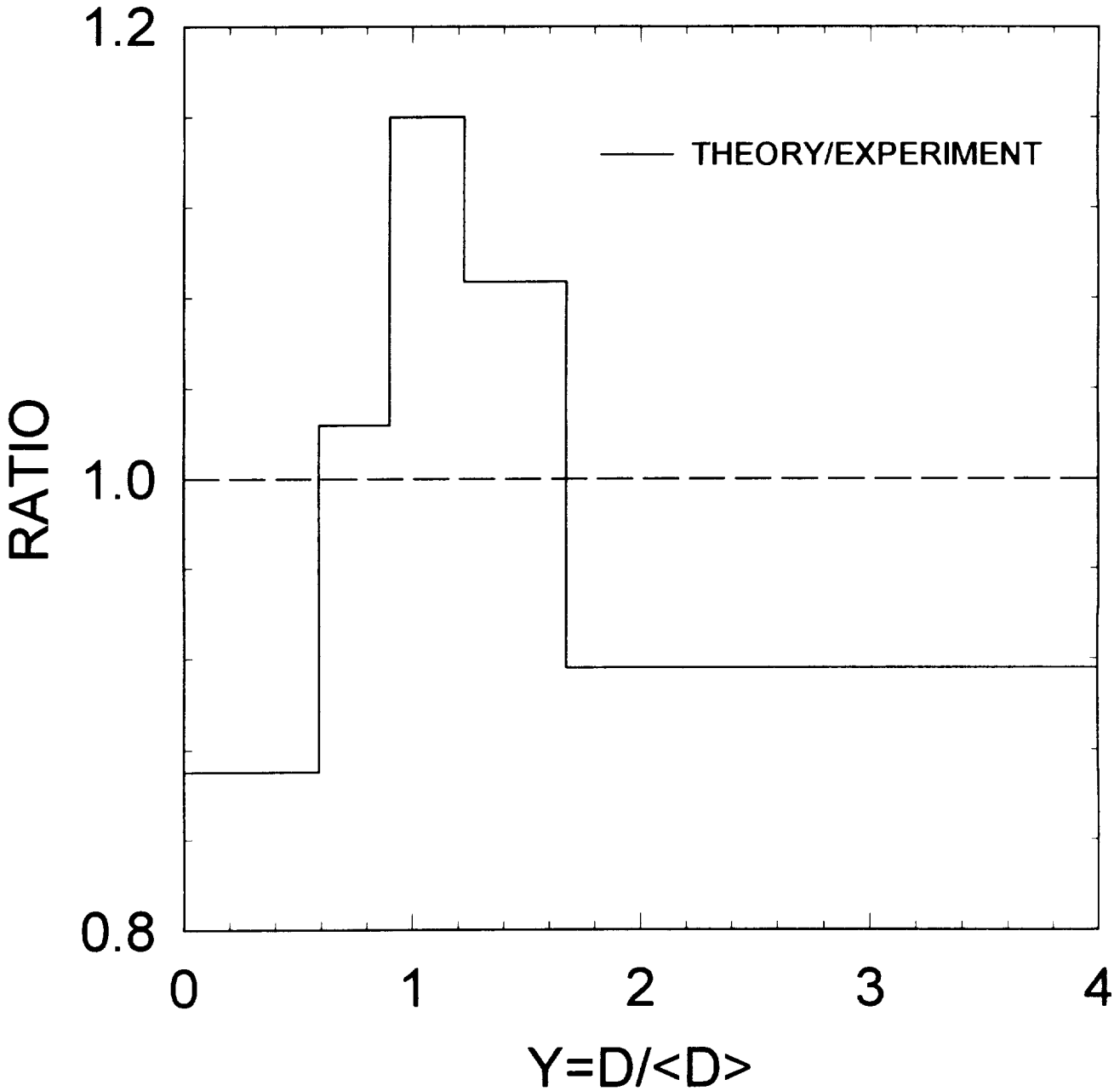

FIG. 3.6

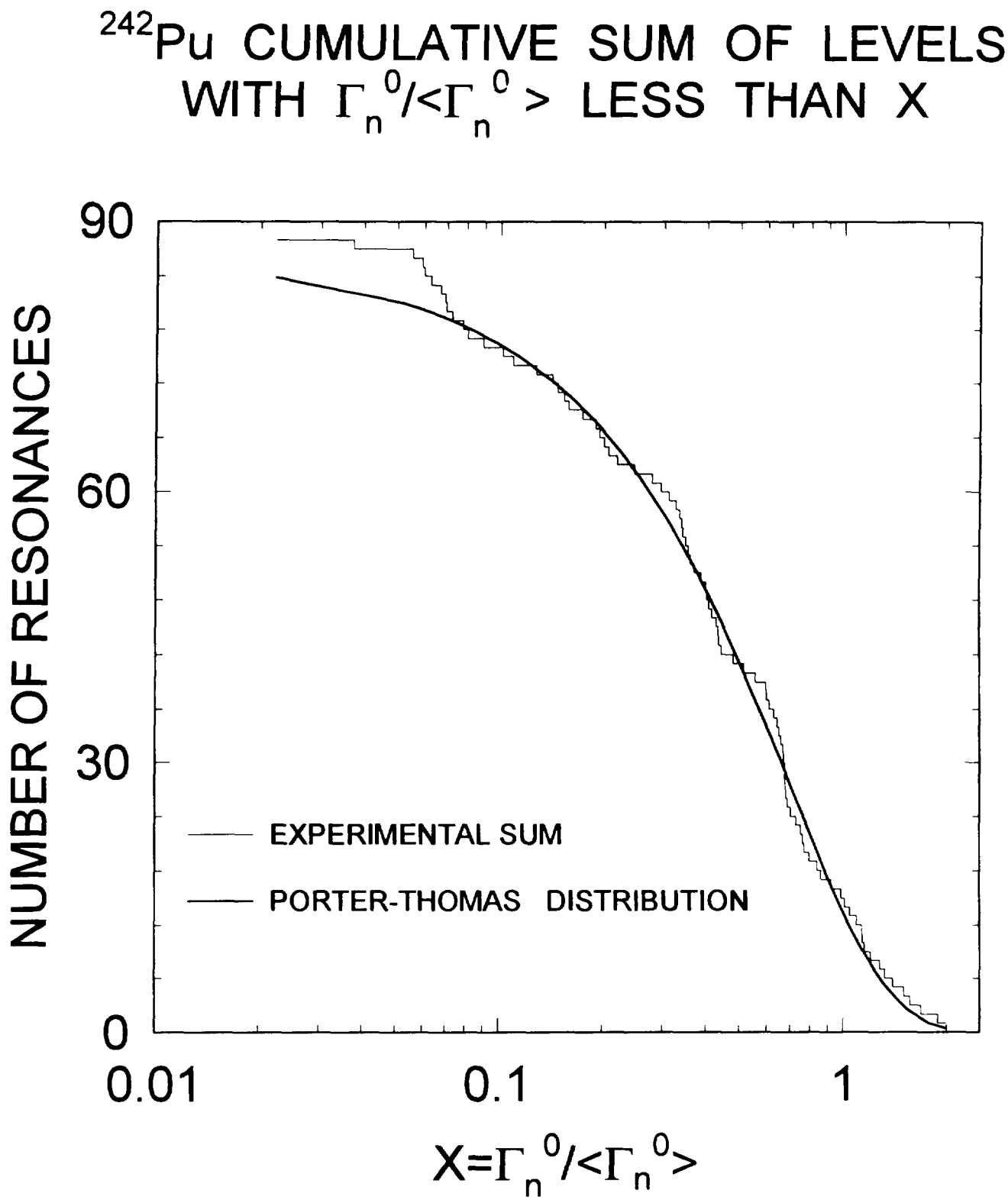
^{242}Pu CUMULATIVE SUM OF LEVELS WITH $\Gamma_n^0/<\Gamma_n^0>$ LESS THAN X
NUMBER OF RESONANCES
90
60
30
0
0.01
0.1
1
EXPERIMENTAL SUM
PORTER-THOMAS DISTRIBUTION
$X=\Gamma_n^0/<\Gamma_n^0>$

FIG.3.7

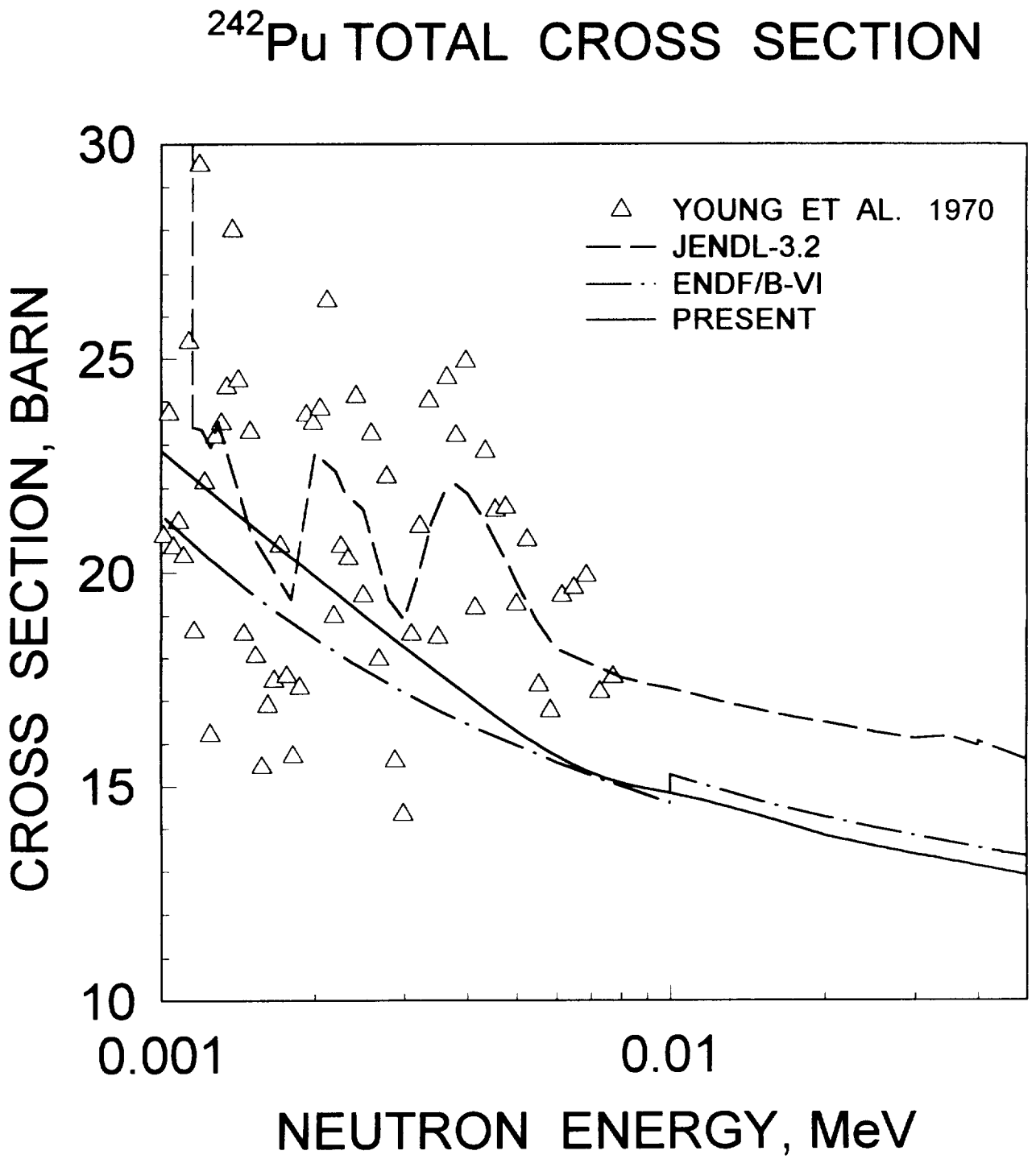
^{242}Pu TOTAL CROSS SECTION
YOUNG ET AL. 1970
JENDL-3.2
ENDF/B-VI
PRESENT
CROSS SECTION, BARN
30
25
20
15
10
0.001
0.01
NEUTRON ENERGY, MeV

FIG.3.8

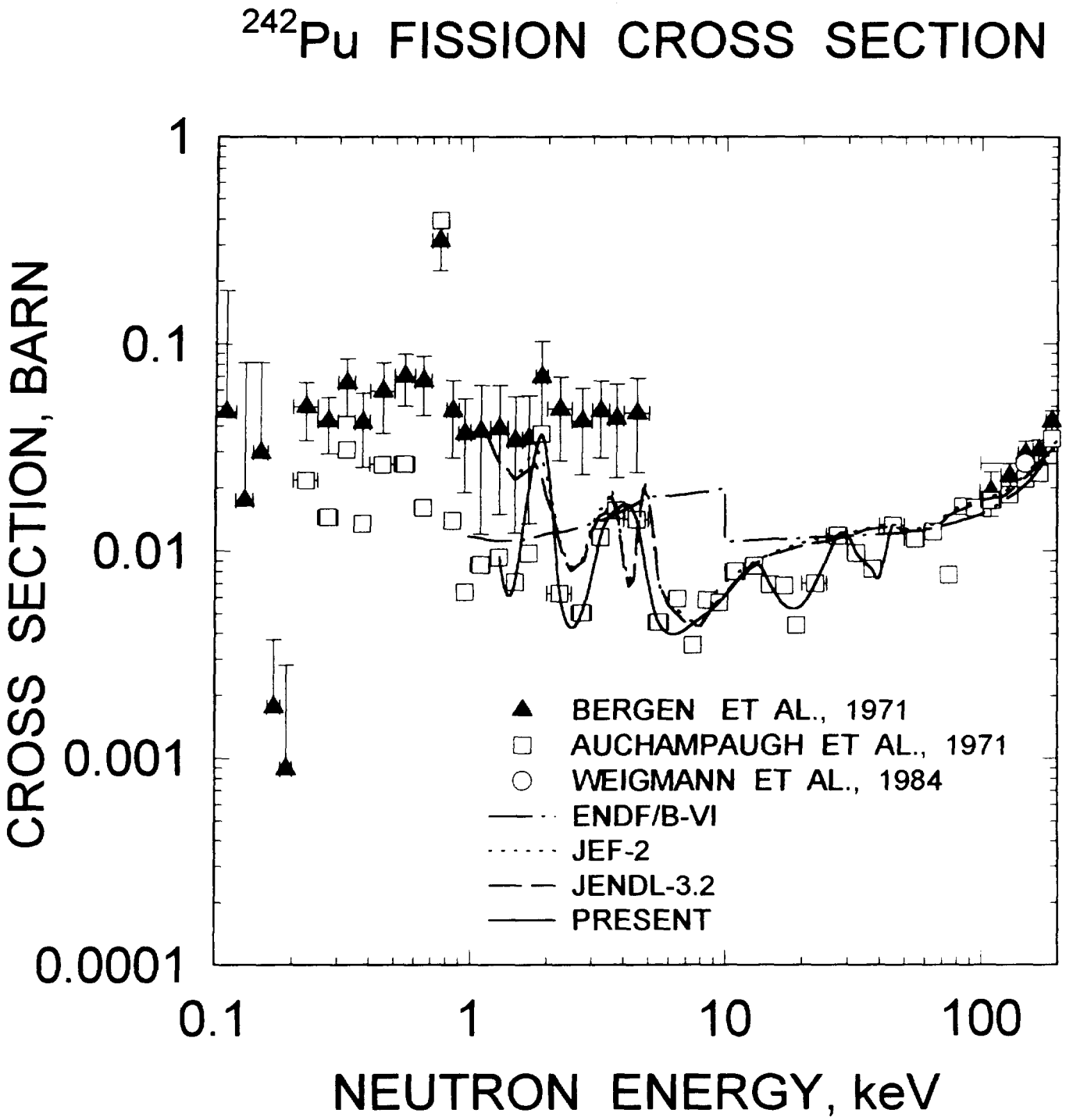
^{242}Pu FISSION CROSS SECTION
CROSS SECTION, BARN
1
0.1
0.01
0.001
0.0001
0.1
1
10
100
NEUTRON ENERGY, keV
BERGEN ET AL., 1971
AUCHAMPAUGH ET AL., 1971
WEIGMANN ET AL., 1984
ENDF/B-VI
JEF-2
JENDL-3.2
PRESENT

FIG.3.9

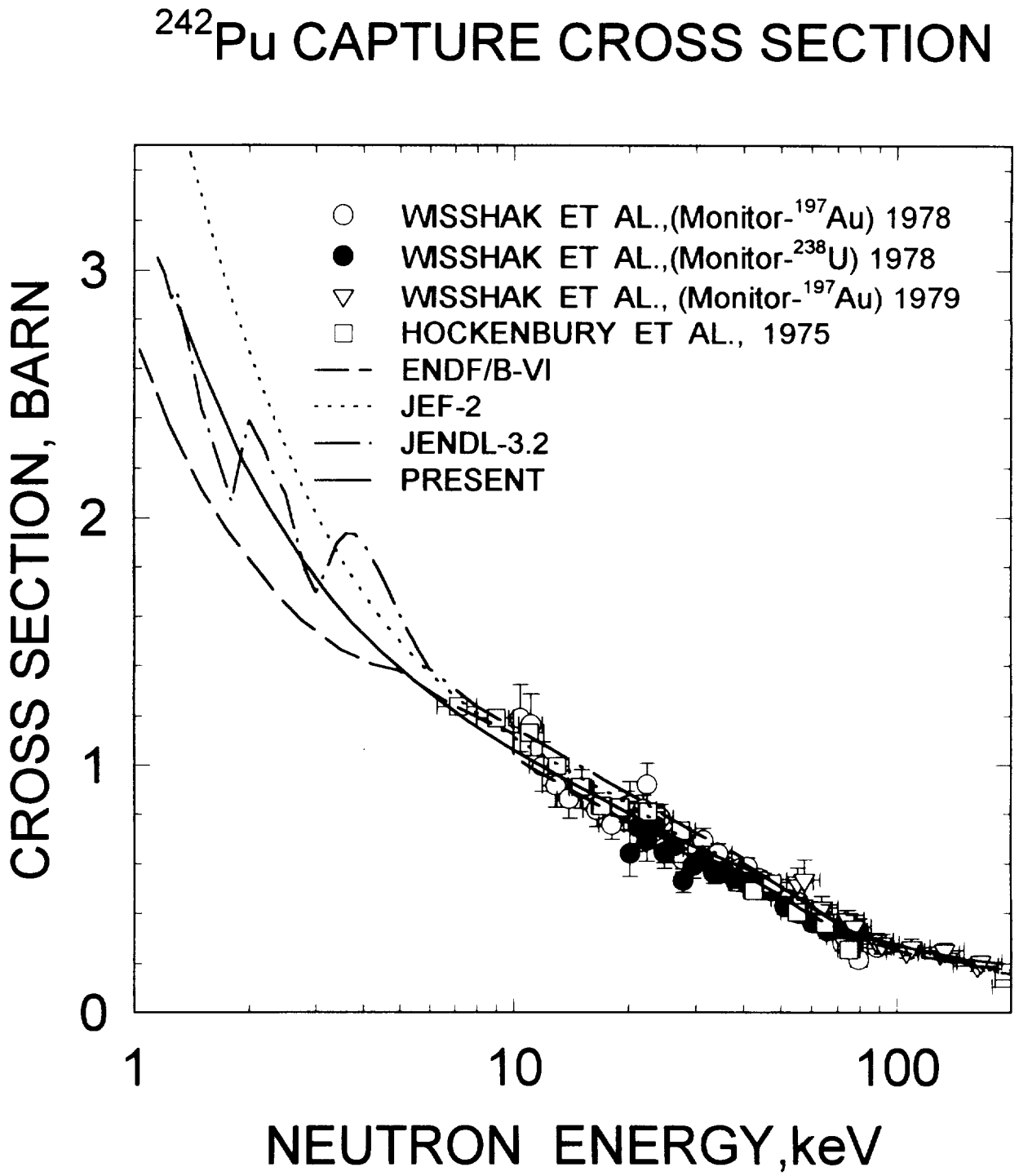
242Pu CAPTURE CROSS SECTION
WISSHAK ET AL.,(Monitor-197Au) 1978
WISSHAK ET AL.,(Monitor-238U) 1978
WISSHAK ET AL., (Monitor-197Au) 1979
HOCKENBURY ET AL., 1975
ENDF/B-VI
JEF-2
JENDL-3.2
PRESENT
CROSS SECTION, BARN
0
1
2
3
1
10
100
NEUTRON ENERGY,keV

FIG.3.10

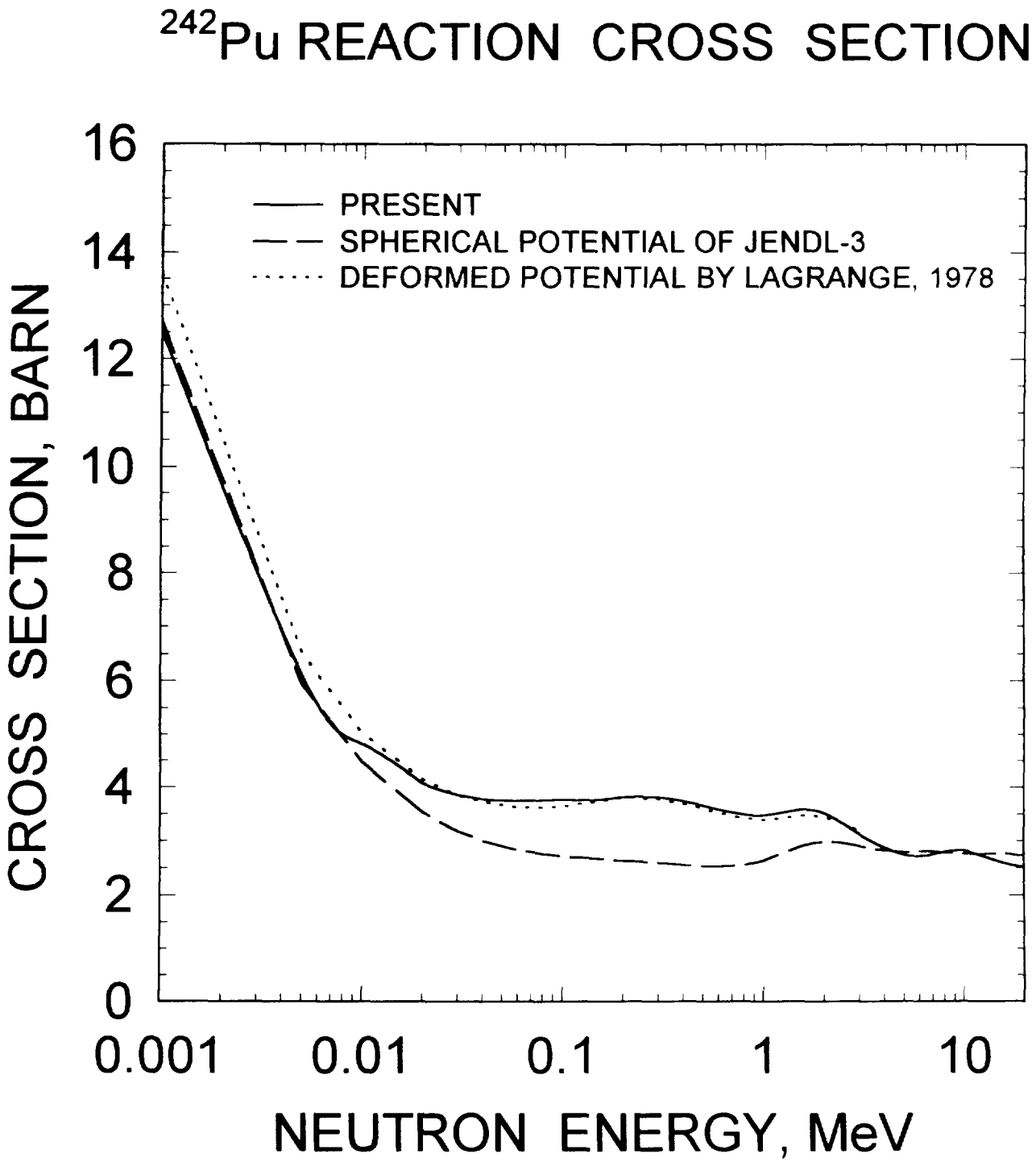
^{242}Pu REACTION CROSS SECTION
PRESENT
SPHERICAL POTENTIAL OF JENDL-3
DEFORMED POTENTIAL BY LAGRANGE, 1978
CROSS SECTION, BARN
16
14
12
10
8
6
4
2
0
0.001
0.01
0.1
1
10
NEUTRON ENERGY, MeV

FIG. 4.1

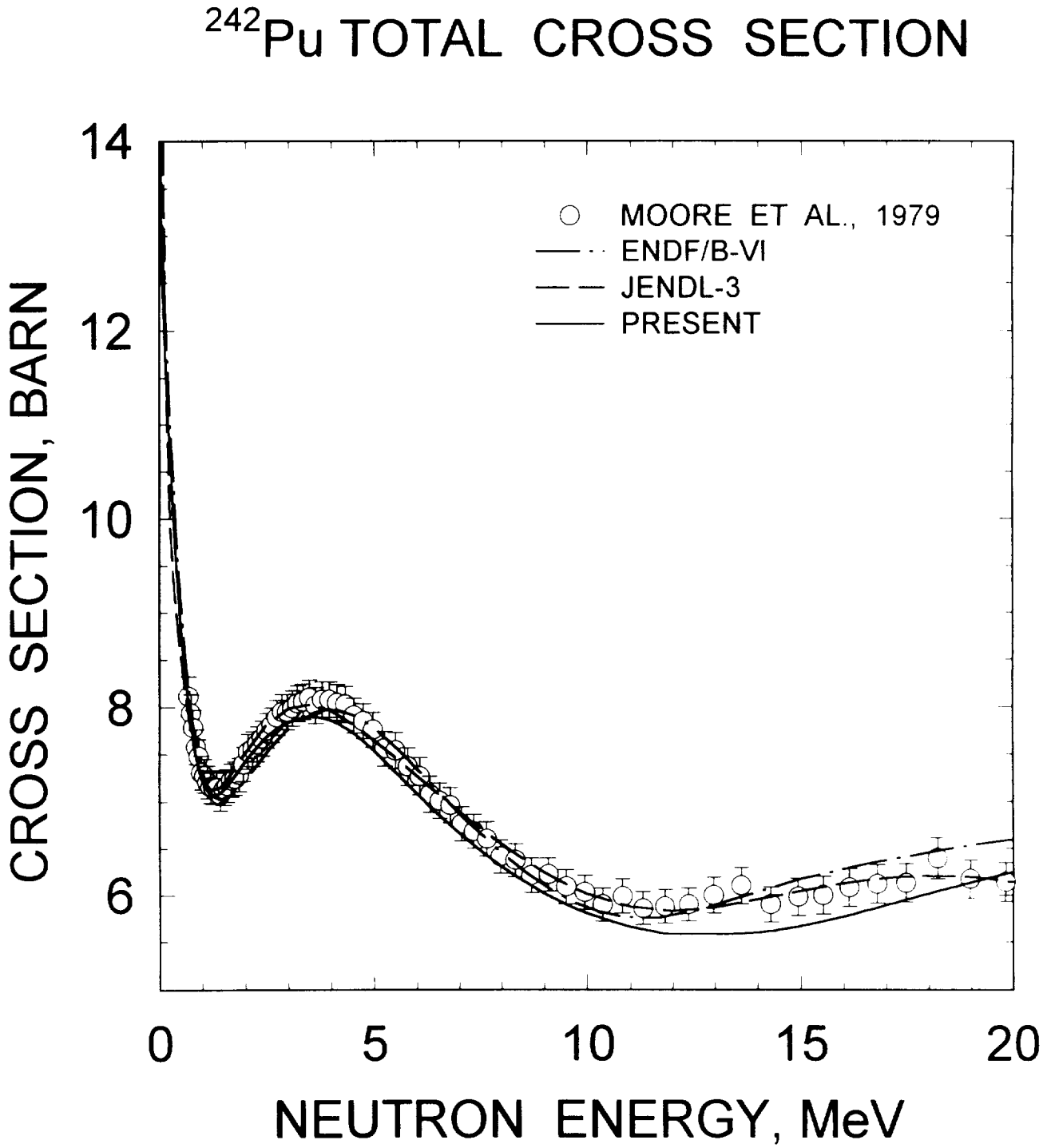
^{242}Pu TOTAL CROSS SECTION
MOORE ET AL., 1979
ENDF/B-VI
JENDL-3
PRESENT
CROSS SECTION, BARN
14
12
10
8
6
0
5
10
15
20
NEUTRON ENERGY, MeV

FIG. 4.2

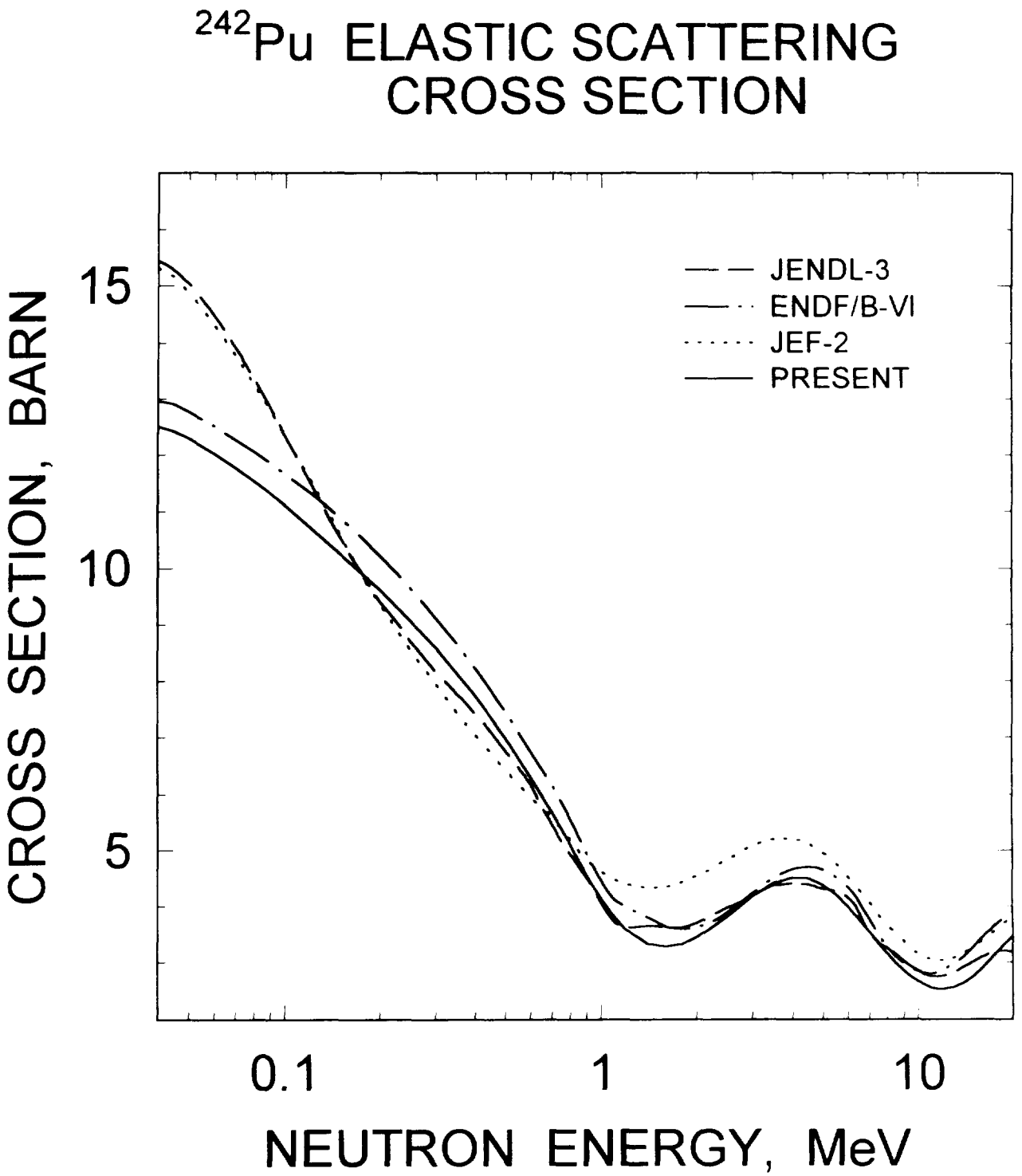
^{242}Pu ELASTIC SCATTERING
CROSS SECTION
JENDL-3
ENDF/B-VI
JEF-2
PRESENT
CROSS SECTION, BARN
15
10
5
0.1
1
10
NEUTRON ENERGY, MeV

FIG. 4.3

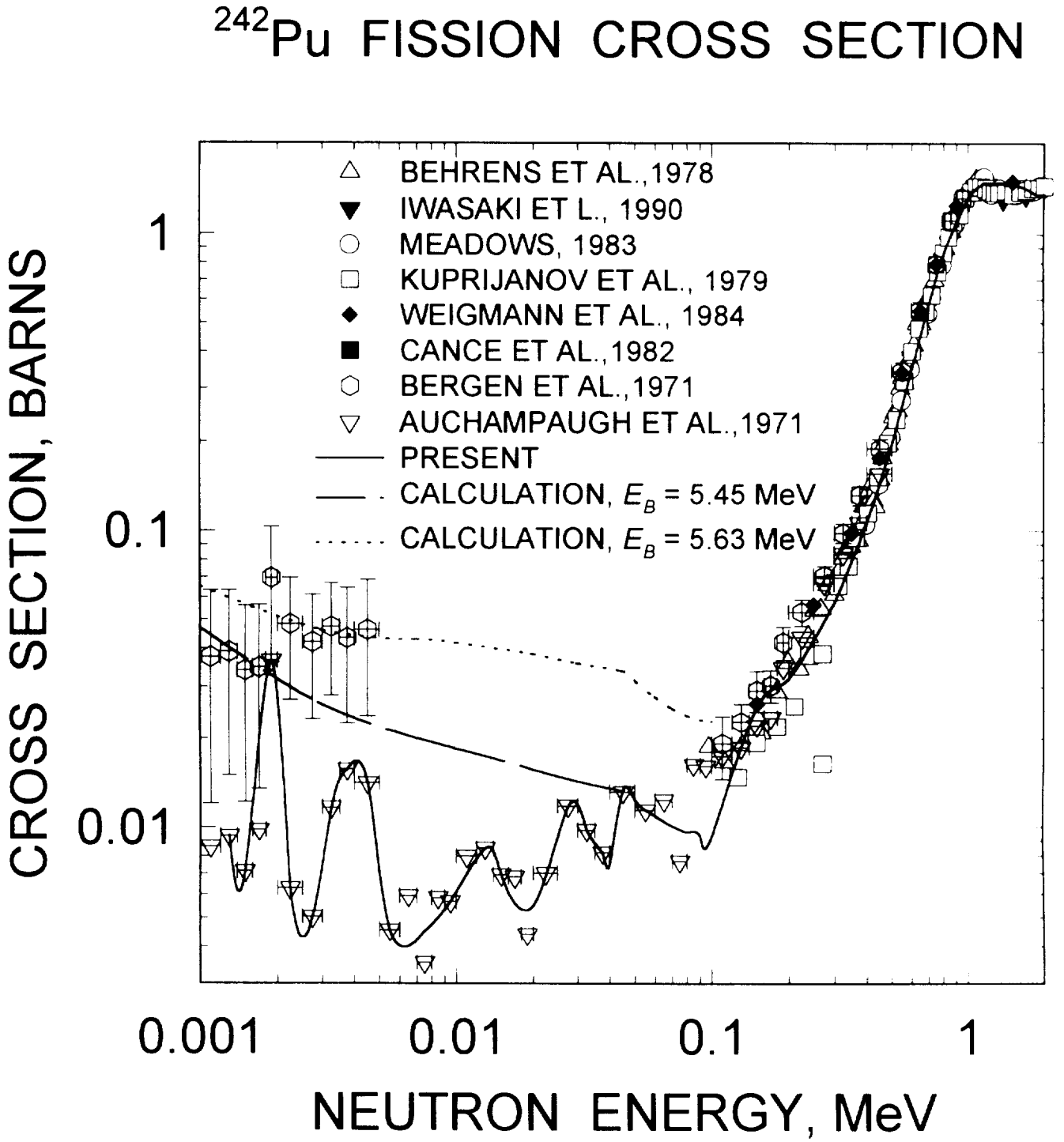
^{242}Pu FISSION CROSS SECTION
BEHRENS ET AL.,1978
IWASAKI ET L., 1990
MEADOWS, 1983
KUPRIJANOV ET AL., 1979
WEIGMANN ET AL., 1984
CANCE ET AL.,1982
BERGEN ET AL.,1971
AUCHAMPAUGH ET AL.,1971
PRESENT
CALCULATION, E_B = 5.45 MeV
CALCULATION, E_B = 5.63 MeV
CROSS SECTION, BARNS
1
0.1
0.01
0.001
0.01
0.1
1
NEUTRON ENERGY, MeV

FIG. 4.4

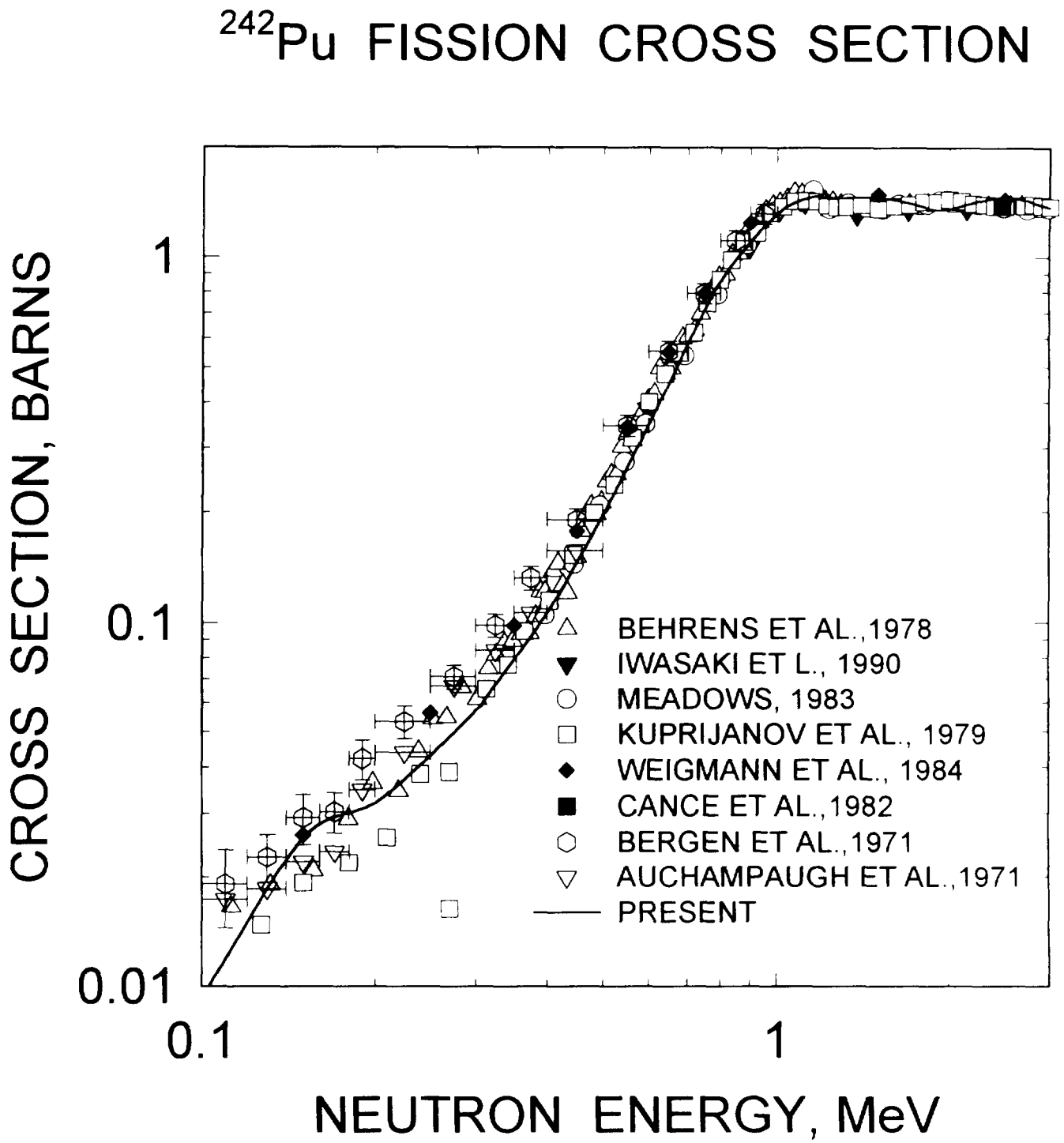
^{242}Pu FISSION CROSS SECTION
CROSS SECTION, BARNS
1
0.1
0.01
0.1
1
NEUTRON ENERGY, MeV
BEHRENS ET AL.,1978
IWASAKI ET L., 1990
MEADOWS, 1983
KUPRIJANOV ET AL., 1979
WEIGMANN ET AL., 1984
CANCE ET AL.,1982
BERGEN ET AL.,1971
AUCHAMPAUGH ET AL.,1971
PRESENT

FIG. 4.5

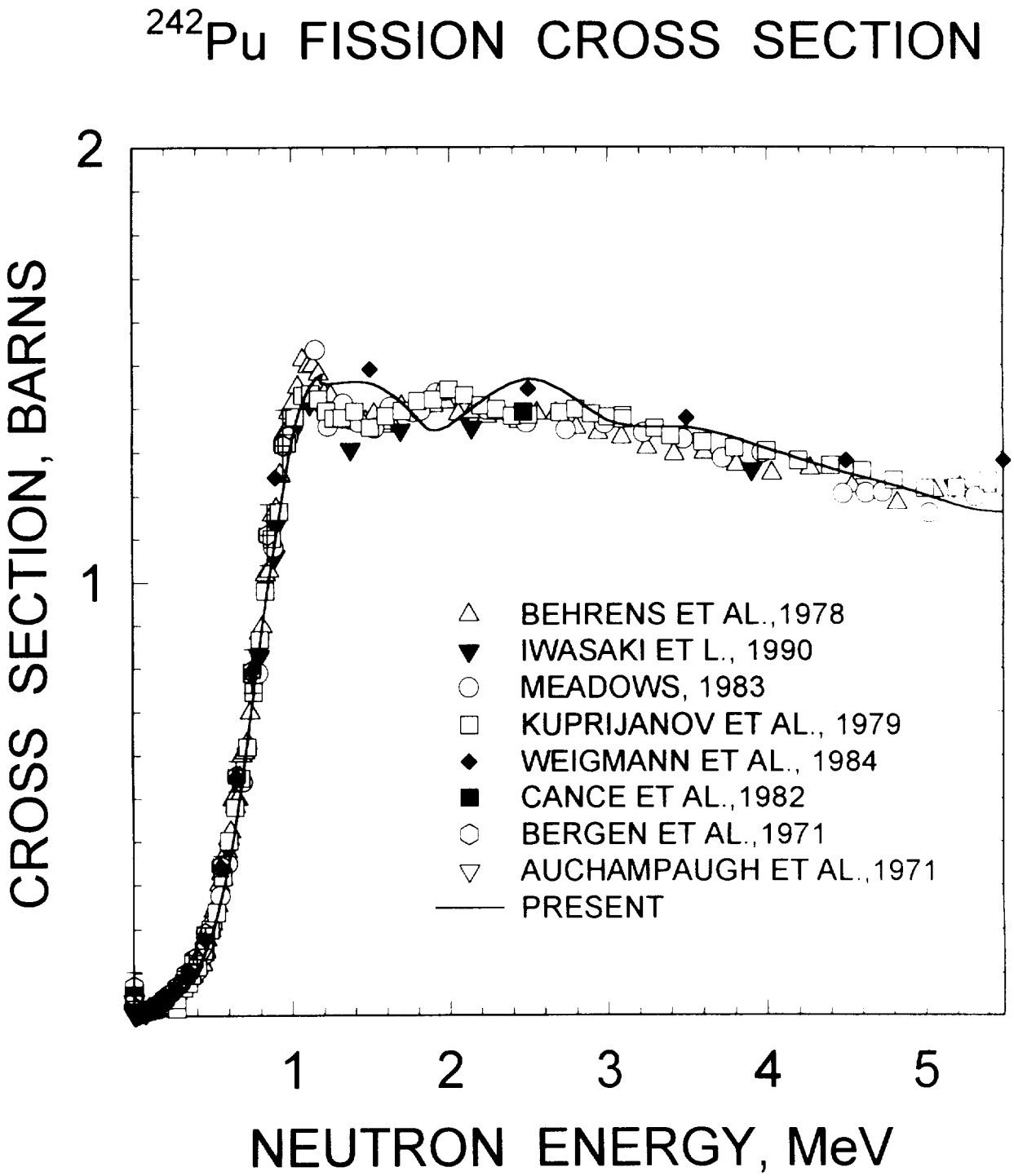
^{242}Pu FISSION CROSS SECTION
CROSS SECTION, BARNS
2
1
1
2
3
4
5
NEUTRON ENERGY, MeV
BEHRENS ET AL.,1978
IWASAKI ET L., 1990
MEADOWS, 1983
KUPRIJANOV ET AL., 1979
WEIGMANN ET AL., 1984
CANCE ET AL.,1982
BERGEN ET AL.,1971
AUCHAMPAUGH ET AL.,1971
PRESENT

FIG. 4.6

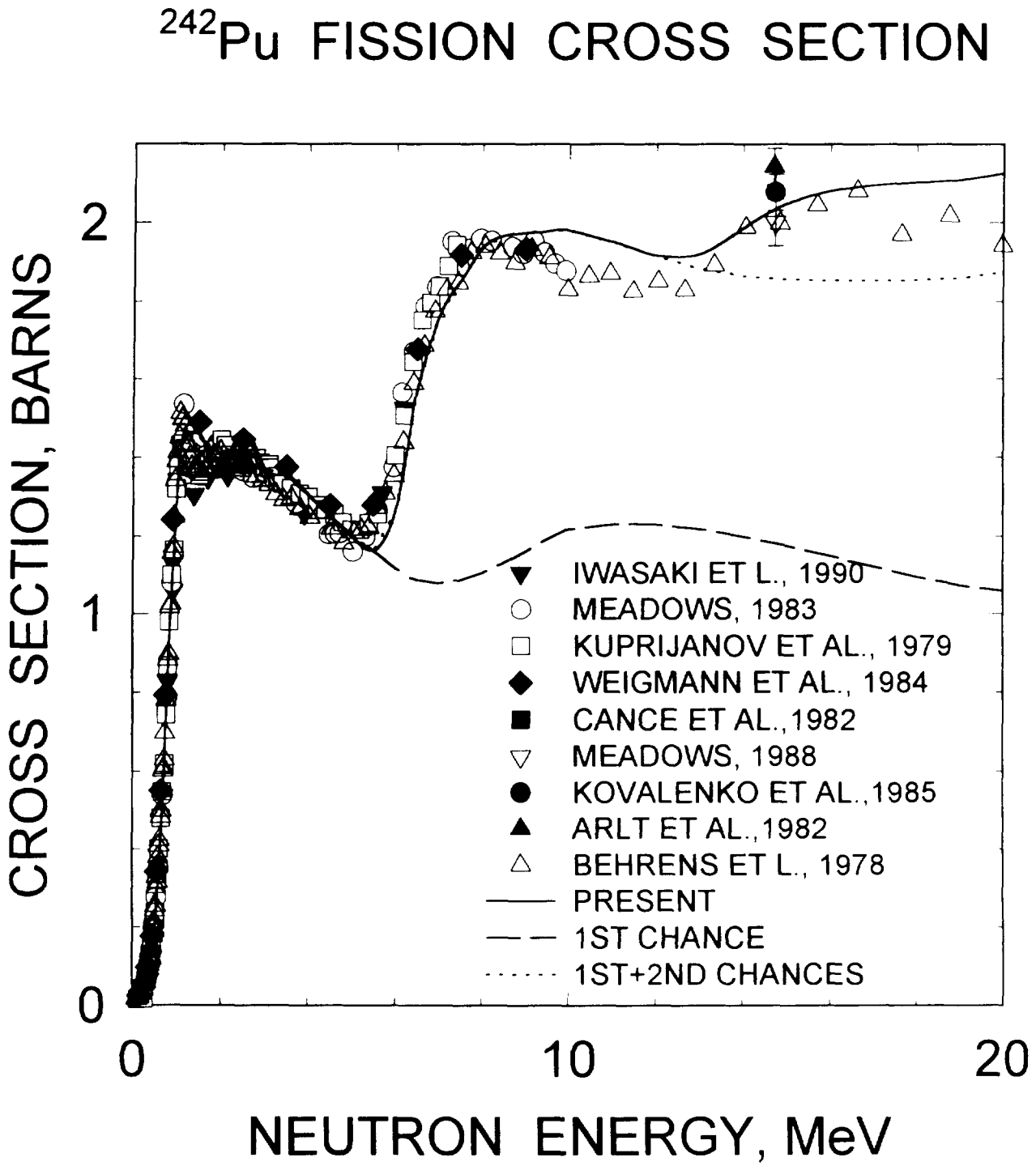
^{242}Pu FISSION CROSS SECTION
CROSS SECTION, BARNS
2
1
0
0
10
20
NEUTRON ENERGY, MeV
IWASAKI ET L., 1990
MEADOWS, 1983
KUPRIJANOV ET AL., 1979
WEIGMANN ET AL., 1984
CANCE ET AL.,1982
MEADOWS, 1988
KOVALENKO ET AL.,1985
ARLT ET AL.,1982
BEHRENS ET L., 1978
PRESENT
1ST CHANCE
1ST+2ND CHANCES

FIG. 4.7

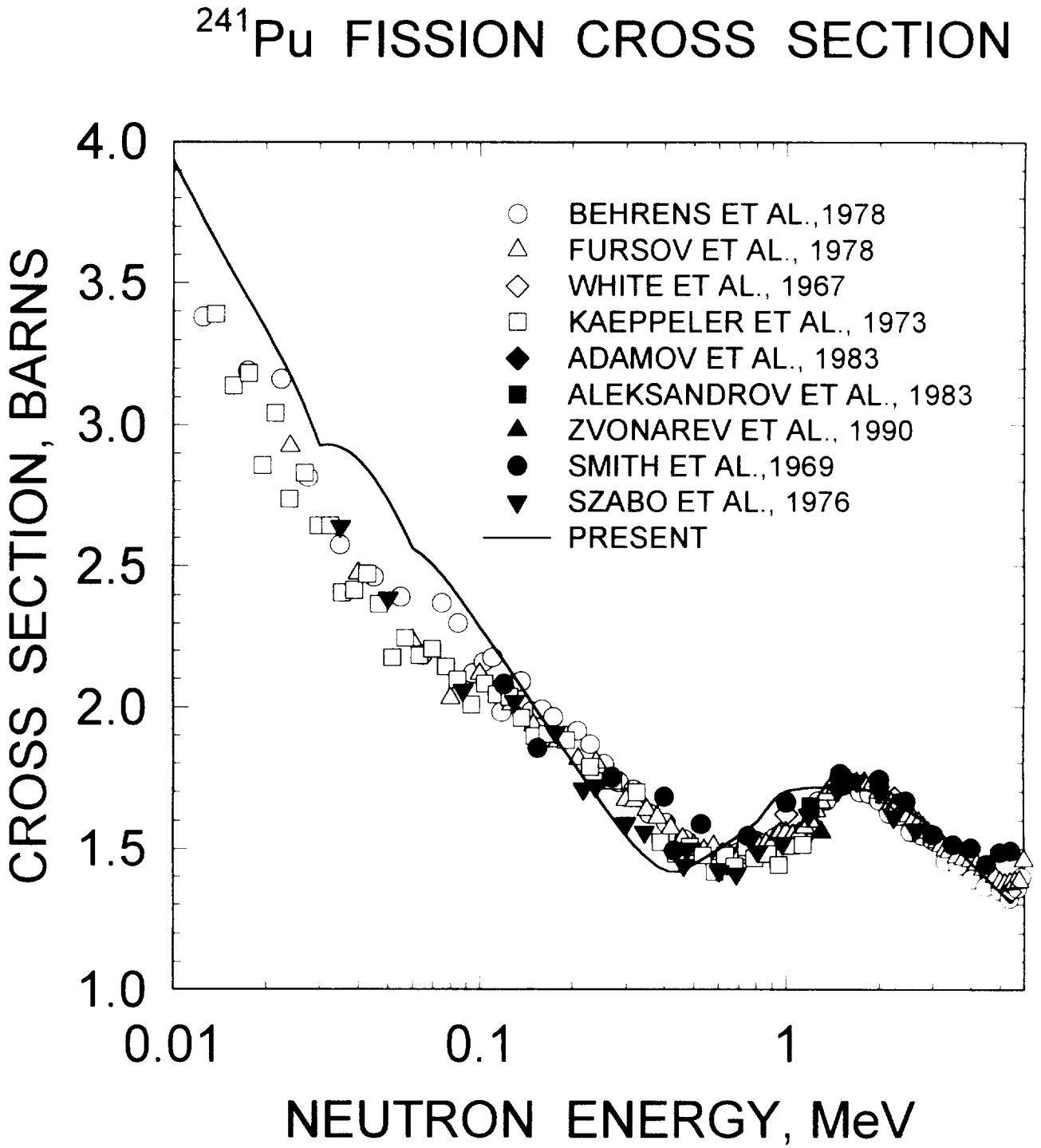
241Pu FISSION CROSS SECTION
CROSS SECTION, BARNS
4.0
3.5
3.0
2.5
2.0
1.5
1.0
0.01
0.1
1
NEUTRON ENERGY, MeV
BEHRENS ET AL.,1978
FURSOV ET AL., 1978
WHITE ET AL., 1967
KAEPPELER ET AL., 1973
ADAMOV ET AL., 1983
ALEKSANDROV ET AL., 1983
ZVONAREV ET AL., 1990
SMITH ET AL.,1969
SZABO ET AL., 1976
PRESENT

FIG. 4.8

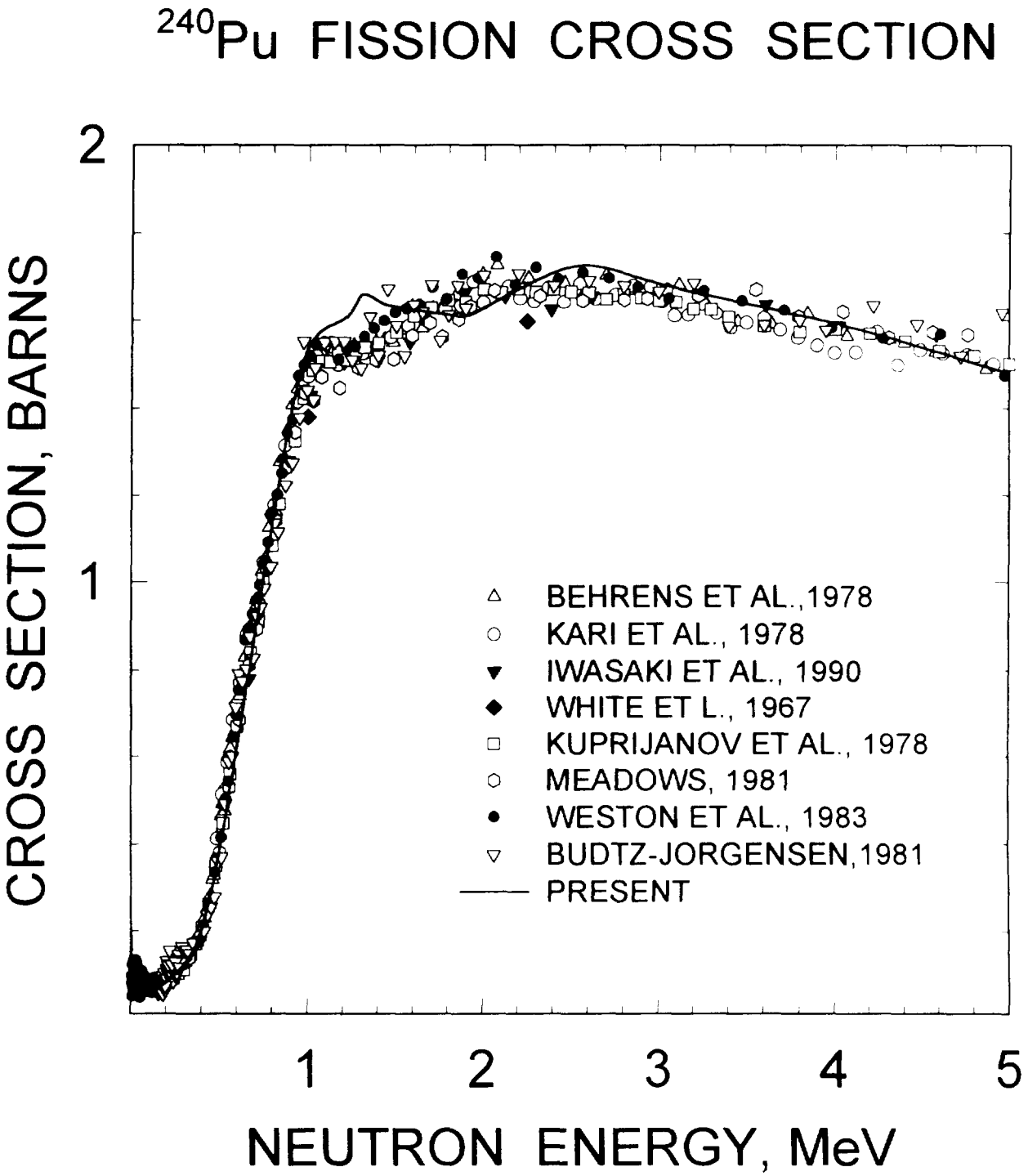
^{240}Pu FISSION CROSS SECTION
CROSS SECTION, BARNS
2
1
1
2
3
4
5
NEUTRON ENERGY, MeV
BEHRENS ET AL.,1978
KARI ET AL., 1978
IWASAKI ET AL., 1990
WHITE ET L., 1967
KUPRIJANOV ET AL., 1978
MEADOWS, 1981
WESTON ET AL., 1983
BUDTZ-JORGENSEN,1981
PRESENT

FIG. 4.9

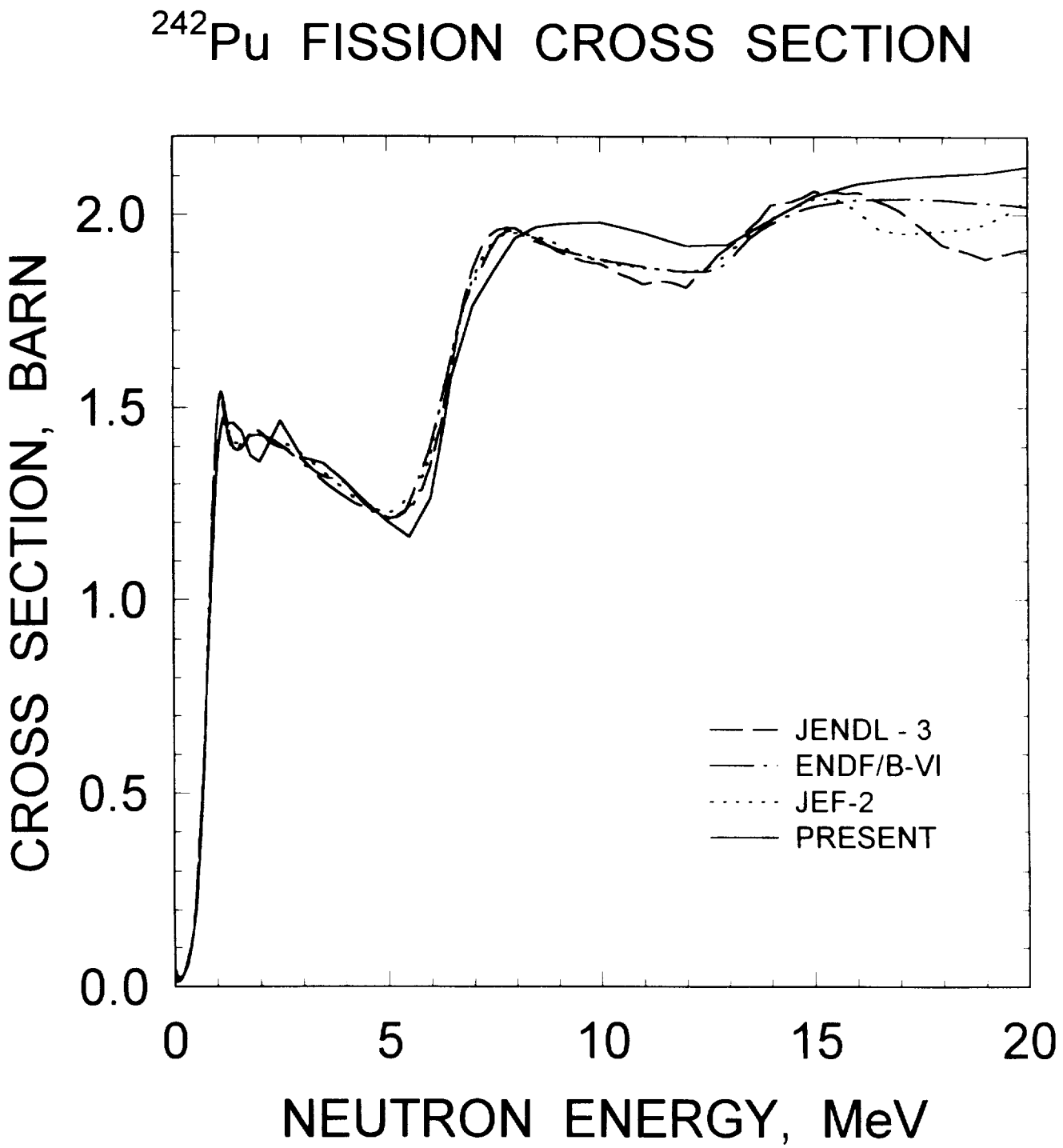
242Pu FISSION CROSS SECTION
CROSS SECTION, BARN
2.0
1.5
1.0
0.5
0.0
0
5
10
15
20
NEUTRON ENERGY, MeV
JENDL - 3
ENDF/B-VI
JEF-2
PRESENT

FIG. 4.10

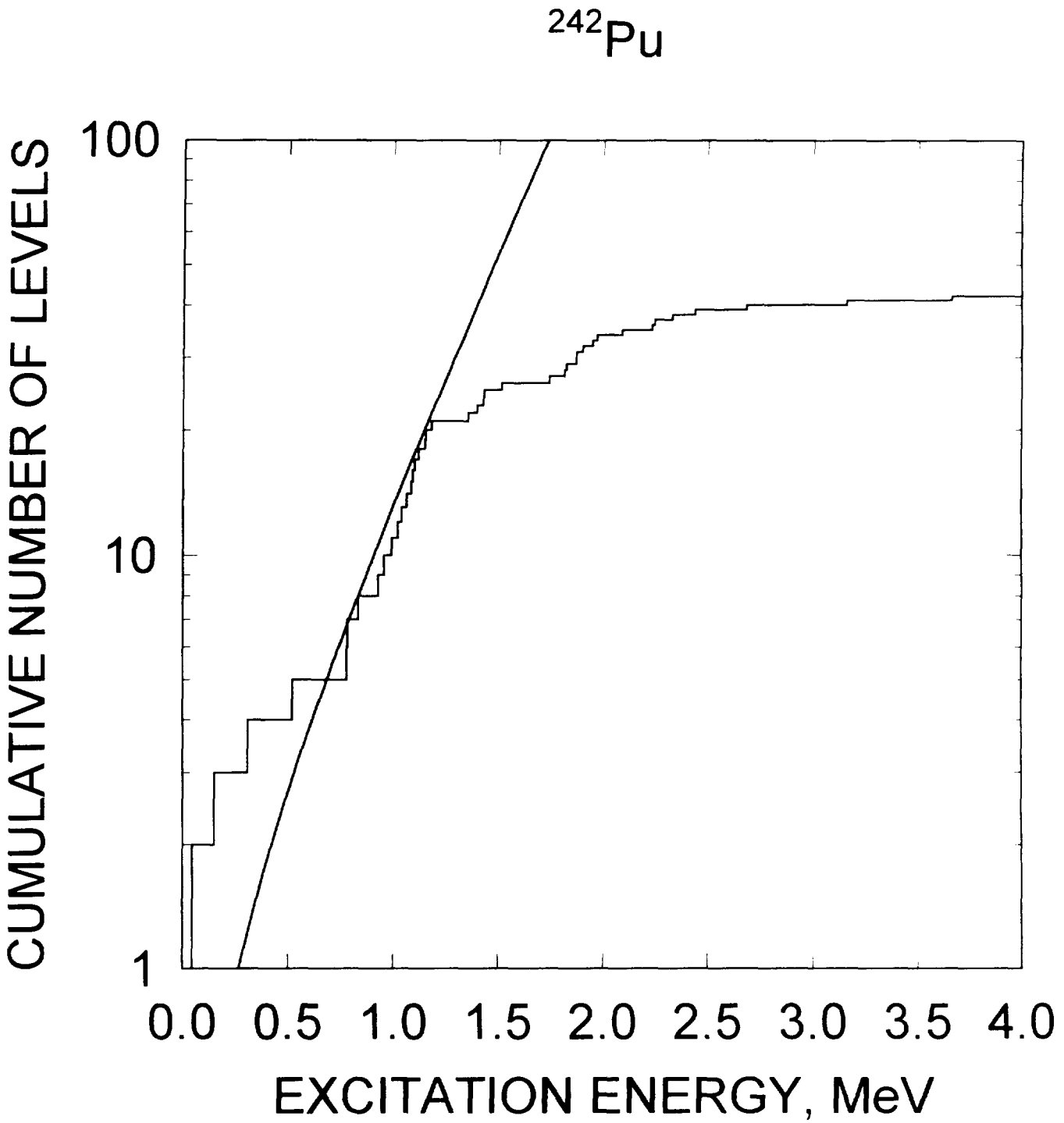
^{242}Pu
CUMULATIVE NUMBER OF LEVELS
100
10
1
0.0
0.5
1.0
1.5
2.0
2.5
3.0
3.5
4.0
EXCITATION ENERGY, MeV

FIG. 4.11

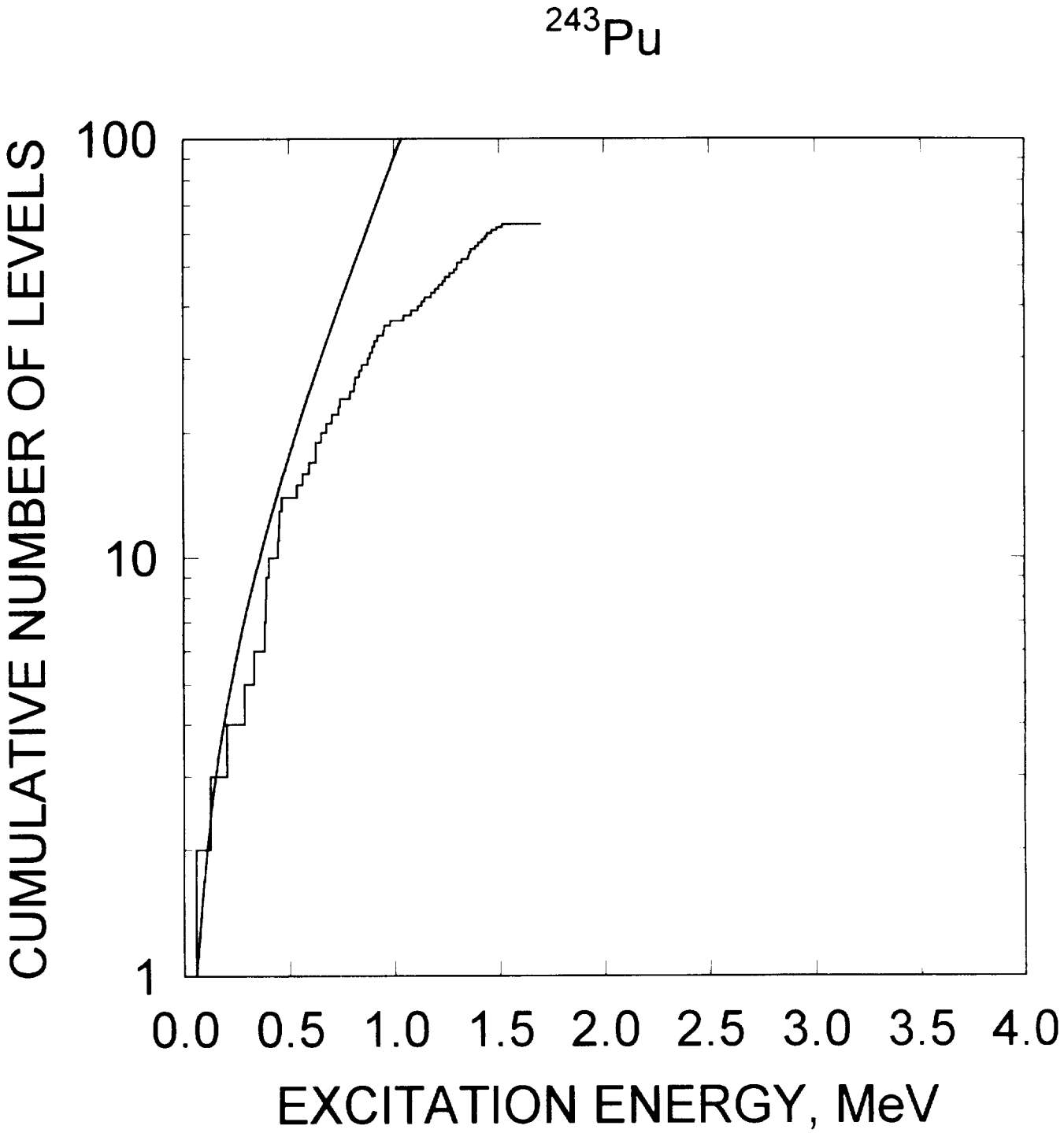
243Pu
CUMULATIVE NUMBER OF LEVELS
100
10
1
0.0
0.5
1.0
1.5
2.0
2.5
3.0
3.5
4.0
EXCITATION ENERGY, MeV

FIG. 4.12

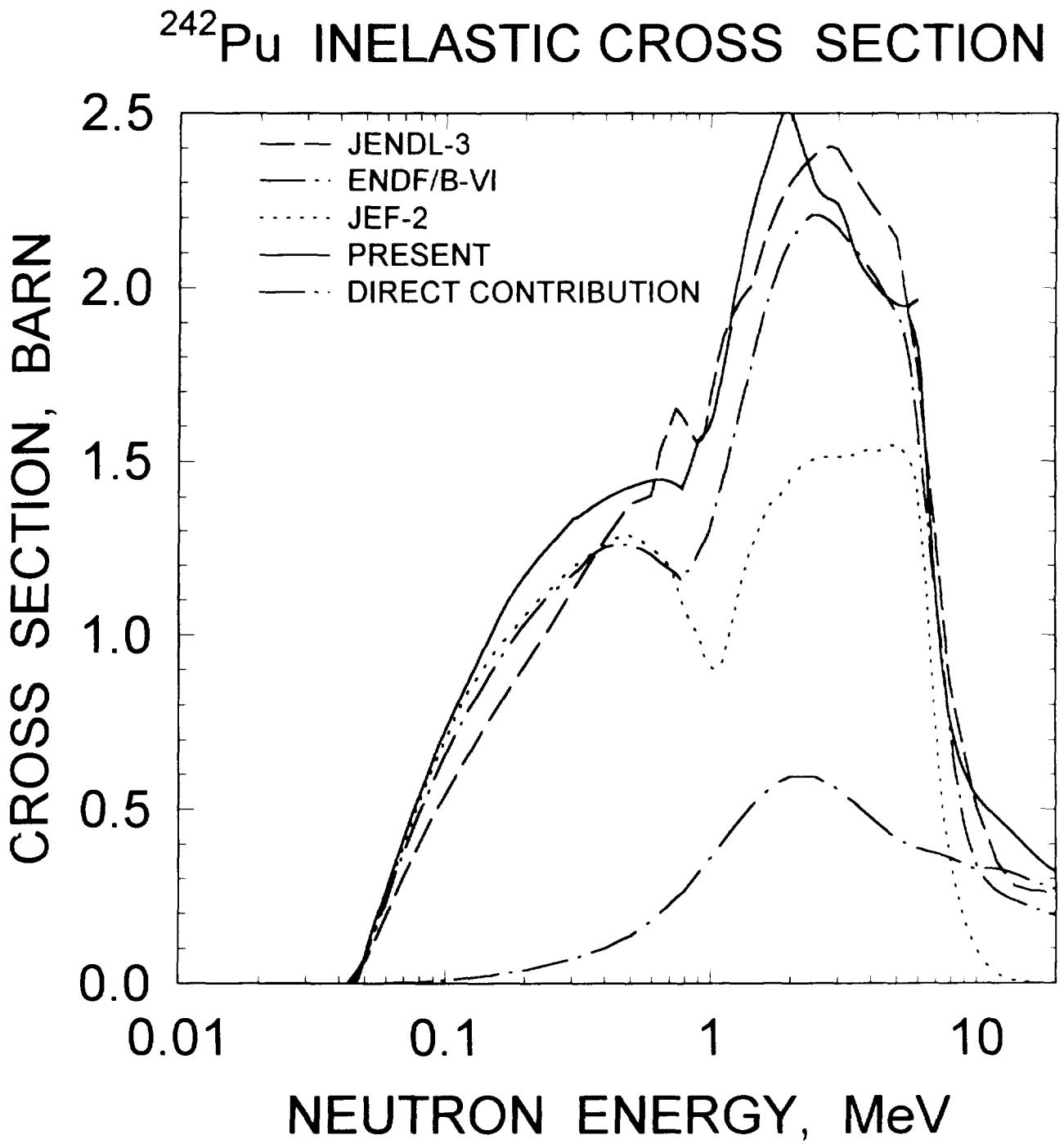
^{242}Pu INELASTIC CROSS SECTION
JENDL-3
ENDF/B-VI
JEF-2
PRESENT
DIRECT CONTRIBUTION
CROSS SECTION, BARN
2.5
2.0
1.5
1.0
0.5
0.0
0.01
0.1
1
10
NEUTRON ENERGY, MeV

FIG. 4.13

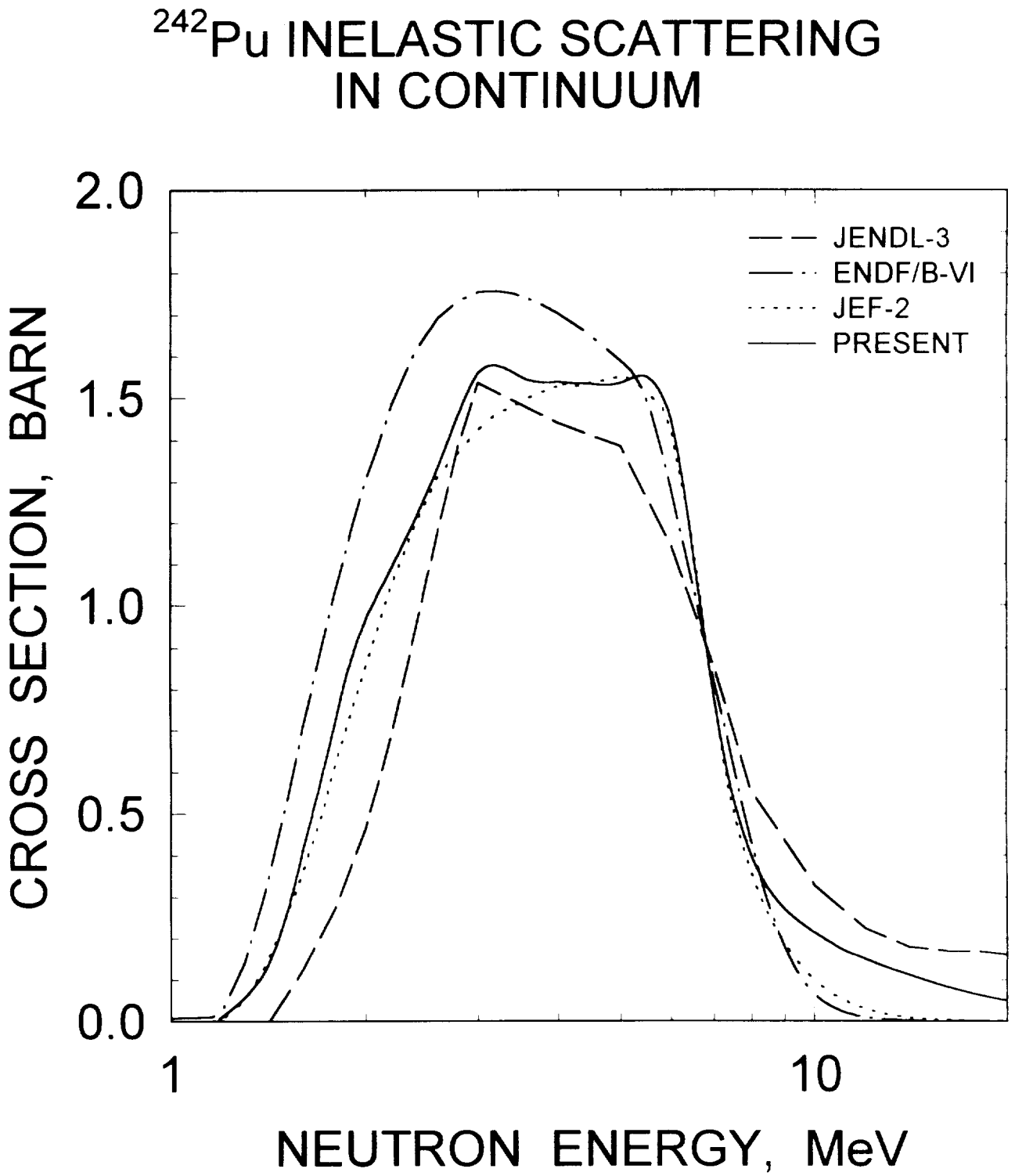
^{242}Pu INELASTIC SCATTERING
IN CONTINUUM
2.0
1.5
1.0
0.5
0.0
CROSS SECTION, BARN
1
10
NEUTRON ENERGY, MeV
JENDL-3
ENDF/B-VI
JEF-2
PRESENT

FIG. 4.14

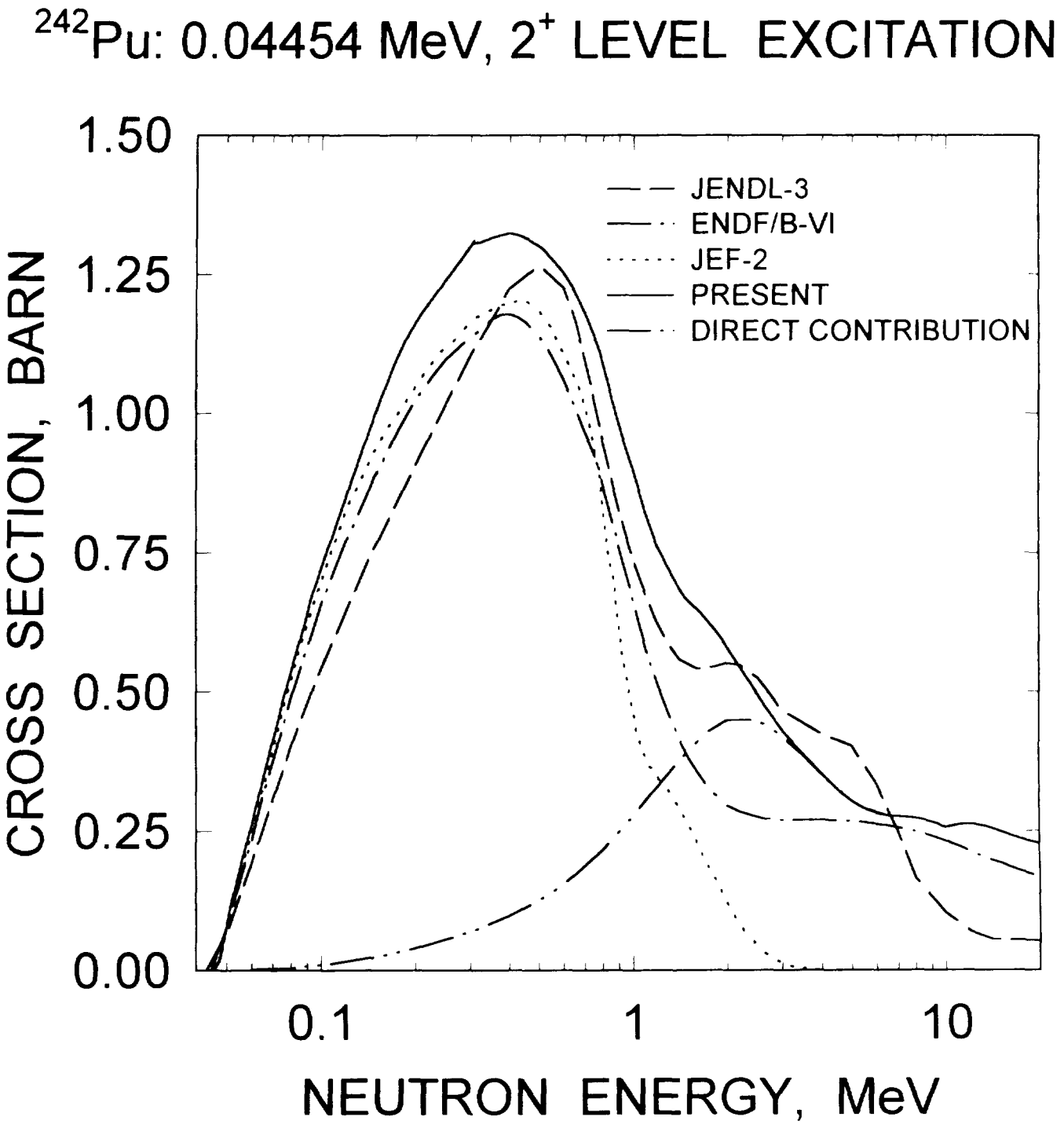
^{242}Pu: 0.04454 MeV, 2^{+} LEVEL EXCITATION
JENDL-3
ENDF/B-VI
JEF-2
PRESENT
DIRECT CONTRIBUTION
CROSS SECTION, BARN
1.50
1.25
1.00
0.75
0.50
0.25
0.00
0.1
1
10
NEUTRON ENERGY, MeV

FIG. 4.15

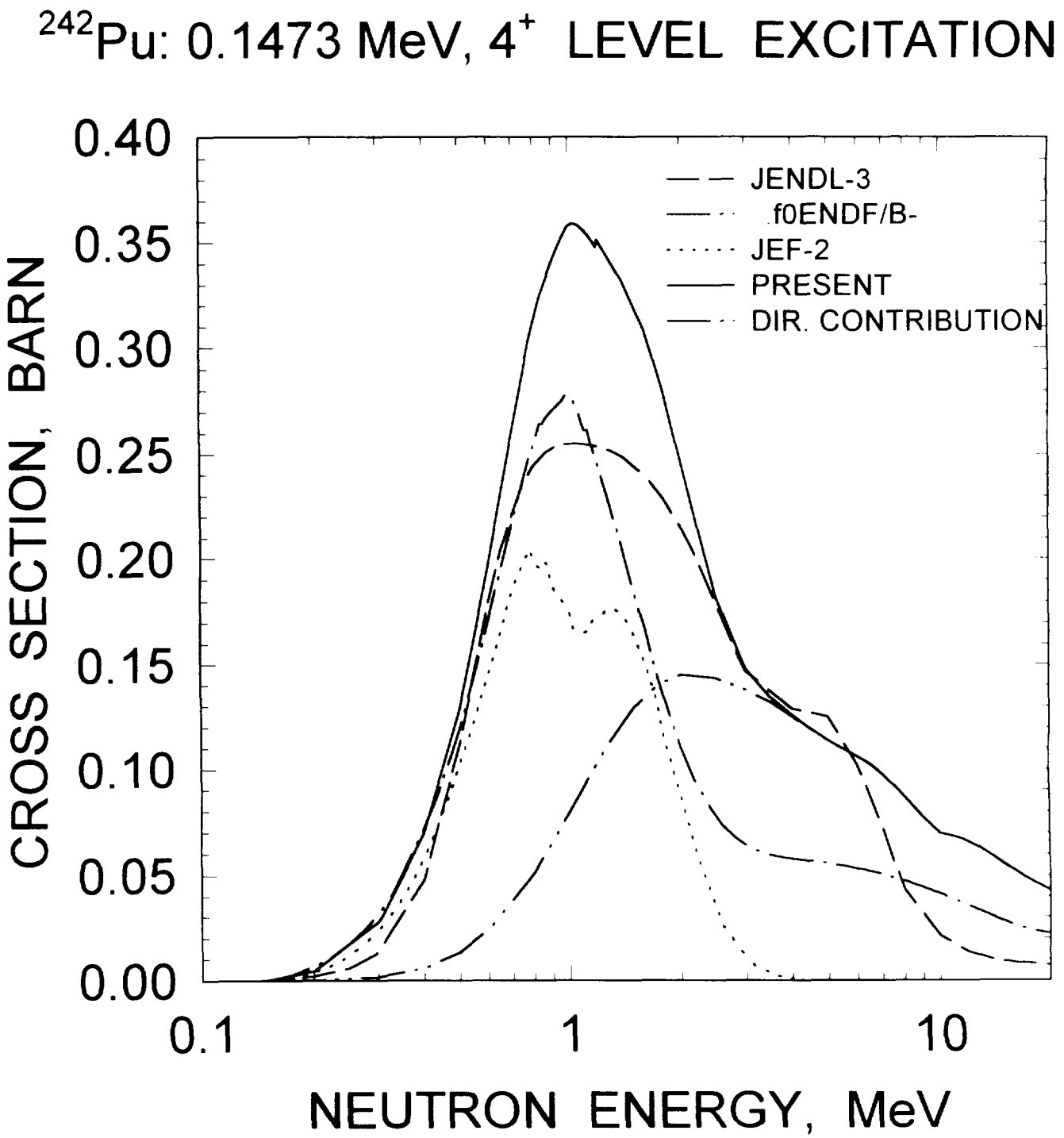
^{242}Pu: 0.1473 MeV, 4^{+} LEVEL EXCITATION
JENDL-3
f0ENDF/B-
JEF-2
PRESENT
DIR. CONTRIBUTION
CROSS SECTION, BARN
0.40
0.35
0.30
0.25
0.20
0.15
0.10
0.05
0.00
0.1
1
10
NEUTRON ENERGY, MeV

FIG. 4.16

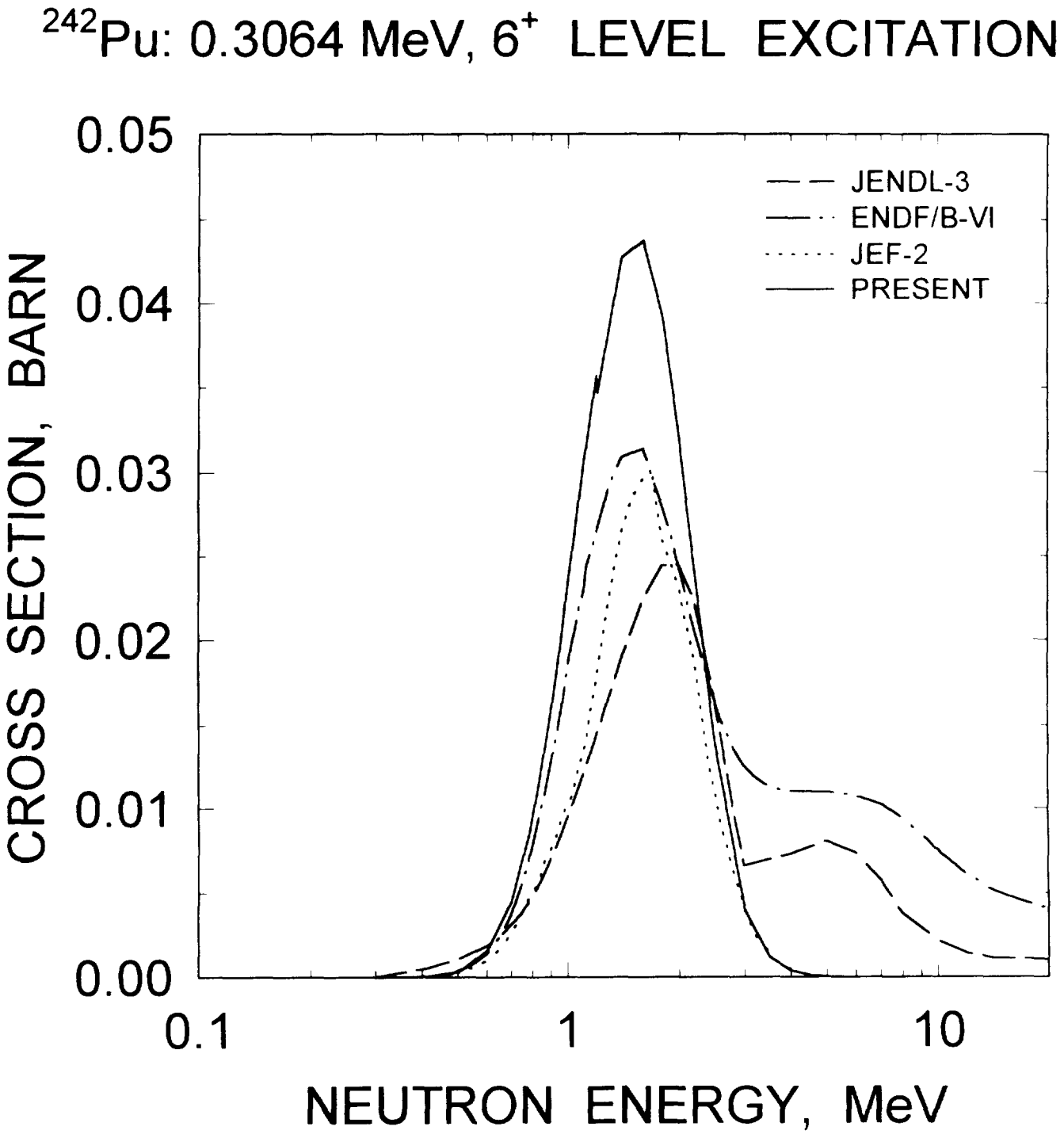
^{242}Pu: 0.3064 MeV, 6^{+} LEVEL EXCITATION
JENDL-3
ENDF/B-VI
JEF-2
PRESENT
CROSS SECTION, BARN
0.05
0.04
0.03
0.02
0.01
0.00
0.1
1
10
NEUTRON ENERGY, MeV

FIG. 4.17

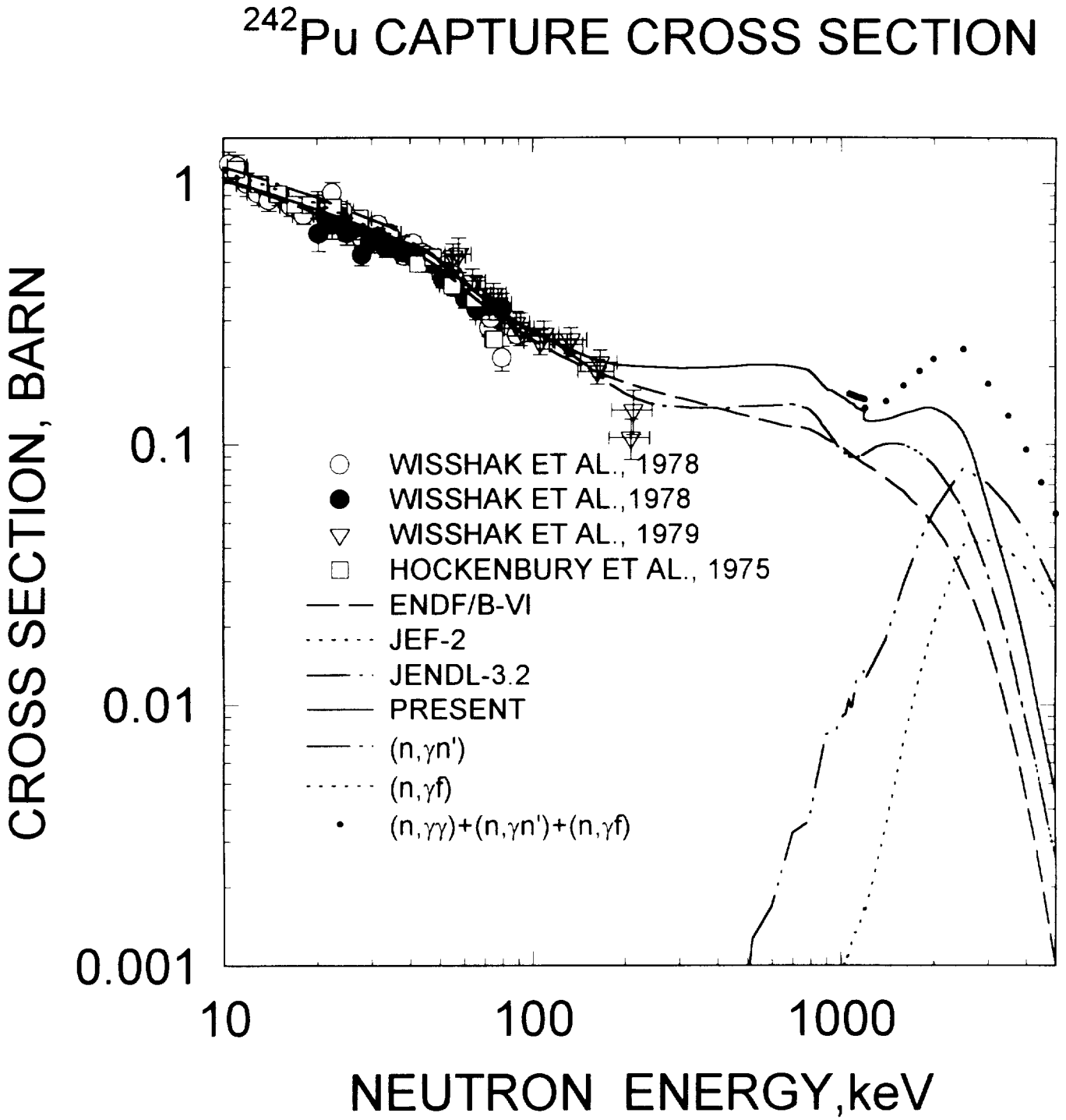
242Pu CAPTURE CROSS SECTION
CROSS SECTION, BARN
1
0.1
0.01
0.001
10
100
1000
NEUTRON ENERGY,keV
WISSHAK ET AL., 1978
WISSHAK ET AL.,1978
WISSHAK ET AL., 1979
HOCKENBURY ET AL., 1975
ENDF/B-VI
JEF-2
JENDL-3.2
PRESENT
(n,γn')
(n,γf)
(n,γγ)+(n,γn')+(n,γf)

FIG. 4.18

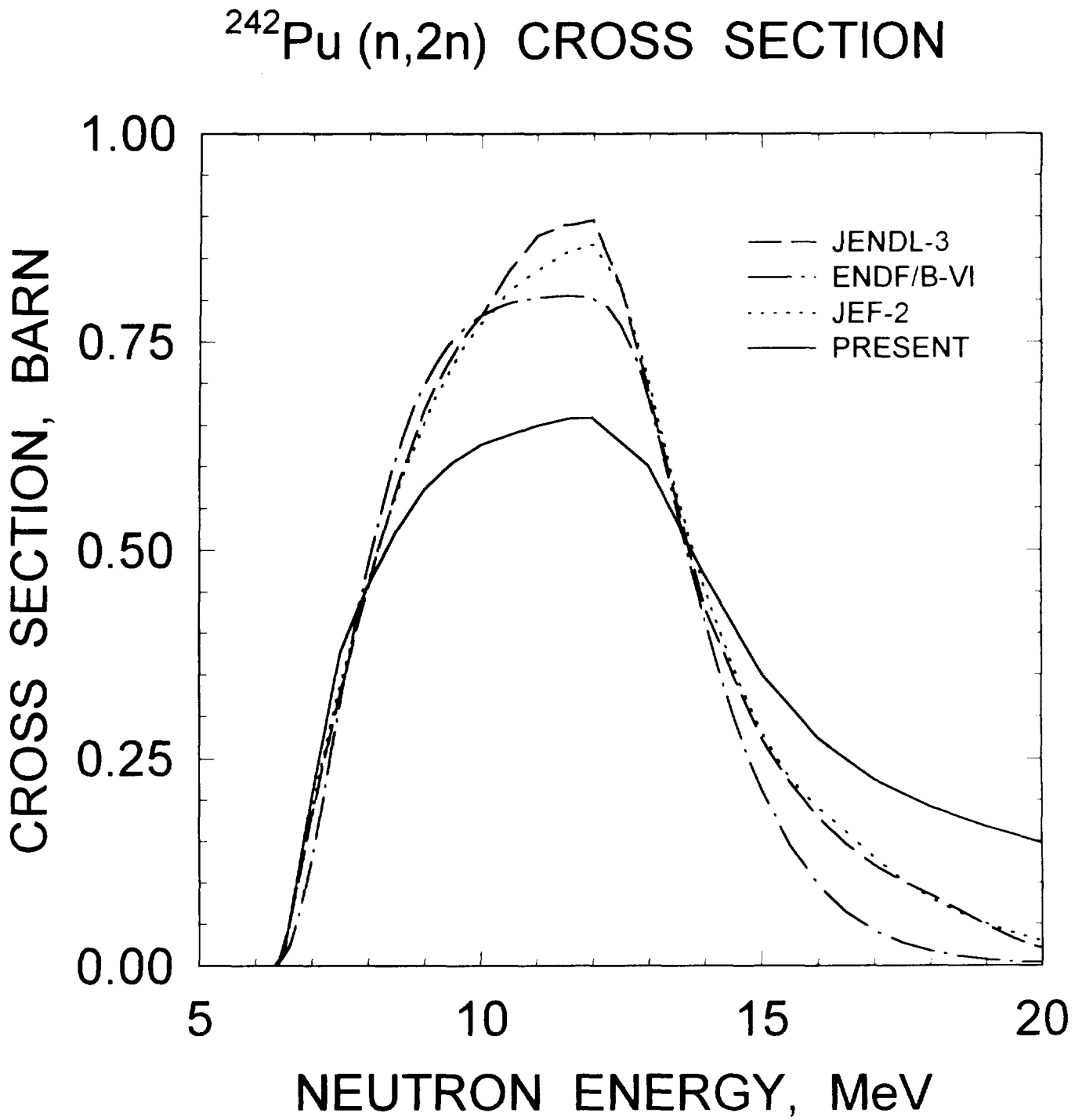
^{242}Pu (n,2n) CROSS SECTION
1.00
0.75
0.50
0.25
0.00
CROSS SECTION, BARN
5
10
15
20
NEUTRON ENERGY, MeV
JENDL-3
ENDF/B-VI
JEF-2
PRESENT

FIG. 4.19

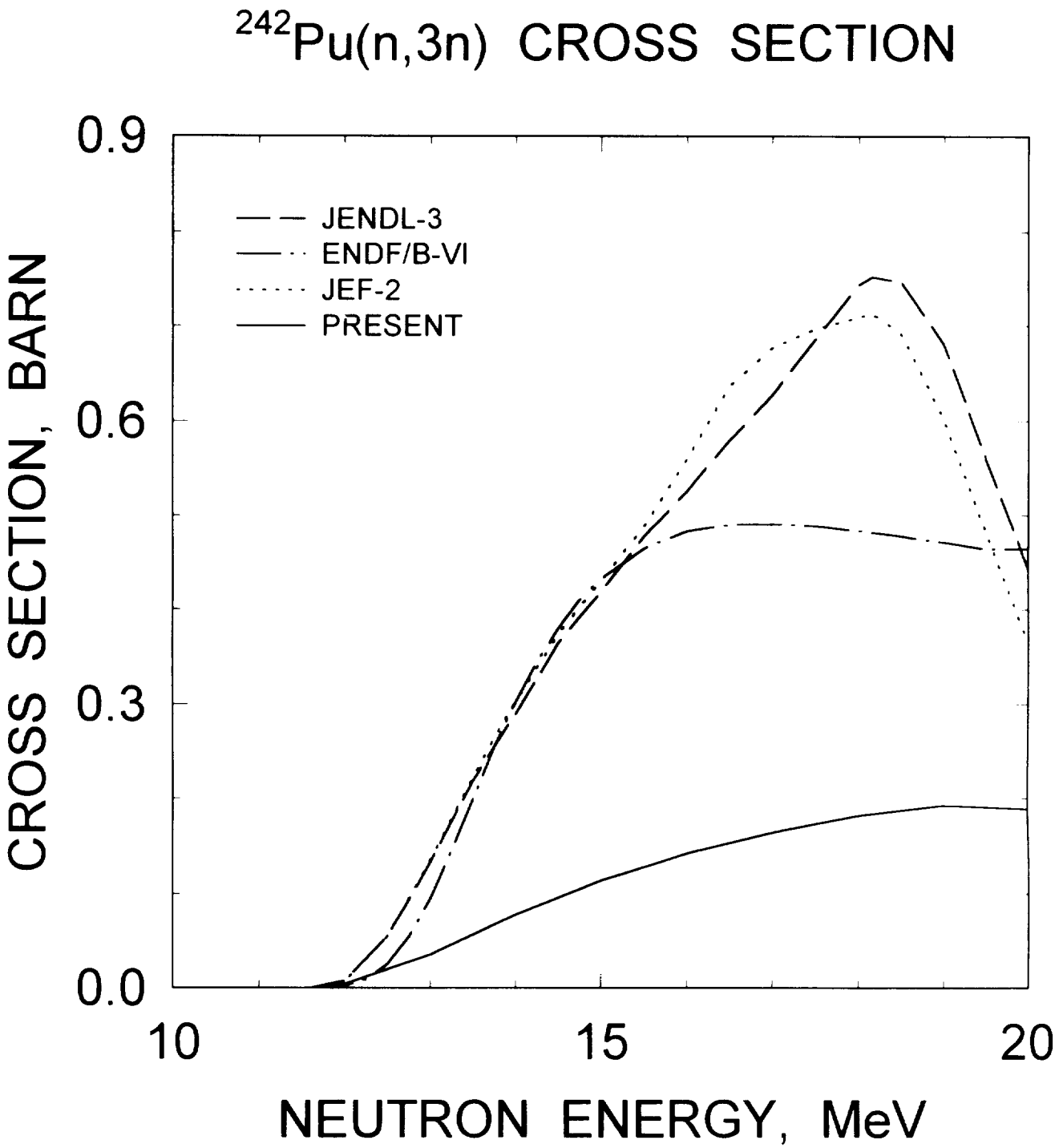
^{242}Pu(n,3n) CROSS SECTION
JENDL-3
ENDF/B-VI
JEF-2
PRESENT
CROSS SECTION, BARN
0.9
0.6
0.3
0.0
10
15
20
NEUTRON ENERGY, MeV

FIG. 4.20

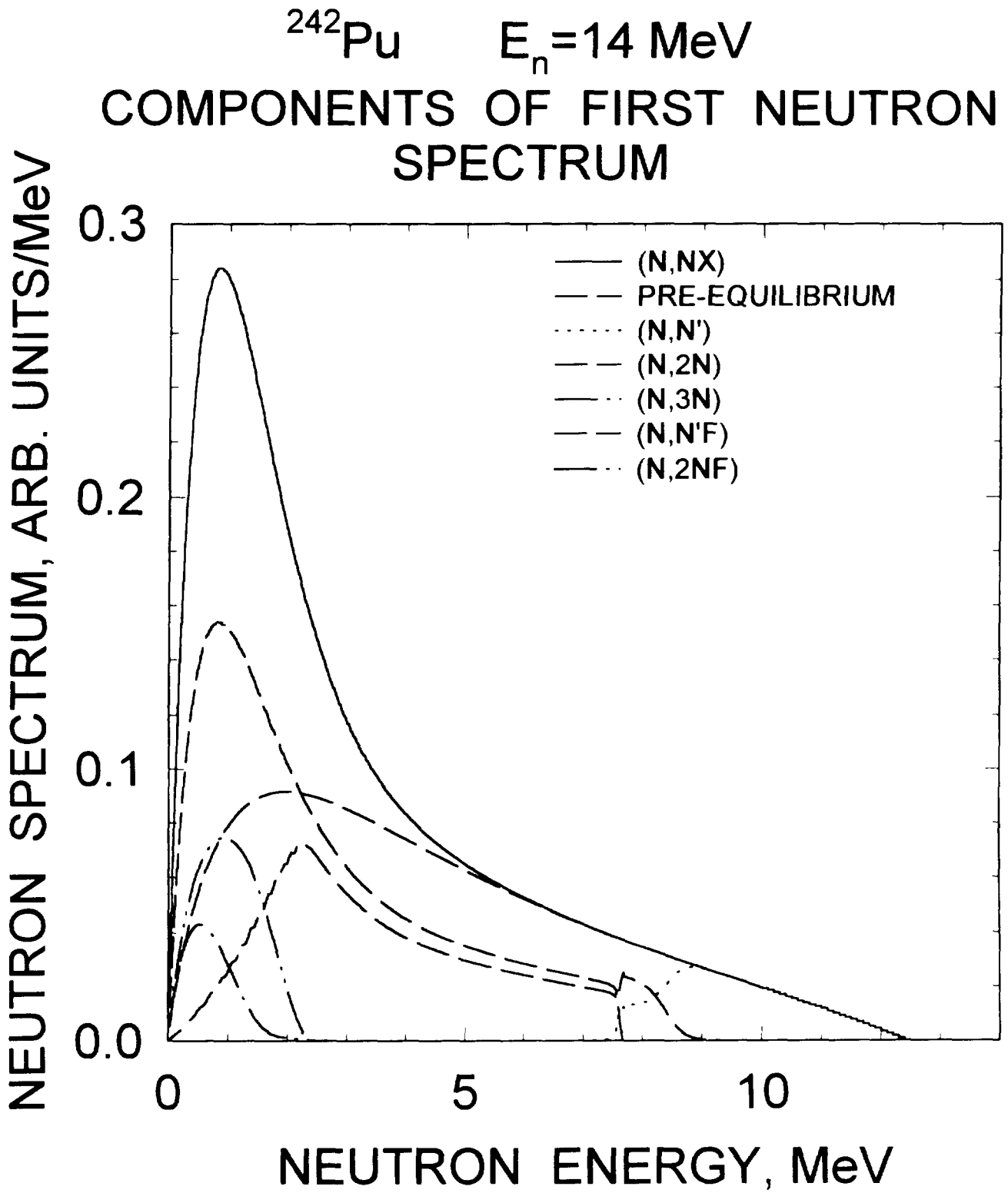
^{242}Pu E_n=14 MeV
COMPONENTS OF FIRST NEUTRON SPECTRUM
NEUTRON SPECTRUM, ARB. UNITS/MeV
0.3
0.2
0.1
0.0
0
5
10
NEUTRON ENERGY, MeV
(N,NX)
PRE-EQUILIBRIUM
(N,N')
(N,2N)
(N,3N)
(N,N'F)
(N,2NF)

FIG.5.1

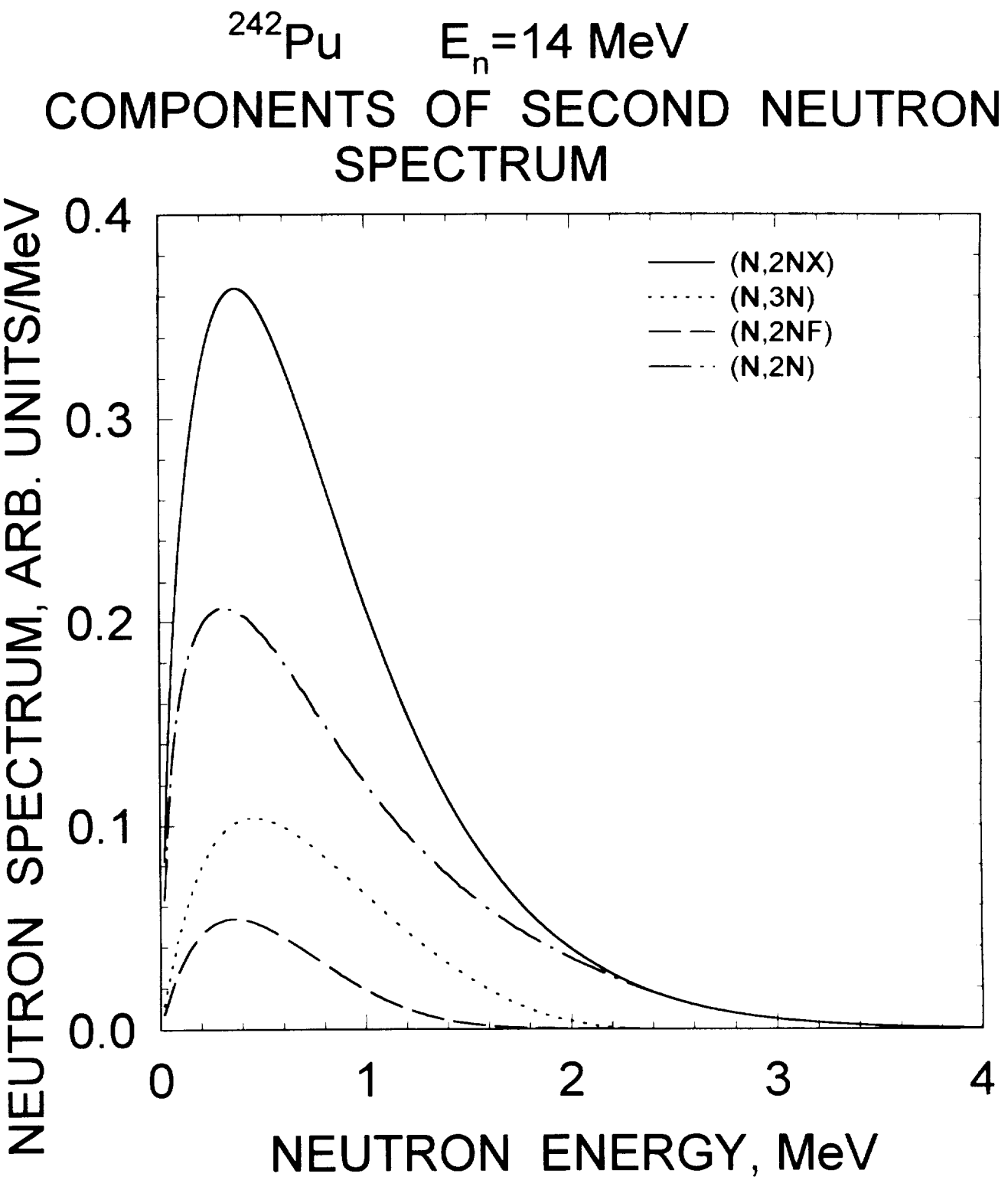
^{242}Pu E_n=14 MeV
COMPONENTS OF SECOND NEUTRON SPECTRUM
NEUTRON SPECTRUM, ARB. UNITS/MeV
0.4
0.3
0.2
0.1
0.0
0
1
2
3
4
NEUTRON ENERGY, MeV
(N,2NX)
(N,3N)
(N,2NF)
(N,2N)

FIG.5.2

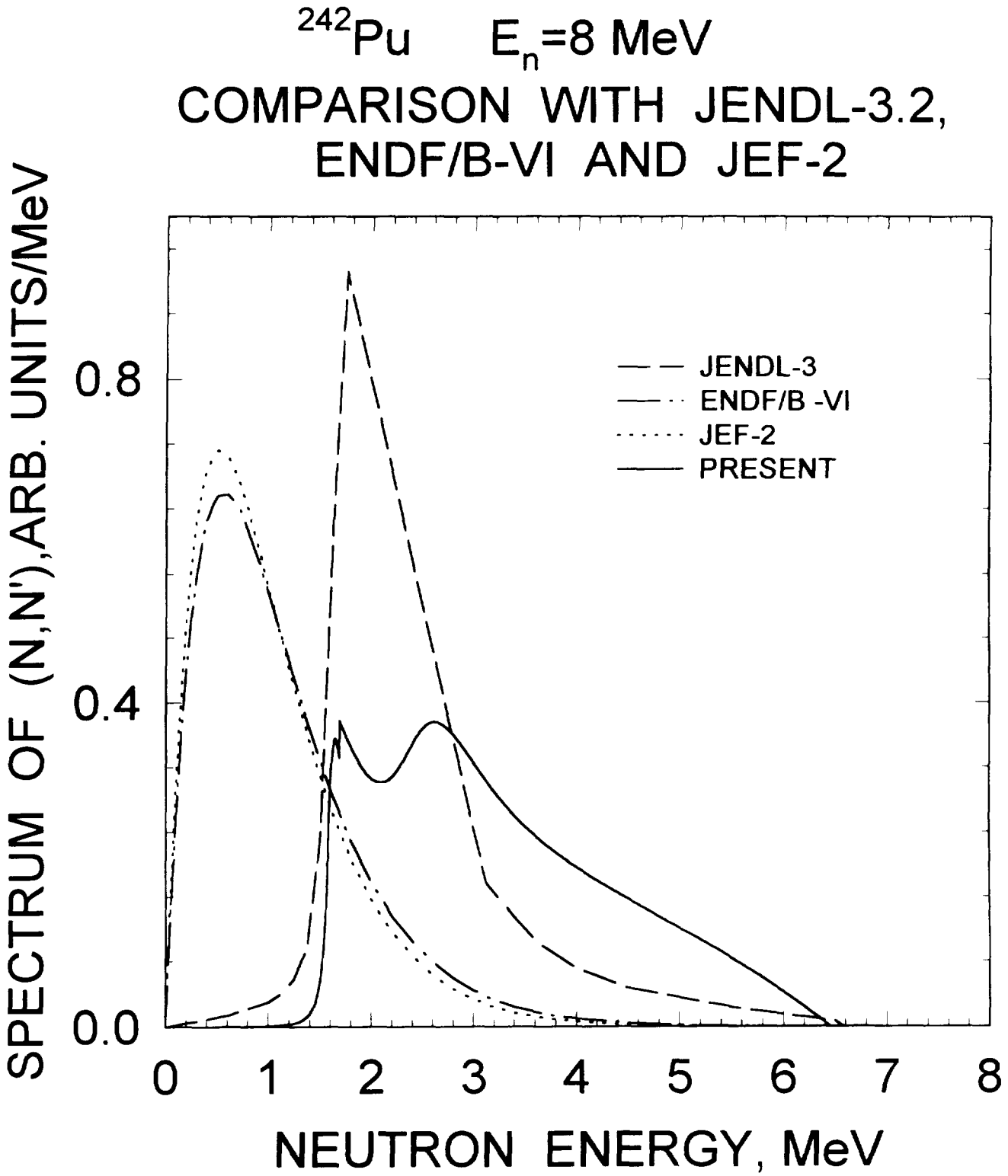
^{242}Pu E_n=8 MeV
COMPARISON WITH JENDL-3.2, ENDF/B-VI AND JEF-2
SPECTRUM OF (N,N'),ARB. UNITS/MeV
0.0
0.4
0.8
0
1
2
3
4
5
6
7
8
NEUTRON ENERGY, MeV
JENDL-3
ENDF/B -VI
JEF-2
PRESENT

FIG.5.3

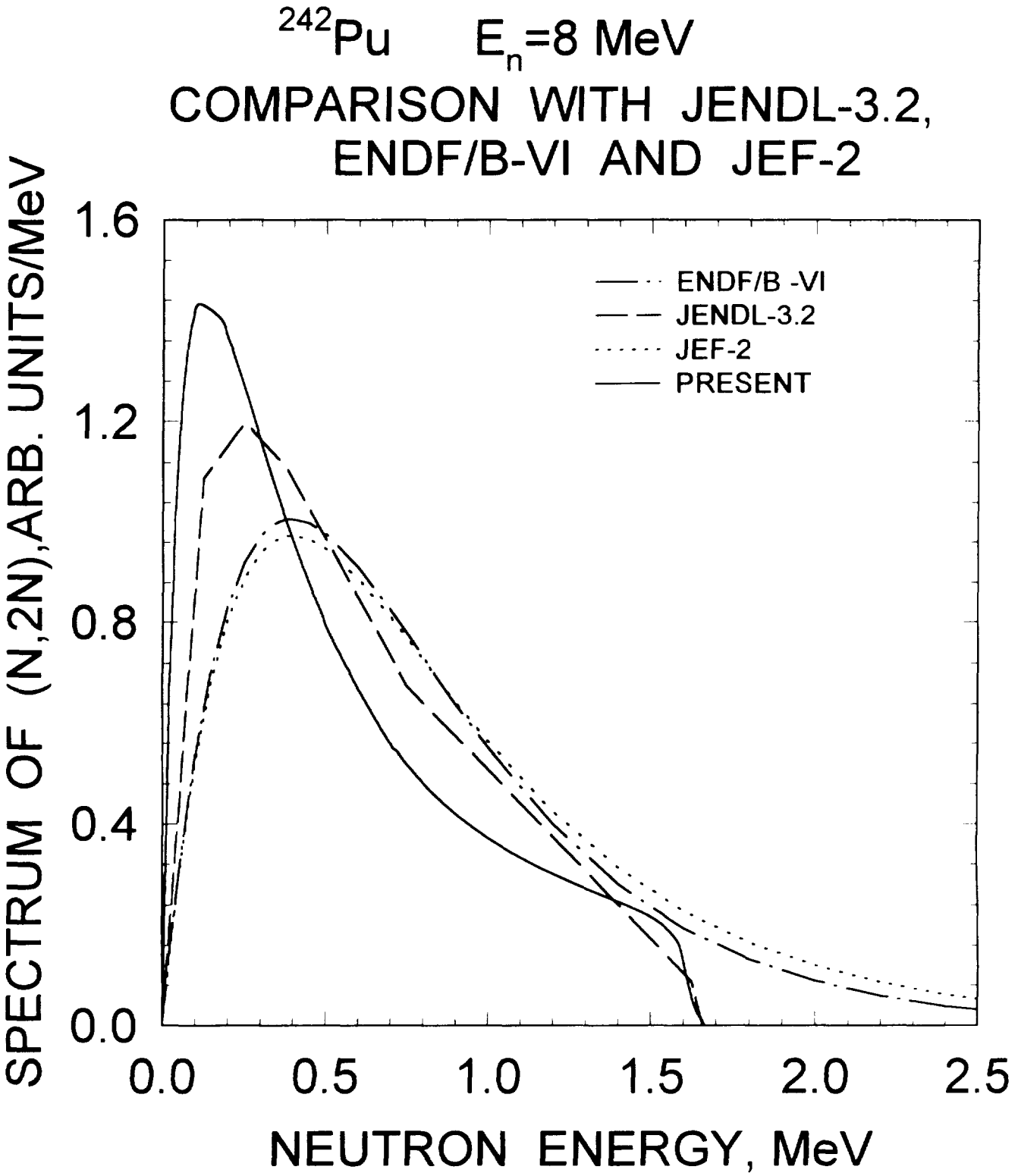
^{242}Pu E_n=8 MeV
COMPARISON WITH JENDL-3.2, ENDF/B-VI AND JEF-2
ENDF/B -VI
JENDL-3.2
JEF-2
PRESENT
SPECTRUM OF (N,2N),ARB. UNITS/MeV
1.6
1.2
0.8
0.4
0.0
0.0
0.5
1.0
1.5
2.0
2.5
NEUTRON ENERGY, MeV

FIG.5.4

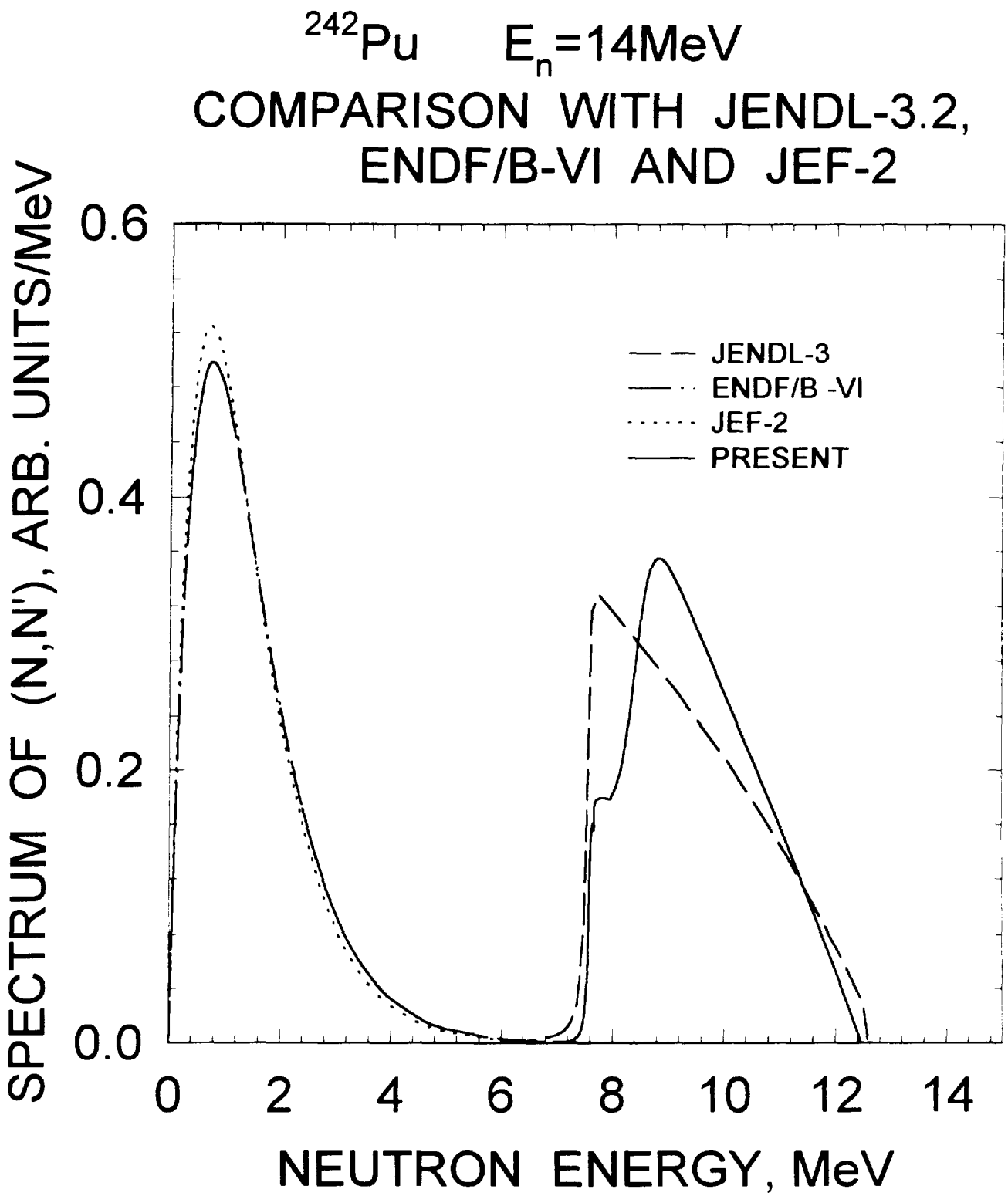
^{242}Pu E_n=14MeV
COMPARISON WITH JENDL-3.2, ENDF/B-VI AND JEF-2
SPECTRUM OF (N,N'), ARB. UNITS/MeV
0.6
0.4
0.2
0.0
0
2
4
6
8
10
12
14
NEUTRON ENERGY, MeV
JENDL-3
ENDF/B -VI
JEF-2
PRESENT

FIG.5.5

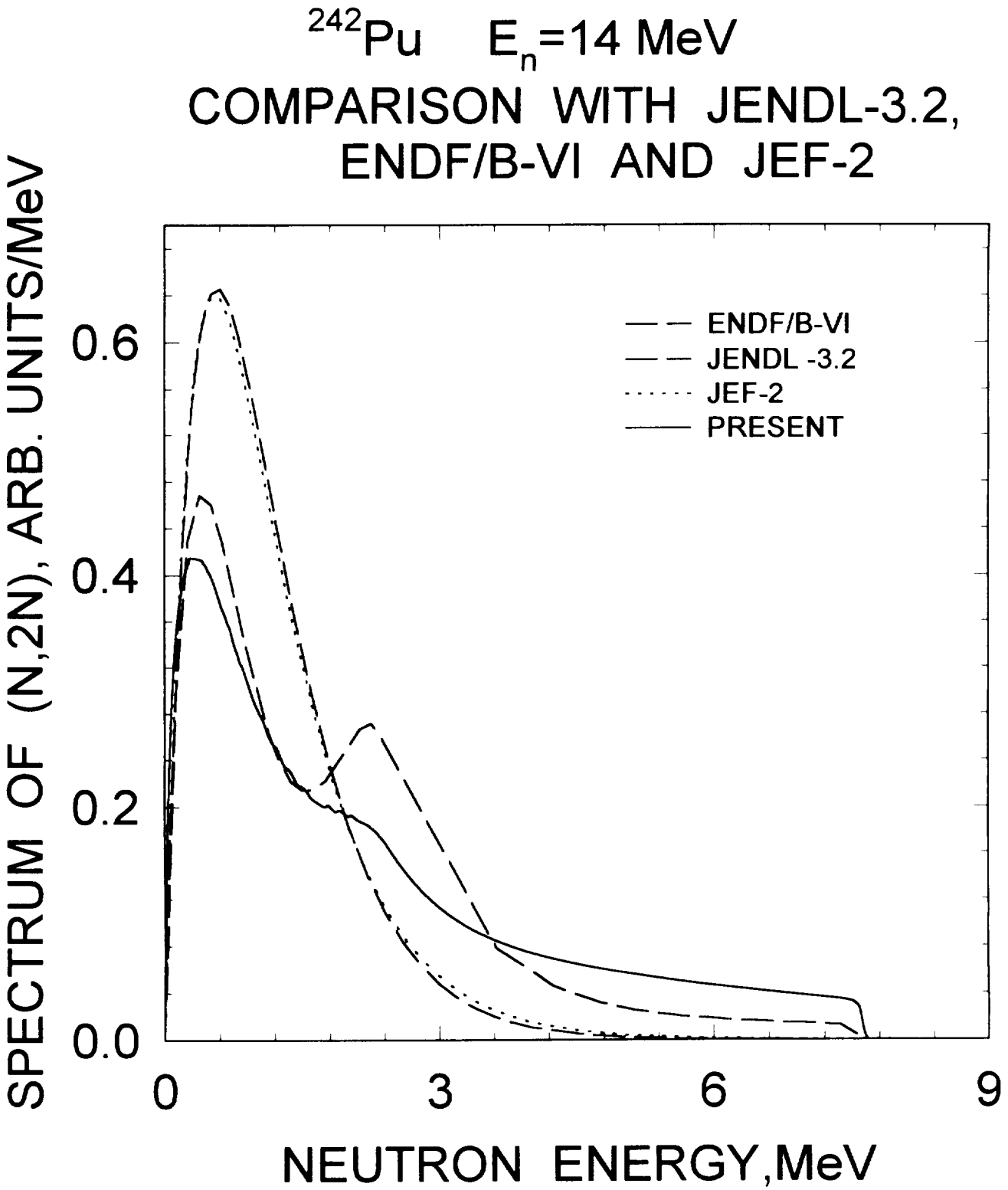
^{242}Pu E_n=14 MeV
COMPARISON WITH JENDL-3.2, ENDF/B-VI AND JEF-2
SPECTRUM OF (N,2N), ARB. UNITS/MeV
0.0
0.2
0.4
0.6
0
3
6
9
NEUTRON ENERGY,MeV
ENDF/B-VI
JENDL -3.2
JEF-2
PRESENT

FIG.5.6

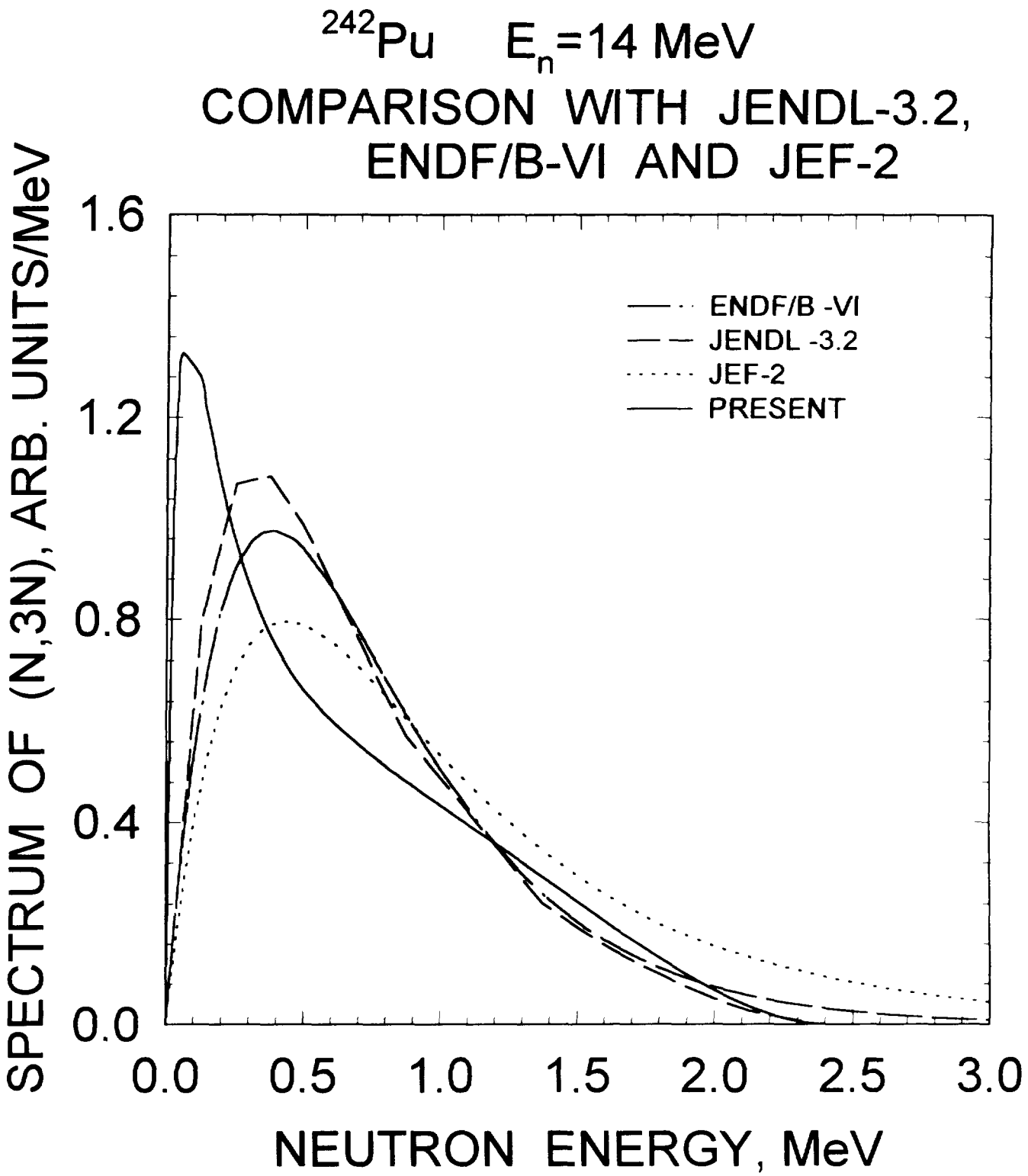
^{242}Pu E_n=14 MeV
COMPARISON WITH JENDL-3.2, ENDF/B-VI AND JEF-2
SPECTRUM OF (N,3N), ARB. UNITS/MeV
1.6
1.2
0.8
0.4
0.0
0.0
0.5
1.0
1.5
2.0
2.5
3.0
NEUTRON ENERGY, MeV
ENDF/B -VI
JENDL -3.2
JEF-2
PRESENT

FIG.5.7

^{242}Pu COMPARISON OF SPECTRA WITH DIFFERENT SHAPES OF THE PROMPT NEUTRON FISSION SPECTRA

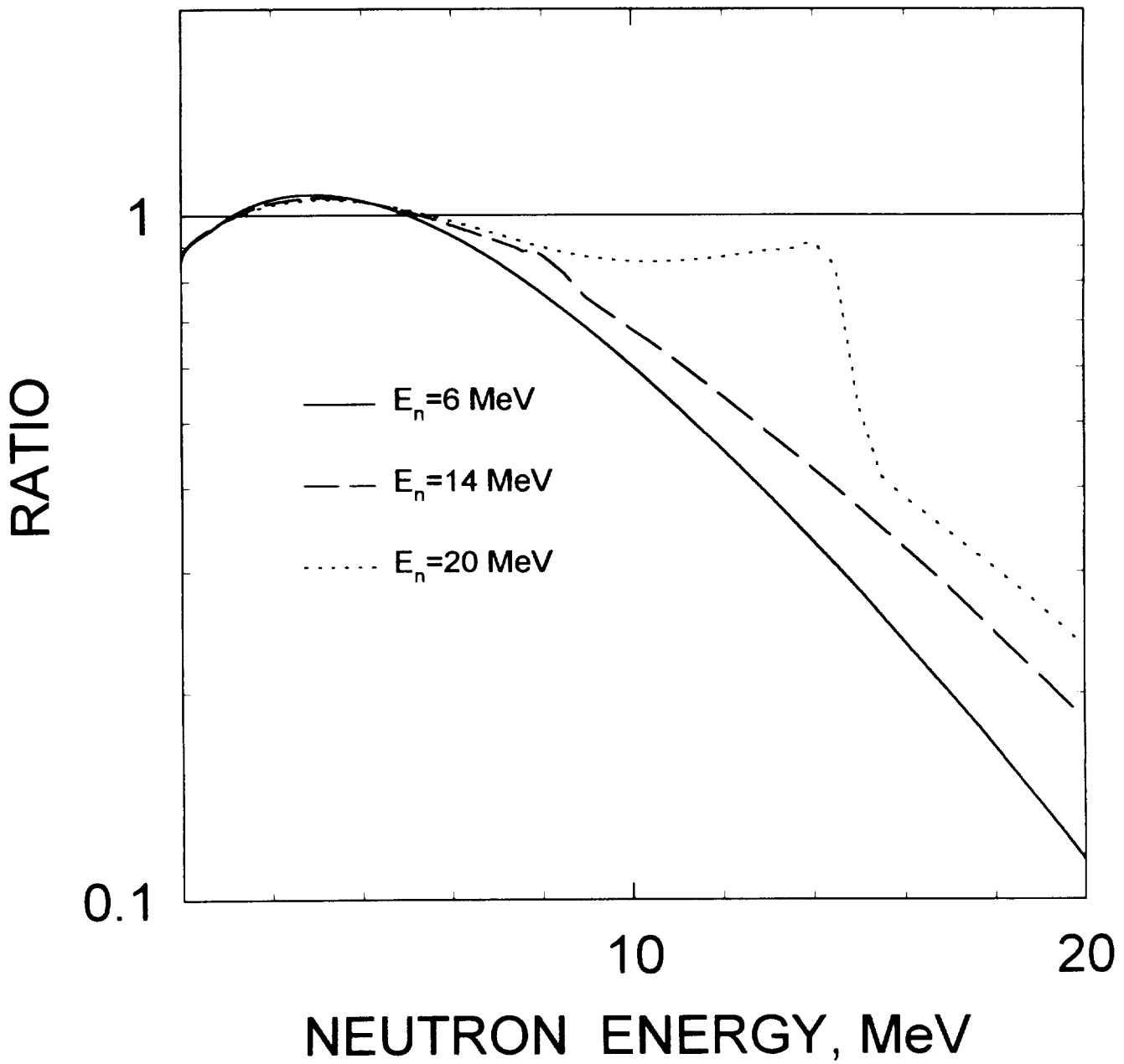

FIG. 5.8

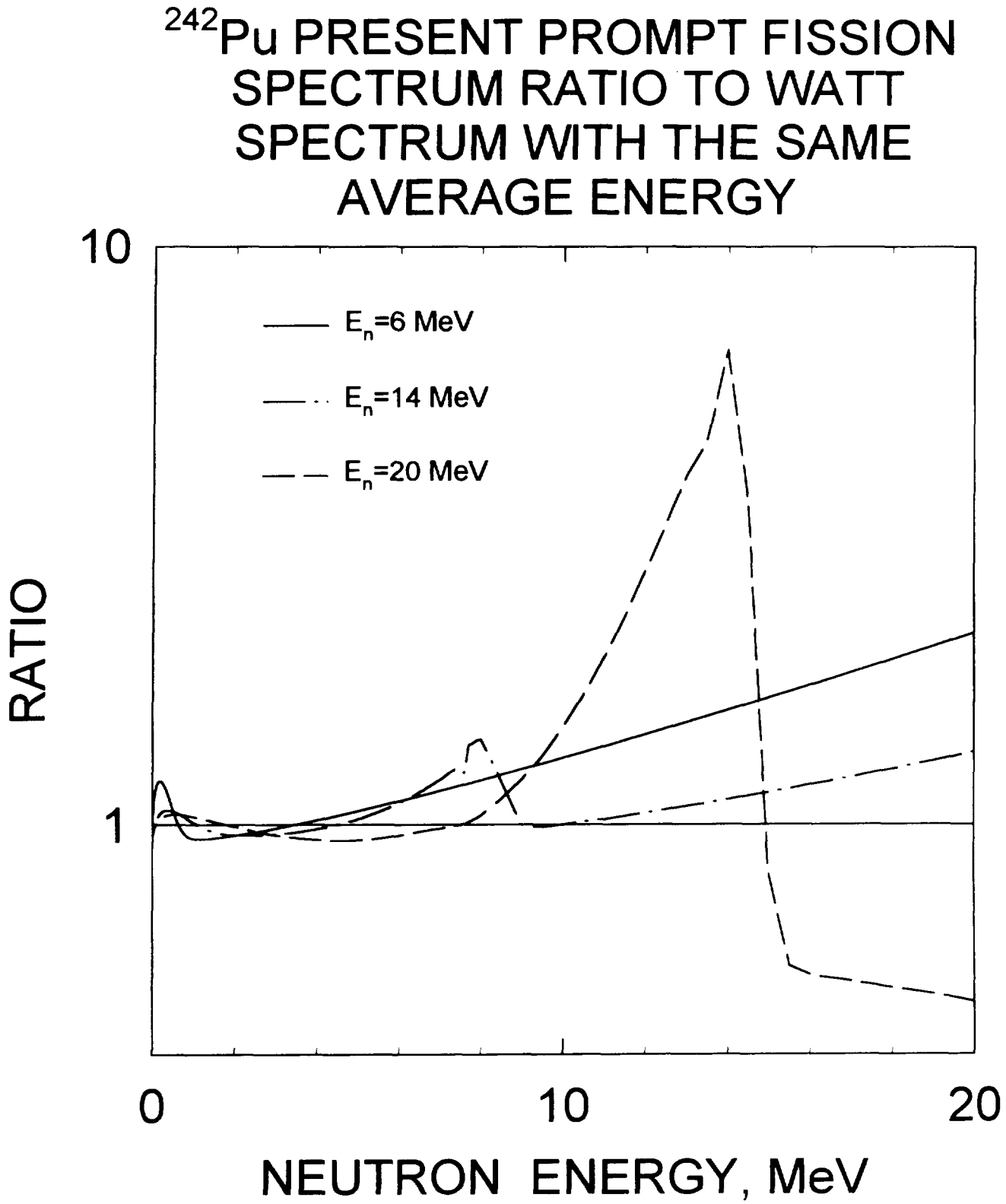
^{242}Pu PRESENT PROMPT FISSION SPECTRUM RATIO TO WATT SPECTRUM WITH THE SAME AVERAGE ENERGY
10
1
RATIO
E_n=6 MeV
E_n=14 MeV
E_n=20 MeV
0
10
20
NEUTRON ENERGY, MeV

FIG. 5.9

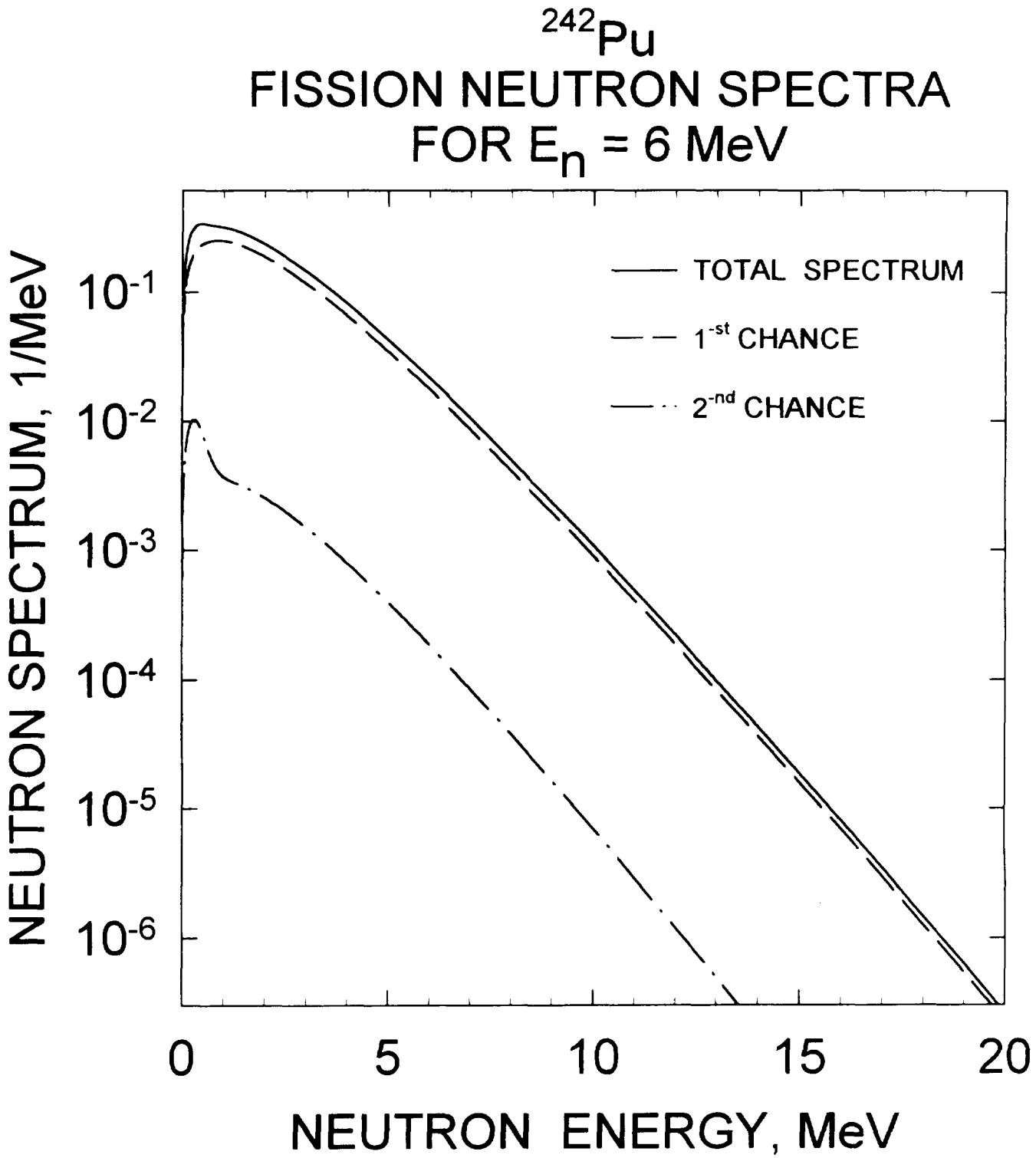
^{242}Pu
FISSION NEUTRON SPECTRA
FOR E_n = 6 MeV
TOTAL SPECTRUM
1-st CHANCE
2-nd CHANCE
NEUTRON SPECTRUM, 1/MeV
10^{-1}
10^{-2}
10^{-3}
10^{-4}
10^{-5}
10^{-6}
0
5
10
15
20
NEUTRON ENERGY, MeV

FIG.5.10

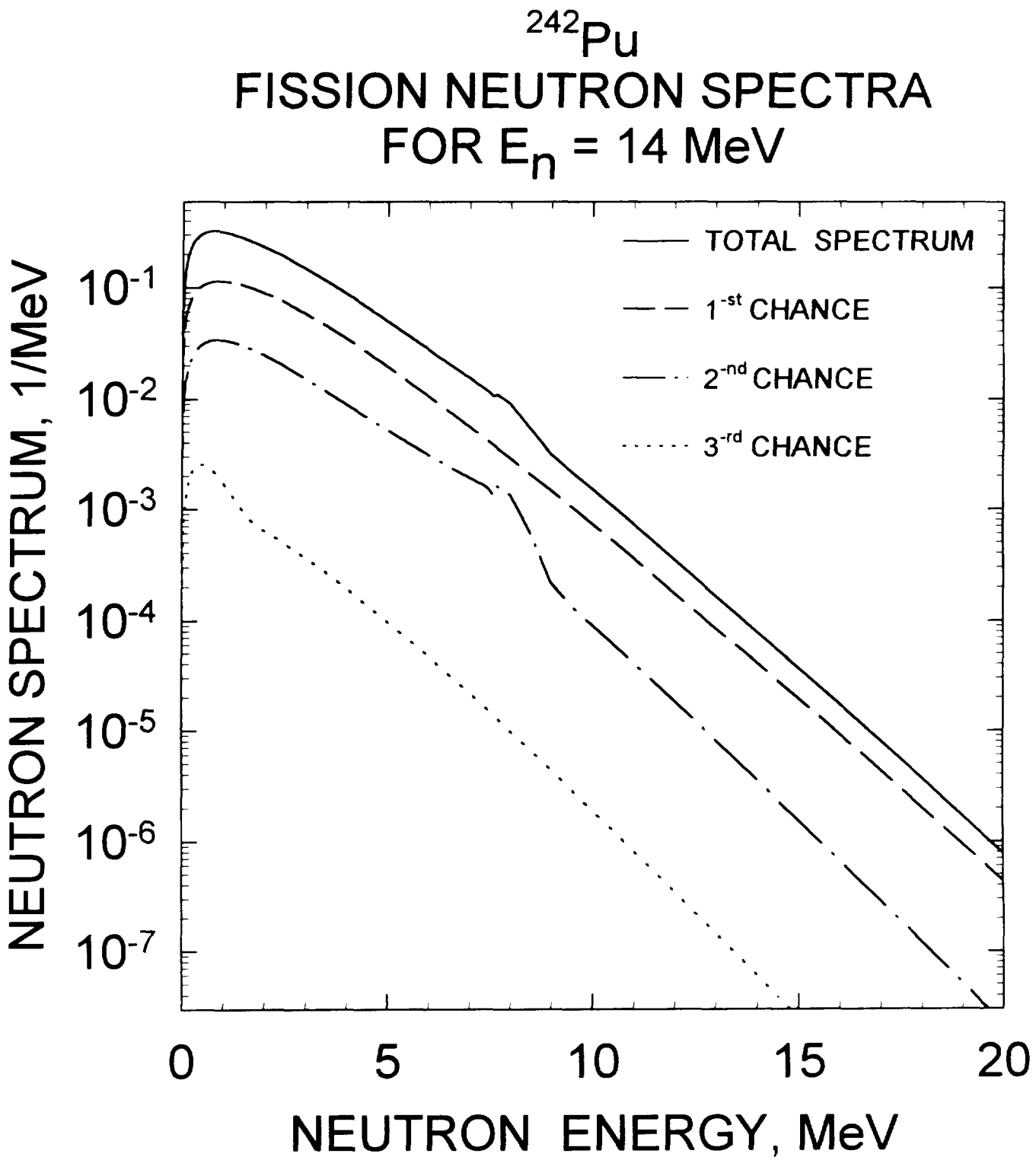
^{242}Pu
FISSION NEUTRON SPECTRA
FOR E_n = 14 MeV
TOTAL SPECTRUM
1-st CHANCE
2-nd CHANCE
3-rd CHANCE
NEUTRON SPECTRUM, 1/MeV
10^{-1}
10^{-2}
10^{-3}
10^{-4}
10^{-5}
10^{-6}
10^{-7}
0
5
10
15
20
NEUTRON ENERGY, MeV

FIG.5.11

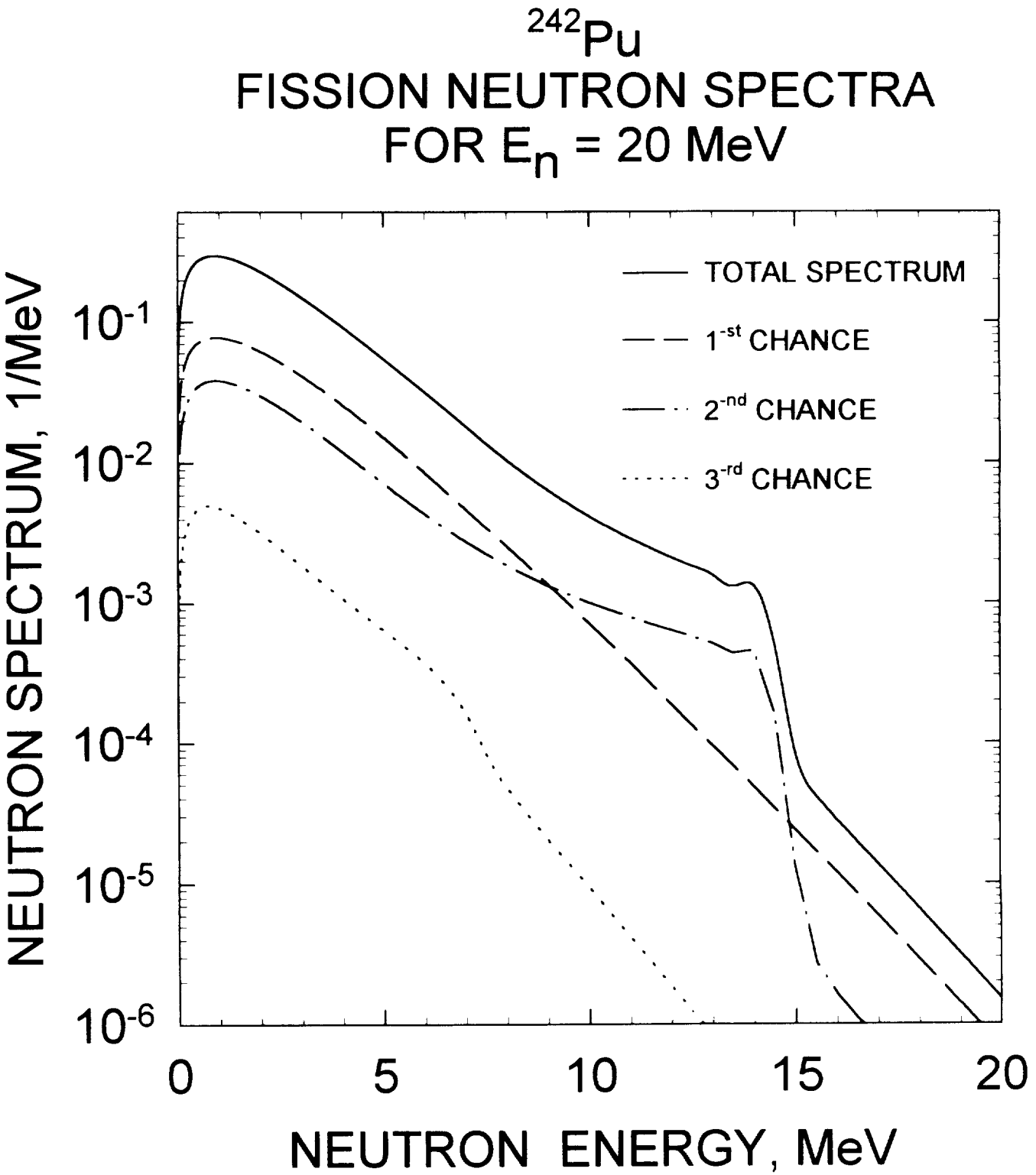
^{242}Pu
FISSION NEUTRON SPECTRA
FOR E_n = 20 MeV
TOTAL SPECTRUM
1-st CHANCE
2-nd CHANCE
3-rd CHANCE
NEUTRON SPECTRUM, 1/MeV
10^{-1}
10^{-2}
10^{-3}
10^{-4}
10^{-5}
10^{-6}
0
5
10
15
20
NEUTRON ENERGY, MeV

FIG.5.12

^{242}Pu COMPARISON OF THE PROMPT NEUTRON FISSION SPECTRUM WITH ENDF/B-VI AND JENDL-3.2 , E_n=15 MeV

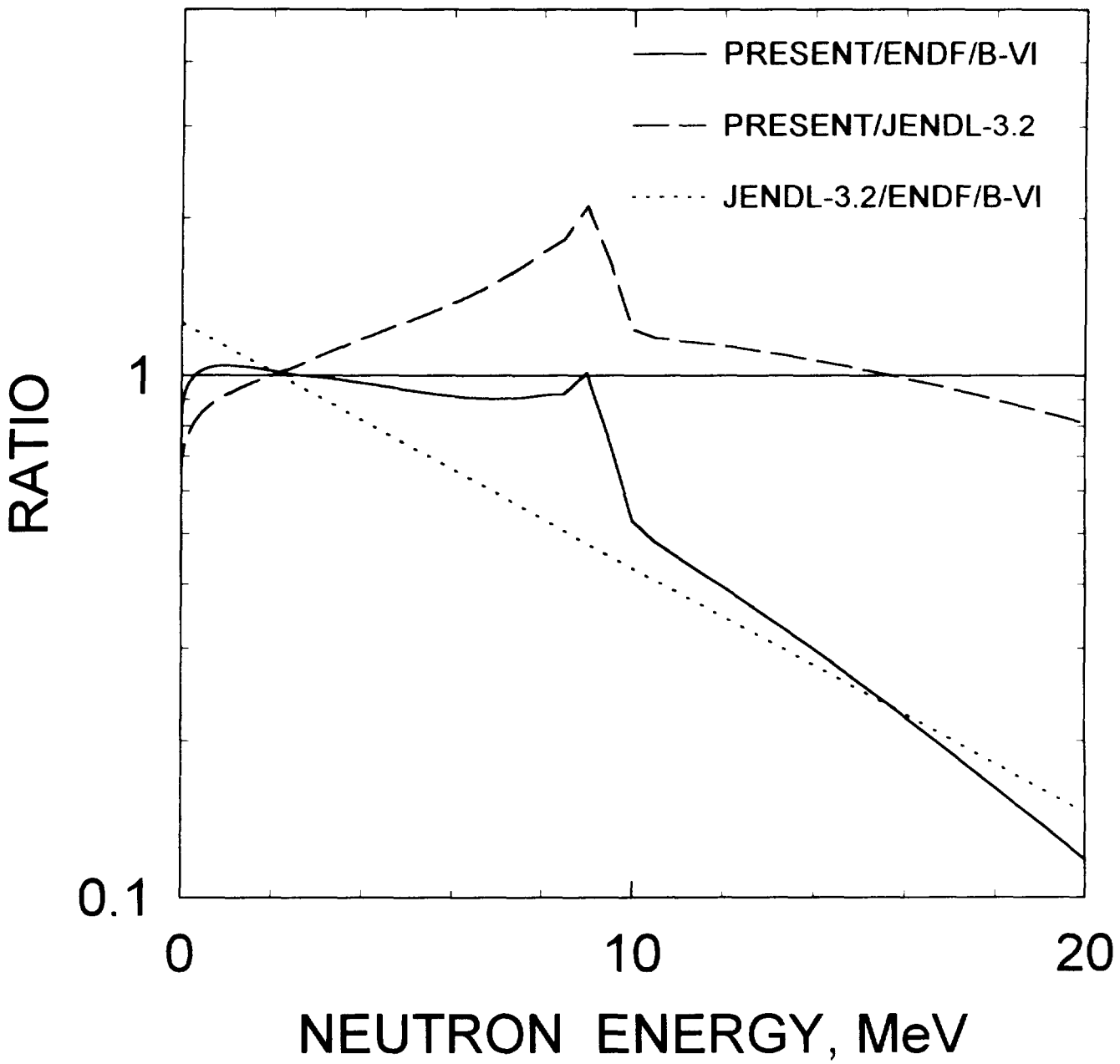

FIG. 5.13

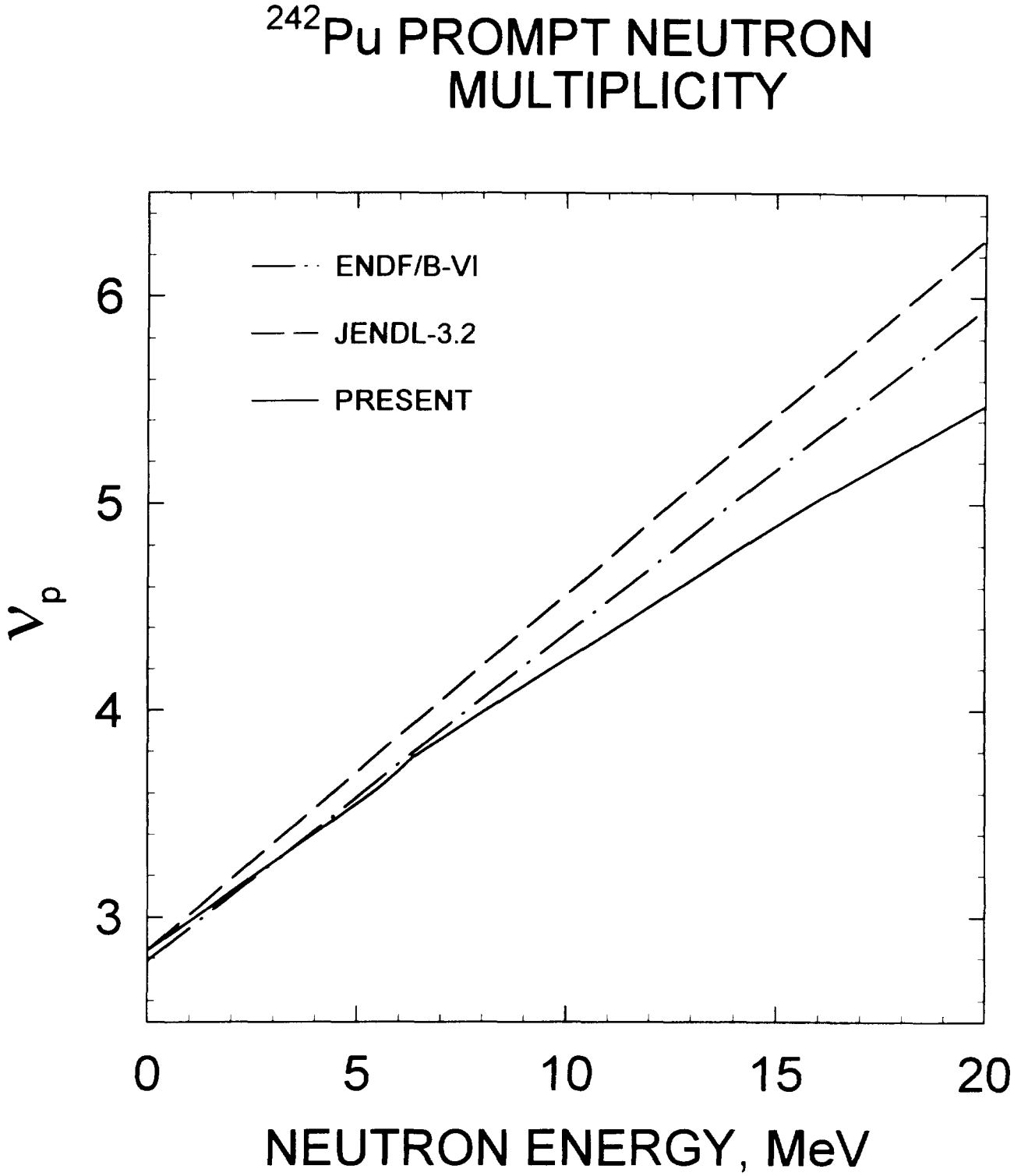
^{242}Pu PROMPT NEUTRON MULTIPLICITY
ENDF/B-VI
JENDL-3.2
PRESENT
ν_p
6
5
4
3
0
5
10
15
20
NEUTRON ENERGY, MeV

FIG.6.1

Nuclear Data Section
International Atomic Energy Agency
P.O. Box 100
A-1400 Vienna
Austria

e-mail: services@iaeand.iaea.or.at
fax: (43-1)20607
cable: INATOM VIENNA
telex: 1-12645 atom a
telephone: (43-1)2060-21710

online: TELNET or FTP: iaeand.iaea.or.at
username: IAEANDS for interactive Nuclear Data Information System
username: ANONYMOUS for FTP file transfer
For users with Web-browsers: http://www-nds.iaea.or.at